HEMODYNAMIC INVESTIGATION OF THE LIVER USING MAGNETIC RESONANCE IMAGING AND COMPUTATIONAL FLUID DYNAMICS

A Thesis
Presented to
The Academic Faculty

by

Stephanie M. George

In Partial Fulfillment
of the Requirements for the Degree
Doctor of Philosophy in the
Wallace H. Coulter Department of Biomedical Engineering

Georgia Institute of Technology
August 2008

HEMODYNAMIC INVESTIGATION OF THE LIVER USING MAGNETIC RESONANCE IMAGING AND COMPUTATIONAL FLUID DYNAMICS

Approved by:

Don P. Giddens, PhD, Advisor
Wallace H. Coulter Department of
Biomedical Engineering
*Georgia Institute of Technology and
Emory University*

Diego R. Martin, MD, PhD
Department of Radiology
Emory University School of Medicine

John N. Oshinski, PhD
Wallace H. Coulter Department of
Biomedical Engineering
*Georgia Institute of Technology and
Emory University*

Raymond P. Vito, PhD
School of Mechanical Engineering
Georgia Institute of Technology

Thomas Heffron, MD
Department of Surgury
Emory University School of Medicine

Date Approved: 27 May 2008

To my parents, John and Susan Gerke, my son, Noah,

and my husband, P.J.

ACKNOWLEDGEMENTS

I would like to thank those who have been supporting me and helping me throughout my doctoral work.

First, I would like to thank my PhD advisor Dr. Don Giddens for your guidance and support throughout my research. Without you I never would have been exposed to the emerging field of liver research. I would like to thank Dr. Diego Martin for your medical expertise and taking the time to work with me and teach me. I would like to thank Dr. John Oshinski for your MR expertise and help on data quality analysis. I would like to thank all members of my thesis committee including the above, Dr. Don Giddens, Dr. Diego Martin, and Dr. John Oshinski, as well as Dr. Ray Vito and Dr. Thomas Heffron whose guidance and suggestions were critical. I would like to thank Dr. Puneet Sharma for his invaluable help in obtaining my MR data.

Thank you to everyone in the Cardiovascular Lab: Amanda, Jin Suo, Annica, Yan, Binjian, Massimiliano, Yi, Sungho and Venkata. Thank you for all the knowledge you have shared. It has been a pleasure working with you and I wish you all the best.

I would also like to thank Dr. Kevin Johnson and Dr. Khalil Salman for your help on image acquisition and processing. I would like to thank those in the Yoganathan Cardiovascular Fluid Mechanics Laboratory for your technical help: Kartik, Diane, Dr. Prasad Dasi and Dr. Philippe Sucosky.

Thank you to Lisa Cox, Joanne Wheatley and Tiffany Easter for all of your administrative support. Without you I never would have had meeting times or meeting places. I would also like to thank Steven Marzec for his invaluable computer and technical assistance.

I would like to thank all of my volunteers for without you this study would not have been possible.

To my husband, P.J., I thank you for your love and support throughout these years. You have calmed me down when stressed and kept me going when necessary. To my son, Noah, you are the light of my life and I love you very much. I wish for you all the educational opportunities you desire. To my parents, thank you for supporting me through all my 24 years of education! Without your love and nurturing from the beginning I would not have been able to achieve what I have achieved. To my brother and sister, Scott and Sarah, you have taught me many lessons throughout the years and your support has also been invaluable. I would also like to thank all of my family and friends who have supported me on this journey. Even across miles the warmth of your love can be felt.

TABLE OF CONTENTS

LIST OF TABLES

LIST OF FIGURES

SUMMARY

Cirrhosis is a leading cause of death in the United States and has severe and costly complications. Because of the clinical significance of cirrhosis, it is important that noninvasive methods be developed to detect cirrhosis early and to monitor its progression with advancing liver disease. Previous studies on portal venous hemodynamics have been performed mainly with ultrasound with mixed results. Magnetic Resonance Imaging offers several advantages over ultrasound including acquisition of both high quality anatomical and hemodynamic information.

Phase-Contrast MR was used to gather velocity data for the portal venous system. Methods were developed to perform registration, segmentation and isolation of the portal vein geometries and velocity data. Computational Fluid Dynamics was also employed to further investigate the flow within the portal vein, beginning with idealized models and then subject specific models.

The idealized models provided a simple initial adaptation of the CFD methodology and provided some insights that were carried forward to the normal subjects and patients such as parabolic-like velocity profiles, streamlining in the portal vein and quasisteady flow assumption.

The data set included nine normal subjects and four patients. Velocity data for the portal vein, superior mesenteric vein, splenic vein and the right or left portal vein were acquired in varying numbers for both data sets. Even with the limited number of subjects a few parameters were significant. Patients with cirrhosis had a significantly increased portal vein area and a significantly decreased average velocity per liver volume and velocity variance. Patients with cirrhosis had a significantly

increased splenic vein area and average flow rate per liver volume. While these results are preliminary due to small sample size, they are promising and require further investigation and more subjects including varying stages of disease.

CHAPTER I

INTRODUCTION

Cirrhosis of the liver is one of the leading causes of death in the United States. Consequences of cirrhosis are portal hypertension (a result of altered hemodynamics, blood flow, in the liver), enlarged spleen, ascites (fluid accumulation in the abdomen), and varices (dilation of intra-abdominal veins that can lead to bleeding and death) [2]. Because of the clinical significance of cirrhosis, it is important that noninvasive methods be developed to detect cirrhosis early and to monitor its progression with advancing liver disease. There is little detailed hemodynamic knowledge available for the normal liver, and therefore departures from physiological hemodynamics that arise from disease are difficult to interpret.

Previous hemodynamic studies have used a variety of imaging methods; Doppler ultrasound, venography, angiography, scintiphotosplenoportography, and percutaneous transhepatic portography [9, 10, 13, 18, 20, 22, 24, 40, 43]. The modalities of Magnetic Resonance Imaging (MRI) and Phase Contrast MRI, a method developed for quantitatively measuring blood flow, have been used limitedly. These methods have the advantage of being completely noninvasive and of providing both anatomical, including vessel area, and hemodynamic information and thus may yield more precise evaluation for improved assessment of cirrhosis in the clinical setting.

This research will examine the use of MRI to investigate normal and diseased portal vein hemodynamics and to potentially identify characteristics for use in clinical diagnoses. A companion technology, computational fluid dynamics (CFD), will be employed to develop computational models of portal vein hemodynamics so that a more thorough understanding of normal and diseased states may be achieved.

Overall Hypothesis: The hemodynamic characteristics of the portal venous system are indicators of liver function, liver disease and progression, specifically of cirrhosis, and can be utilized to improve the clinical evaluation and management of patients.

Specific Aim 1: Develop an idealized, but physically representative model of the portal venous system to preliminarily investigate portal venous flow and study the effect of boundary conditions and geometric shape on flow patterns.

Specific Aim 2: Characterize hemodynamics in the normal adult portal venous system.

Specific Aim 3: Characterize hemodynamics in the portal venous system in patients with cirrhosis and portal hypertension.

Specific Aim 4: Identify differences in hemodynamic characteristics of the portal venous system between normal and diseased subjects.

The **main purpose** of this work is to understand portal venous hemodynamics in greater detail than is currently known and to investigate the potential of relating this knowledge to the progression of liver disease. If a relationship between hemodynamic characteristics and disease can be developed using the methodology, this knowledge may ultimately be used to non-invasively determine stages of cirrhosis; assess the risk of portal hypertension, ascites, and varices; develop and evaluate accurate treatment plans; and possibly improve the index used for transplant wait list status. Thus, this research may set the stage for a number of translational clinical investigations of liver-related diseases.

CHAPTER II

BACKGROUND AND SIGNIFICANCE

2.1   Liver Anatomy and Physiology

The liver is the largest solid organ and gland in the body weighing approximately 1500 grams. It is located predominantly in the upper right quadrant of the abdomen. The liver appears glossy and is red in color, wrapped in a fibrous capsule. The anterior surface is triangular in shape and contains two main lobes, the right and left (Figure 1). There are also two accessory lobes, the caudate and quadrate, that are visible on the posterior surface of the liver. Ligaments connect the liver to the diaphragm and abdomen wall, providing stability [4].
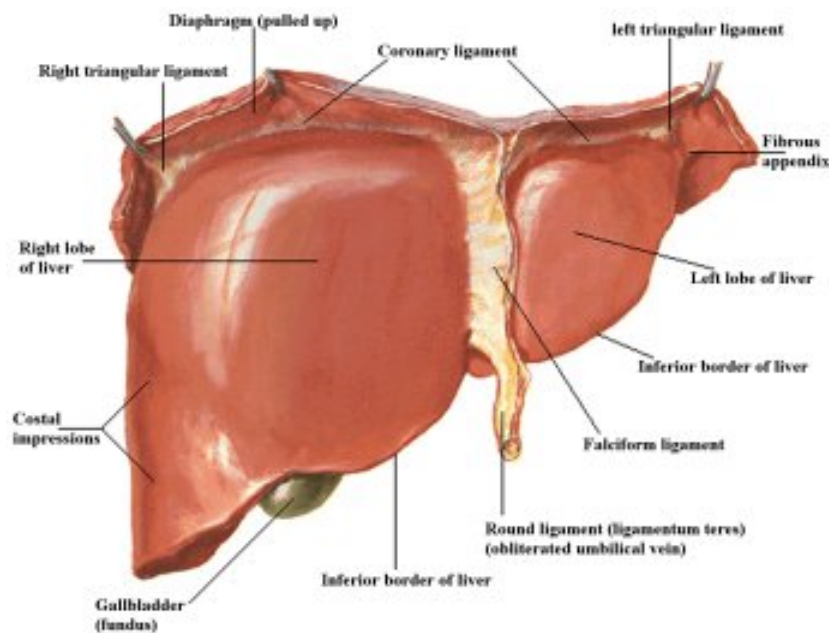
Figure 1: Anterior View of Liver [5]

The structural unit of the liver is the lobule, which is formed by the connective tissue capsule (Figure 2). The hepatic lobule is roughly hexagonal in shape and is

separated from other lobules by the interlobular septum. There are about one million lobules in the liver each with a diameter of 0.5-2mm [5]. The lobule is made up of plates of hepatocytes that radiate from a central vein in the center. At the vertices of the lobule is an area called the portal triad (Figures 2 & 3), which contains an artery, vein, and bile duct [5]. While the lobule is the structural unit, the acinus is the functional unit. The acinus is an elliptical mass of hepatocytes with zones that radiate out from the vascular system (Figure 3). Zone 1 is closest to the vasculature while zone 3 is farthest away [5].
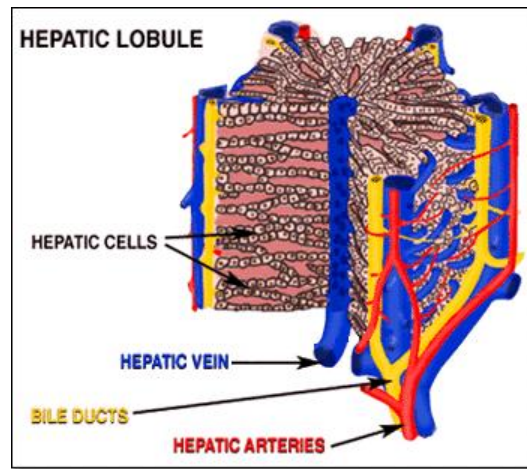
Figure 2: Hepatic Lobule [4]
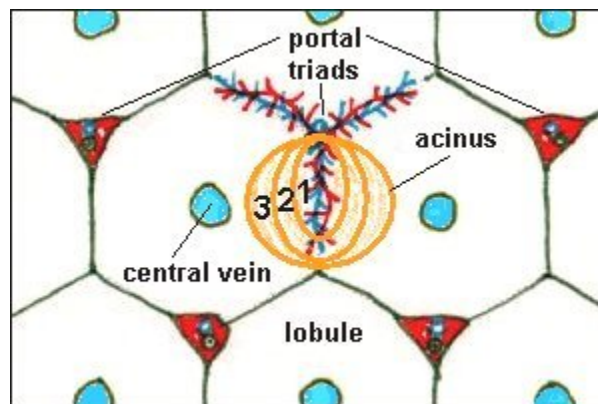
Figure 3: The Acinus [5]

The liver receives blood from two sources, the hepatic artery and the portal vein. The blood from the portal vein supplies 80% of the liver's blood and contains nutrients that were absorbed from the digestive tract [28]. The liver vasculature can be seen in Figure 4. Sinusoids are low pressure vascular channels which receive blood at the portal triad region from terminal branches of the portal vein and hepatic artery (Figure 5). The blood then passes through the sinusoid into the central vein where it empties into the hepatic vein and eventually the inferior vena cava. There is only one direction of flow, with no recirculation.

Vena Cava

Hepatic Vein

Celiac Trunk off Aorta

LIVER

Stomach

Gall Bladder

Spleen

Portal Vein

Superior Mesenteric Vein

Hepatic Artery

Splenic Vein
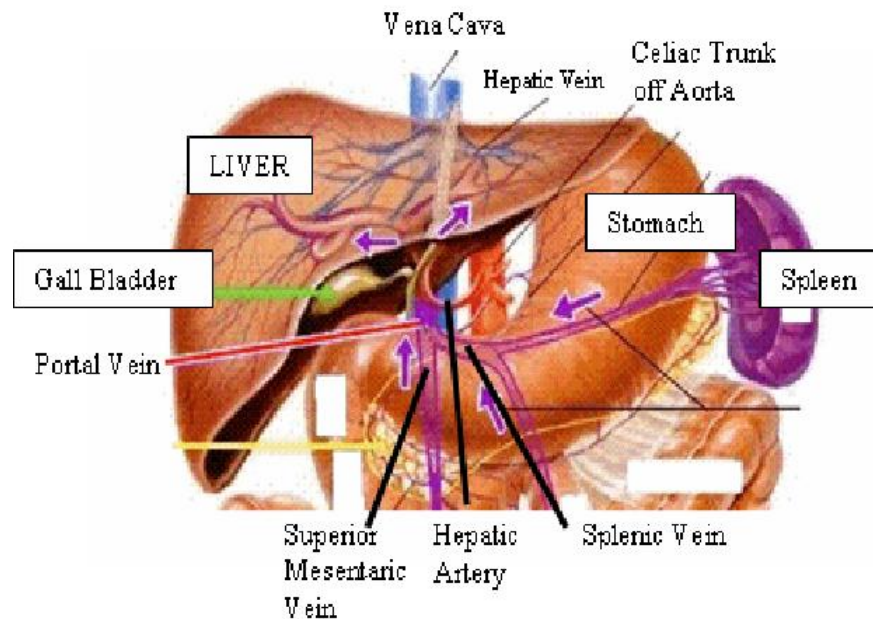
Figure 4: Liver Vasculature [4]

There are several sinusoidal lining cells. The first are endothelial cells, which are unlike other endothelial cells. They have fenestrae or holes, which are about 1000A in diameter that control the interchange between the blood and the perisinusoidal space. The endothelial cells are unique because they lack a basal lamina. Kupffer cells lie on the luminal surface of the endothelium. They are monocyte derived cells that engulf pathogens, cell debris, and damaged blood cells. They can also present antigens that

will stimulate an immune response. Kupffer cells also store iron, some lipids, and heavy metals. Hepatic Stellate cells (HSC), also known as Ito cells and fat storing cells, have many functions. They synthesize apolipoproteins and prostaglandins, produce cytokines and express membrane receptors, synthesize the extracellular matrix, and are involved with matrix degradation. HSCs have the ability to contract the sinusoid, regulating sinusoidal diameter and tone. After an injury HSCs can be activated causing excessive proliferation [5]. The last group of cells is the Pit cells, which are natural killer cells that fight against tumor cells and viral infections [8]. The hepatocytes perform the metabolic, endocrine, and secretory functions of the liver. They are bipolar cells with the apical side facing the sinusoid and the lateral sides joining other hepatocytes and forming bile canaliculi [5]. The sinusoid and sinusoidal lining cells can be seen in Figure 5.
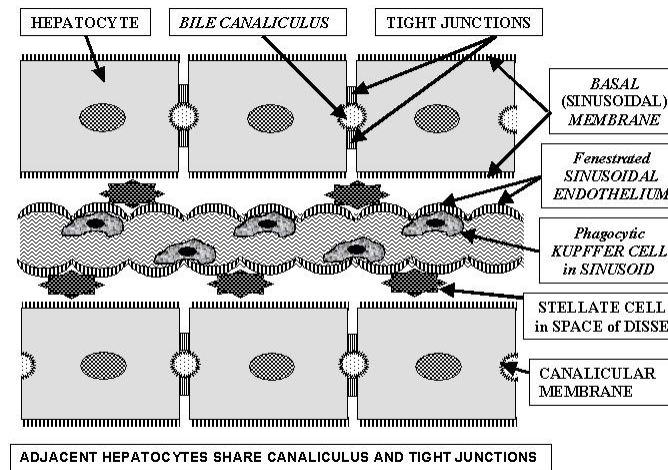
Figure 5: Sinusoid [2]

The liver has three main categories of functions; metabolic regulation, hematological regulation, and bile synthesis and secretion. The general function of the metabolic regulation is to remove and store excess nutrients and correct deficiencies, depleting stored reserves and synthetic activities. The liver is involved in carbohydrate

6

metabolism by stabilizing blood glucose levels. The liver manages lipid metabolism by regulating the circulating levels of triglycerides, fatty acids, and cholesterol. The liver can also synthesize lipoproteins, cholesterol, and phospholipids. The liver removes excessive amino acids from circulation and uses them to synthesize proteins or converts them to lipids or glucose for storage. The liver is responsible for removal of waste products from the blood, which are then inactivated and stored or excreted. The liver performs deamination, which produces ammonia that is then excreted by the kidneys. Vitamins A, D, E, K, and B12 are absorbed and stored in the liver until needed. Hemoglobin is processed for its iron content, which is converted to ferritin and stored. Last, the liver removes and breaks down circulating drugs. How fast the liver does this is taken into account in the dosage of medicines [28].

The general function of the liver's hematological regulation is to regulate and filter the blood. As mentioned previously, Kupffer cells have the ability to engulf cells and debris in the blood and present antigens, stimulating an immune response. The liver is responsible for synthesizing and releasing into circulation blood plasma proteins such as albumins, transport proteins, clotting proteins, and compliment proteins. Circulating hormones are also removed in the liver, which is the primary site for absorption and recycling of epinepherine, norepinephrine, insulin, thryroid hormones, and steroid hormones. Antibodies are absorbed and broken down releasing the amino acids to be recycled. Toxins that are lipid soluble are absorbed and stored in the liver forever, such as DDT, while other toxins are removed and broken down or excreted in bile [28]. Fluid and proteins flow from the blood into the perisinusoidal space which collects into lymphatic capillaries. Half of the lymph is formed in the liver [5].

The last function of the liver is bile synthesis and secretion which will be discussed in detail in the biliary system.

2.2 Biliary System

The biliary system consists of organs and ducts that are involved in the production and transportation of bile (Figure 6). The function of the system is to remove organic anionic compounds from circulation and aid in digestion. Bile is a greenish yellowish fluid that consists of waste products, cholesterol, water, small amounts of ions, bilirubin and bile acids [3]. The first step in the bile formation process is the uptake of organic anionic compounds by the hepatocytes. Organic anionic compounds include organic anions such as bilirubin and bromsulfophthalein (BSP), and bile acids [8].
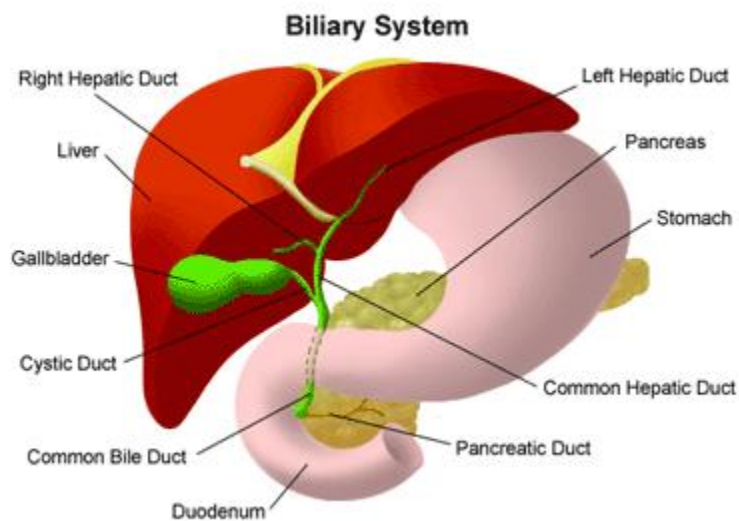
Figure 6: Biliary System [3]

Bile acid production is a major pathway for removing cholesterol. There are two types of bile acids, cholic acid and chenodeoxycholic acid. Once synthesized they are secreted into the bile canaliculi, which is emptied into the small intestine where the bile acids help with fat digestion. They are reabsorbed and again taken up by the liver. This is called enterohepatic recirculation (Figure 7); 95% of bile acids undergo this process and are recycled 6-10 times daily [2].

Another major component of bile is bilirubin, which is the end product of the degradation of the heme group from hemoproteins. Bilirubin is toxic but is rendered
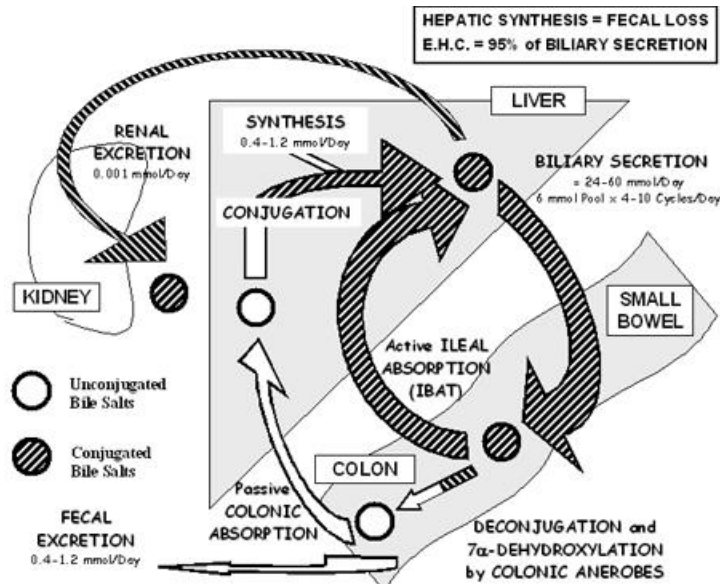
Figure 7: Recycling of Bile Acids [2]

harmless by binding to albumin and rapid excretion by the liver. It is taken up by hepatocytes by facilitated diffusion that requires chlorine. Once inside the cell, bilirubin must be conjugated if it is not already, and then it is secreted into the bile canaliculi [8].

The bile canaliculi (Figure 8) are half tubules that are carved out of the hepatocyte surface. They are formed by tight junctions which provide a barrier for leakage into and out of the canaliculi. The bile canaliculus contains actin and microvilli and is supported by a complex cytoskeleton [8].
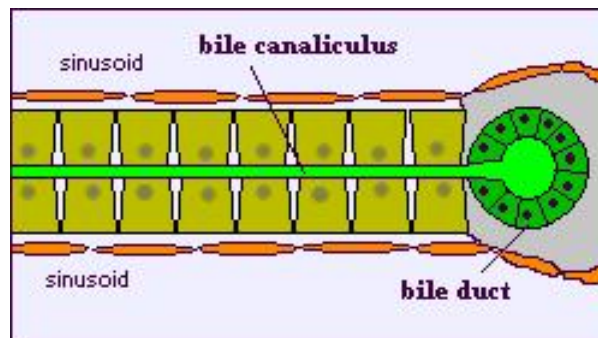
Figure 8: Bile Canaliculus [5]

Bile formation is initiated by active secretion of bile acids and other organic anionic compounds. There are two components. The first is the bile acid dependent fraction which is related to secretion via the ATP-dependent bile salt export pump (BSEP). The second is the bile acid independent fraction related to secretion of other organic anions by ATP dependent Multi-Drug Resistant Protein 2 (MRP2). Both cases generate osmotic gradients that induce water flow from the sinusoid [2]. Control of bile formation and flow is dependent on the supply of bile acids, which is related to the rate of bile acid recirculation. Vagal stimulation is also a weak stimulant. There are several gastrointestinal hormones involved such as cholecystokinin (CCK), a weak stimulant, gastrin, a weak stimulant, secretin, a strong stimulant for ductal bile formation, glucagons, a modest stimulant, and somatostatin, a strong inhibitor [2].

After the bile is secreted into the bile canaliculus, it is collected in a system of ducts that lead to the right and left hepatic ducts and then to the common hepatic duct. The hepatic duct then joins the cystic duct from the gall bladder to form the common bile duct, which connects to the duodenum through the sphincter of Oddi (Figure 9). When bile is not needed, it is diverted into the gall bladder. After food is eaten, the gallbladder contracts releasing the bile [3]. Contraction of the bile canaliculi involves signaling between cells via gap junctions. The contractions occur in peristaltic waves at about 1.5-3 contractions per minute [8]. As the bile moves along the ducts its composition is changed by the epithelial cells lining the duct, the cholangiocytes. The changes include altering the water and electrolyte content.
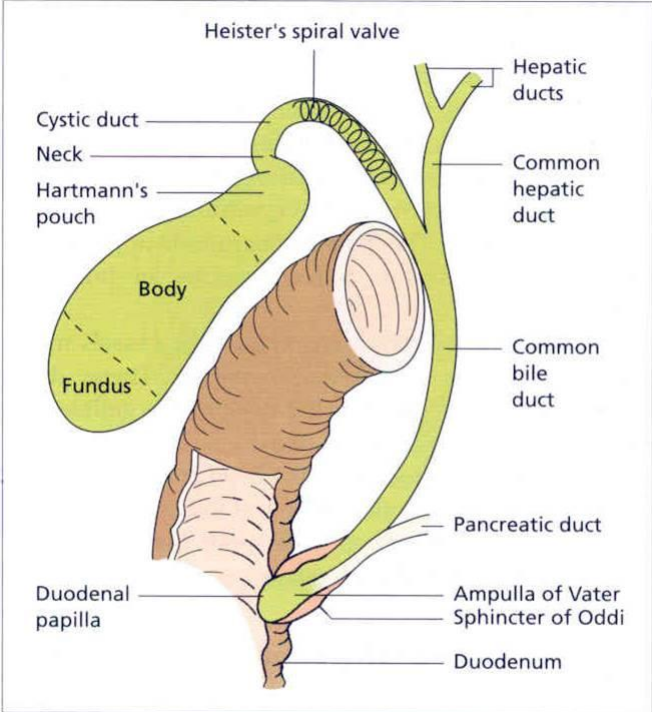
Figure 9: Extrahepatic Bile Ducts [36]

2.3 Liver Disease

Cirrhosis is one of the leading causes of death in the United States and is the final common histological pathway for a wide variety of liver diseases [2]. Cirrhosis is a diffuse hepatic process characterized by fibrosis and the conversion of normal liver architecture into structurally abnormal nodules [36]. Common causes of cirrhosis include Hepatitis C (26%), Alcoholic liver disease (21%), Hepatitis C plus alcoholic liver disease (15%), Cryptogenic causes (18%), Hepatitis B (15%), and misc (5%) [36].

A serious complication relating to cirrhosis is portal hypertension, which is high blood pressure in the portal vein. Portal hypertension is caused by altered hemodynamics in the liver. One alteration is increased resistance to flow of blood through the liver and a second is a large increase in the amount of blood trying to enter the liver from the splanchnic circulation [36]. A normal hepatic venous pressure gradient is 3-6 mmHg. Above that range is portal hypertension with a threshold for ascites at 8 mmHg and another threshold for varices at 12 mmHg [36].

Causes of increased resistance of blood flow into the liver can be presinusoidal, intrasinusoidal, or postsinusoidal (Figure 10). Presinusoidal causes include blockage of the main portal vein or annular fibrosis of intrahepatic portal venules. Intrasinusoidal causes are mainly due to cirrhosis and include subendothelial deposition of collagen in the space of disse, distortion from regenerating nodules, constriction due to synthesis of NO and increased vasocontrictors (endothelin), and impaired hepatic removal and increased consumption of endotoxins or compression by tumors. Postsinusoidal causes include veno-occlusive disease, obstruction of small hepatic venules, Budd Chiari Syndrome, obstruction of the main hepatic vein, and severe right side congestive heart failure [36].

Increased splanchnic flow can be caused by a hyperdynamic circulation state found in cirrhosis. Cirrhosis brings increased synthesis of NO, increased systemic glucagon concentration, decreased sensitivity to vasoconstrictors and increased cardiac output
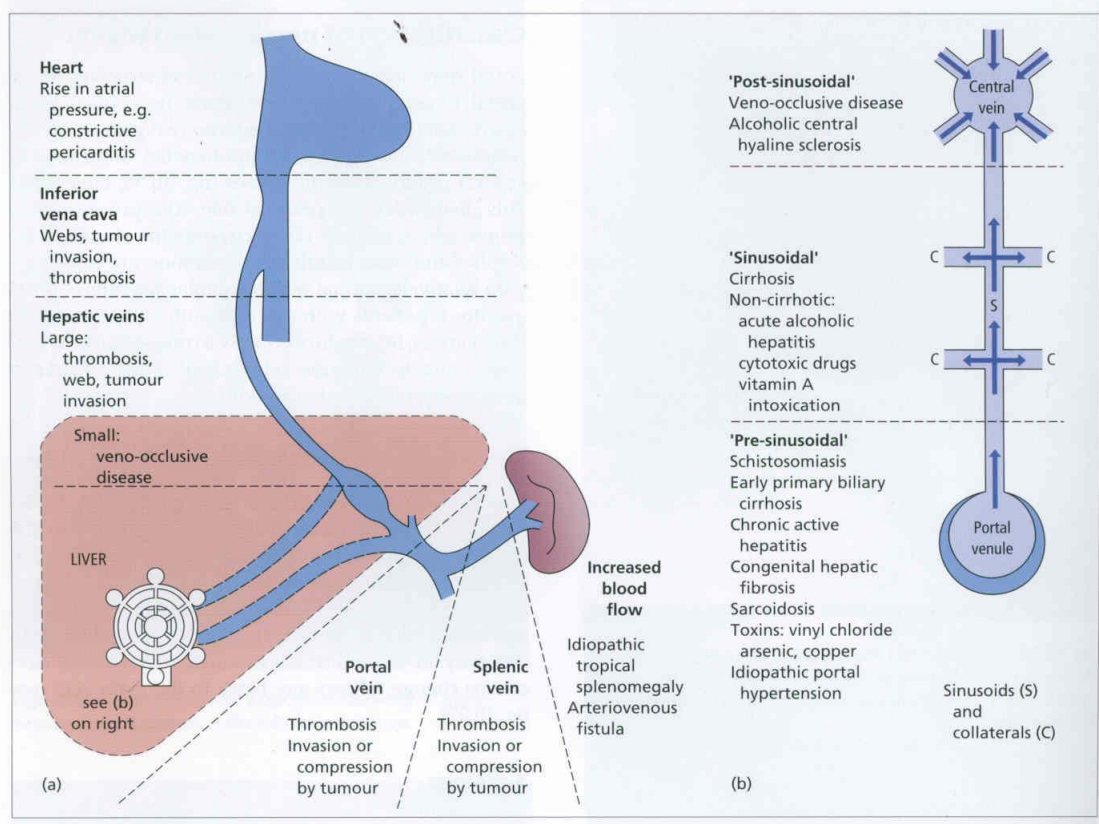
Figure 10: Causes of Portal Hypertension [36]

[36].

Consequences of portal hypertension (PH) include enlarged spleen, portal venous collaterals to systemic veins bypassing the liver (varices), accumulation of fluid in the peritoneal cavity (ascites), and edema [36]. Common varices are gastroesophageal, retroperitoneal, periumbilical, rectal, and diaochragmatic-perisopheageal (Figure 11) [36]. Variceal hemorrhage is the most common complication associated with PH. Of patients with cirrhosis, 90% develop varices, 30% of varices bleed, and the first epidsode of variceal hemorrhage carries an estimated 30-50% mortality rate [36].

Treatment for PH includes decreasing intrahepatic vascular resistance using NO precursors and blocking angiotensin II and endothelin receptors. Another treatment is to constrict splanchnic arterioles to decrease portal venous flow using beta-adrenergic
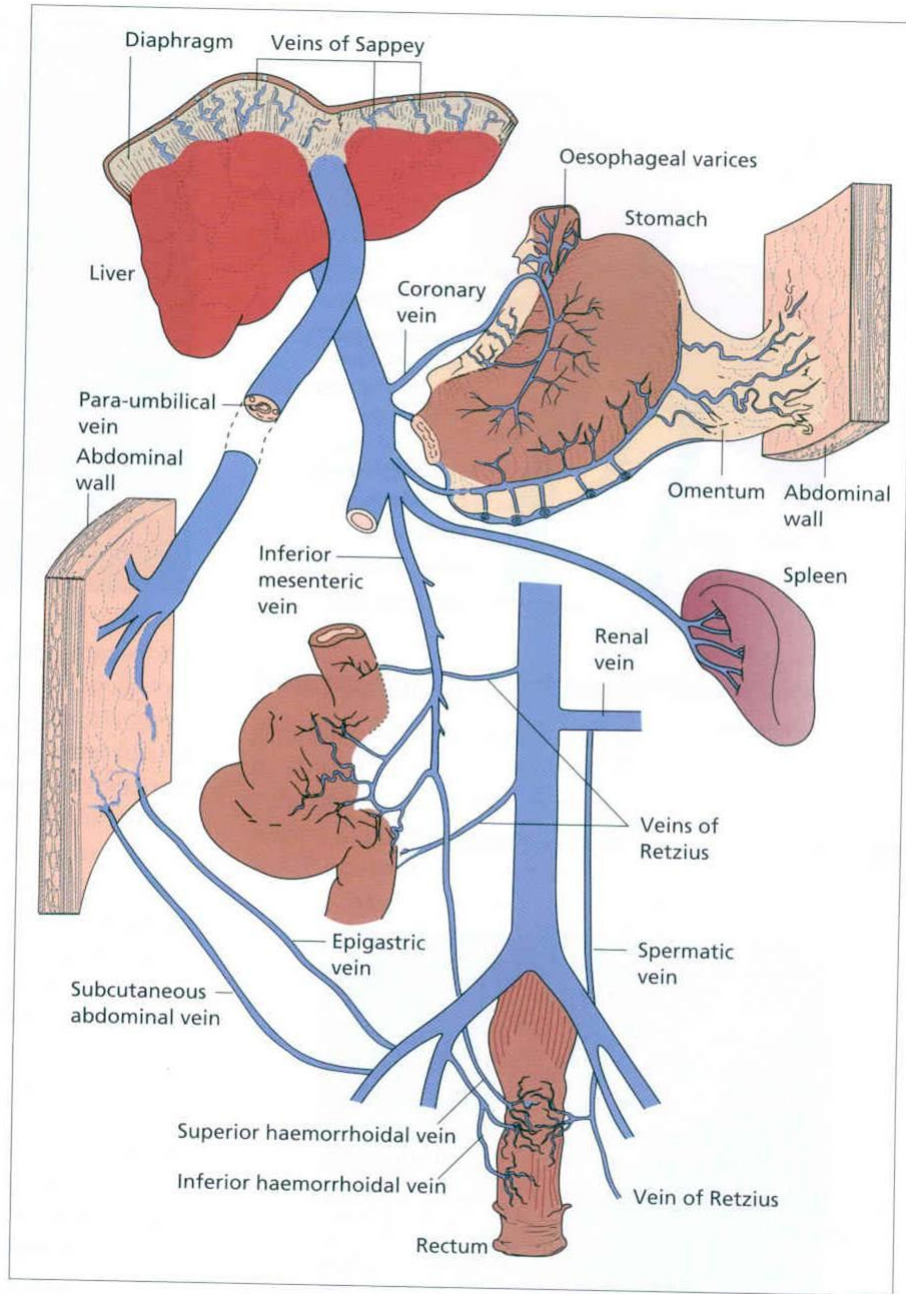
Figure 11: Common Varices [36]

antagonist and splanchnic selective vasopressin analogue. A third option is to inhibit splanchnic vasodilation by decreasing NO synthesis by inhibiting eNOS, using endo-toxin formation in the gut and inhibiting CCK, VIP and glucagon receptors. A fourth treatment option is to decrease intravascular volume using diuretics and restricting sodium. The last treatment option is to decompress the portal system by diverting blood to the systemic circulation using a surgical splenorenal or porto-caval shunt or the transjugular intrahepatic porto-systemic shunt (TIPS) (Figure 12) [36].
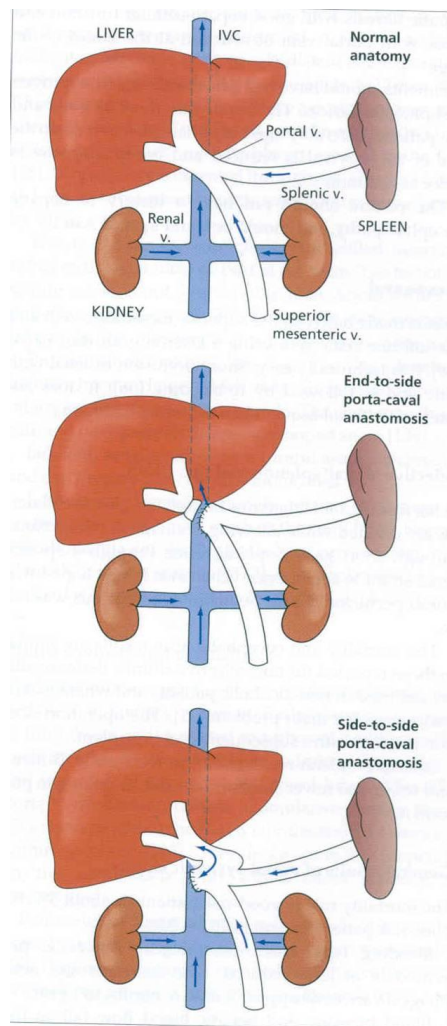
Figure 12: Liver Shunts [36]

2.4   Liver Transplantation

Over the past several decades, the need for livers has increased more rapidly than the availability of livers as illustrated in Figure 13. The next figure gives the number of people on the waiting list for various organs as of April 21, 2008 (Figure 14). The data were provided by the United Network for Organ Sharing (UNOS). While the kidney accounts for most of the people on the waiting list (77%), the liver has the second largest number of people (17%). The mortality of the waiting list has increased 575% from 1988 to 1997 [7].
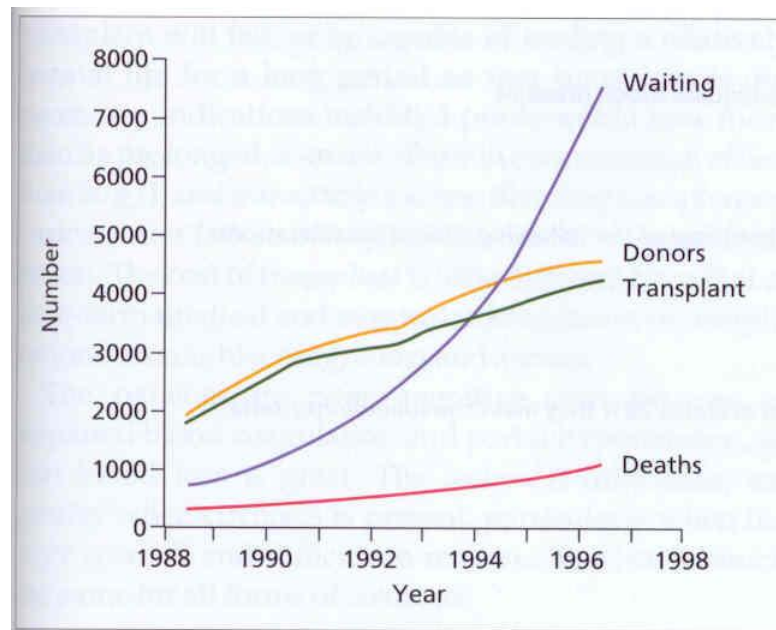
Figure 13: Available vs. Waiting Livers [36]
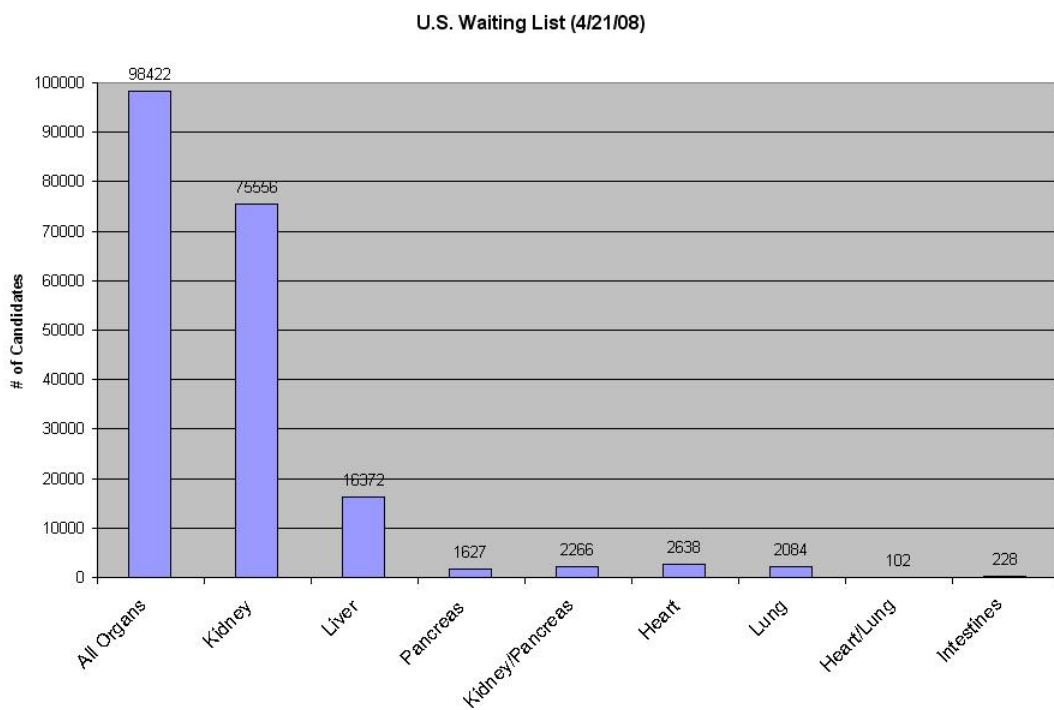
Figure 14: U.S. Waiting List by Organ [7]

Candidates for transplantation include cirrhosis, primary metabolic disease, acute liver failure, malignant disease, cholestatic liver disease, and others. Criteria for transplantation are partially based on the Child-Pugh Scoring System (Figure 15) which takes into account encephalopathy, ascites, bilirubin and albumin levels, prothrombin time, and type of disease. UNOS's criteria places candidates into four statuses, Status 1 is top priority and then 2A, 2B, and 3 [36].

Child–Pugh scoring system to assess severity of liver disease

	Points		
	1	2	3
Encephalopathy (grade)	None	1–2	3–4
Ascites	Absent	Slight or controlled by diuretics	At least moderate despite diuretic treatment
Bilirubin (mg/dl)	<2	2–3	>3
Albumin (g/dl)	>3.5	2.8–3.5	<2.8
Prothrombin time (seconds prolonged)	<4	4–6	>6
Or INR	<1.7	1.7–2.3	>2.3
For primary biliary cirrhosis, primary sclerosing cholangitis or other cholestatic liver diseases: bilirubin (mg/dl)	<4	4–10	>10

Figure 15: Child-Pugh Score [36]

Donors must be between the ages of 2 months and 60-65 years of age. The livers are matched blood type specific, but can be mismatched in emergency situations. The donor livers are tested for Hepatitis B and C viral markers, CMV antibodies, and HIV [36].

There are four different types of liver transplant surgeries; Orthotopic, Piggyback, Split Liver, and Living Donor. Orthotopic liver transplantation takes an average of 8 hours operative time. Before this however, the donor liver is harvested. First, the inferior vena cava (IVC) is cut above the liver and then below the liver. An aortic patch is created that includes the celiac trunk and the superior mesenteric

artery (SMA). The celiac trunk and mesenteric artery are separated unless there are accessory hepatic arteries stemming from the SMA. The portal vein is cut about 1-2 cm. from its origin and the bile duct is also cut. The common, external, and internal iliac arteries and veins are also harvested in case grafts are necessary [30]. In the recipient, the liver is removed with the attached portion of the IVC. Some patients that can not withstand having their IVC and their portal vein clamped are put on veno-venous bypass. Venous blood from the leg and portal vein are rerouted through a pump into an arm vein. The order of anastomoses is first the supra-hepatic IVC, intra-hepatic IVC, portal vein, hepatic artery, and last the bile duct (Figure 16).
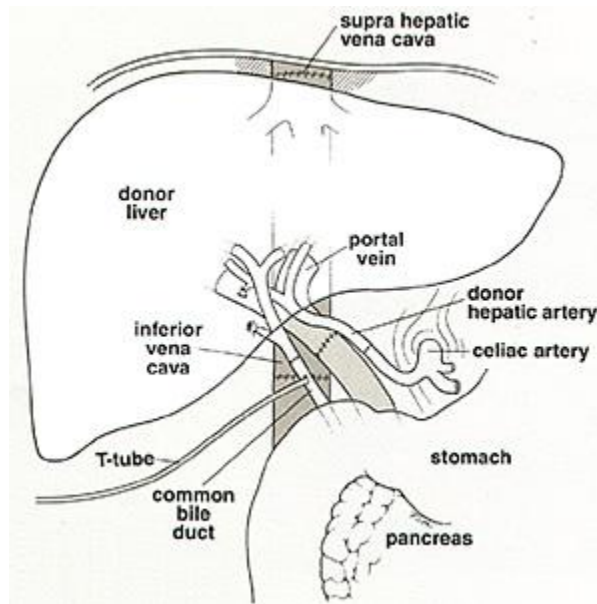
Figure 16: Anastomoses [6]

For both the hepatic artery and the portal vein, if there is not enough length, an artery or vein graft from the donor maybe used. It is important not to put the artery or vein in tension. Artery anastomoses are sometimes sewn with a growth factor patch that helps to prevent anastomotic strictures. When bile duct sizes are mismatched, the problem can be handled in three ways; one bile duct can be cut up the side expanding the opening, for two small bile ducts both ends will be cut to increase the diameter at the anastomoses, and with large to small bile ducts the

larger duct will be stitched over [30].

Before the bile ducts are anastomosed, a T-tube is put in place that allows bile to drain outside the body. This is a precaution because it is dangerous to have a build up of bile in the body. If the recipient's bile duct is too badly damaged, a roux-en-Y procedure can be performed where the intestines are transected and one end is attached to the donor bile duct while the other end is reattached to the intestines [30].

The next type of liver transplant is the piggyback transplant, in which the recipient's IVC is left intact. This recipient may then not require a veno-venous bypass. The top of the donor IVC is anastomosed to the recipient's hepatic vein stumps.

Due to the high demand for livers, donor livers have been split to give to two people. This was initially done in children where there is a restriction in how large the donor liver can be. The donor liver is usually separated into the right and left lobes as seen in Figure 17 [30].
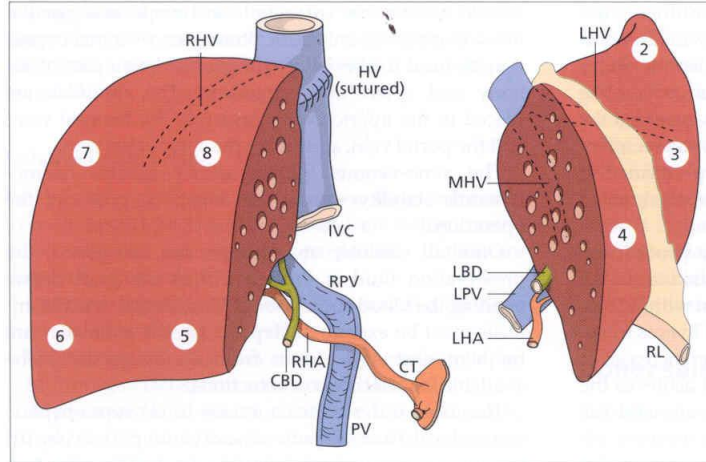
Figure 17: Split Liver Transplant [36]

A living donor can also donate a portion of their liver. The size of the recipient and the risk to the donor dictates which portion of the liver is donated. In typical adult donor, the left lobe with all the major vessels remains in the donor and the right side goes to the recipient [30]. The liver regenerates almost to pre-surgery mass

in eight weeks [6]. A typical living donor transplant can be seen in Figure 18.
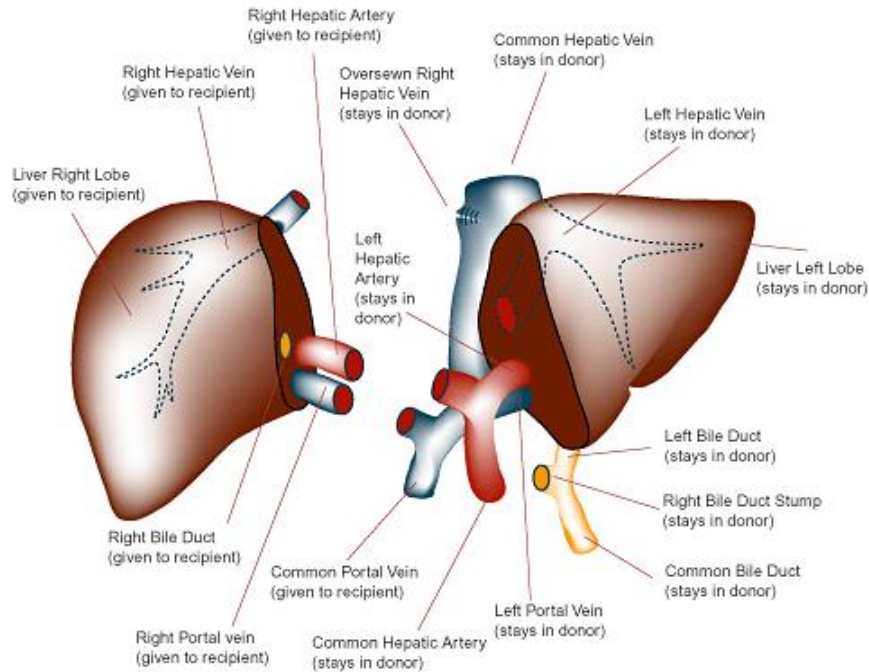
Figure 18: Living Donor Transplant [6]

Among the most feared complications of liver transplants are vascular complications which occur in about 2-25% of the cases [29] [17]. One such vascular complication is hepatic artery thrombosis (HAT), which is more frequent in children. This is possibly because of discrepancy in arterial size and lack of sufficient magnification to see the artery [17]. Thrombosis of the hepatic artery occurs more often than thrombosis of the portal vein or IVC. After transplant, the patient undergoes routine ultrasound for the first few days and then at longer intervals. HAT is often discovered this way and angiography is performed to confirm. Treatment options include thrombectomy and donor or synthetic arterial graft. But the main course of action is retransplantation (50%) [29] [37]. Hepatic artery stenosis (HAS) is also a problem which again is diagnosed via ultrasound and confirmed by angiography. Treatment includes revision of the anastomoses, repositioning of the artery, saphenous vein patch, and aortic interposition graft [30]. Reduction in hepatic artery blood flow can present as biliary

complications because the hepatic artery is the only source of oxygenated blood to the bile ducts. Detection and correction must occur within 24 hours or the biliary epithelium will die and the liver will fail [17]. Portal vein thrombosis is rare and has many causes such as twists and kinks in the vein, anastomotic strictures, excessive length of vein and many more. Treatment involves thrombectomy, venous graft, and anticoagulation therapy. Portal vein strictures occur at tight anastomoses, kinks and twists, or where external pressure is applied. Diagnosis is made using ultrasound and angiography. Treatment includes revision of anastomoses, transhepatic portal vein catheterization, and percutaneous transhepatic angioplasty with or without a stent placement. Hepatic vein stricture and thrombosis occur infrequently and are diagnosed by ultrasound and venography. Treatment includes percutaneous transhepatic angioplasty, stenting, and retransplantation [30].

Biliary complications are usually caused by anastomotic strictures, which develop mainly from technical complications. Treatment includes internal stent, percutaneous balloon dilation, reanastomoses, and if not previously done, a roux-en-Y anastomosis [30].

2.5 Significance

Based on the above knowledge, several conclusions can be drawn. The first is that the liver is an *important* organ that provides many life affecting functions. The second is that incidence of and deaths due to liver disease are *increasing*, and the gap between need and supply of transplantable livers is *increasing*. Thus, being able to more accurately diagnose and treat individuals as well as determine risk of complications such as portal hypertension and varices are of growing importance and will affect a growing number of patients.

CHAPTER III

PORTAL VENOUS HEMODYNAMICS

Previous studies have focused on the portal vein and its left and right branches, the splenic vein, the spleen, and splenic artery using a variety of methods including Doppler ultrasound (the most popular), limited MR, venography, angiography, scintiphotosplenoportography, and percutaneous transhepatic portography [9, 10, 13, 18, 20, 22, 24, 40, 43]. Measurements include velocity, flow rate, and area/diameter. Indices used for venous comparison include hepatic venous pressure gradient (HVPG), venous pulsatility index (VPI) and congestion index (CI) defined as:

$$HVPG = free\,hepatic\,venous\,pressure - wedged\,hepatic\,venous\,pressure \quad (1)$$

$$VPI = (max\,frequency\,shift - min\,frequency\,shift)/max\,frequency\,shift \quad (2)$$

$$CI = Vessel\,area/max\,velocity \quad (3)$$

Measurements used for arterial comparison include velocity, flow rate, and area/diameter. Indices used include the above congestion index as well as pulsatility index (PI) and resistive index (RI) defined as:

$$PI = (peak\,systolic\,velocity - end\,diastolic\,velocity)/\,mean\,velocity \quad (4)$$

$$RI = (peak\,systolic\,velocity - end\,diastolic\,velocity)/peak\,systolic\,velocity \quad (5)$$

3.1 Portal Vein

In general with cirrhosis, many studies that include US and MR measurements, have found a significant decrease in portal blood velocity (PBV) [9, 15, 20, 31, 32, 40, 43].

Zoli et al. [45] found that in diseased subjects a PBV of less than 10 cm/s characterized a shorter survival rate and that the prognostic significance of the Child-Pugh score increased when PBV was included. Nanashima et al. [32] and Taourel et al. [38] correlated PBV, measured non-invasively, to HVPG. Another study though, of 375 patients showed no correlation between PBV and HVPG [15]. Therefore the correlation is still inconclusive. Since HVPG is an invasive measurement, correlation to a non-invasive parameter may eliminate the need for the invasive test illustrating the importance of such as correlation. Nanashima et al. [32] also showed a low correlation between MR PBV measurements and US PBV measurements, which further supports the use of MR to measure PBV.

The difference in portal blood flow (PBF) between normal subjects and patients remains unclear. Kayacetin et al. [20] and Vyas et al. [40] found a significant decrease in PBF in patients, but Yin et al. [43] found a significant increase in PBF. Several other studies found no significant difference between the two groups [9,15,22,31]. With cirrhosis the resistance to flow in the liver increases, but flow from the splenic vein increases which can maintain normal PBF even under portal hypertensive conditions. Again there are mixed findings on the correlation of PBF to HVPG [15, 38]. The ratio of SV flow to PV flow was found to increase and in some cases doubled with cirrhosis [22,43]. Since the portal vein connects two collateral beds, it is hypothesized that the flow within the portal vein would be steady, however, Gallix et al. [14] found that in healthy individuals the portal vein had a small venous pulsatility index (VPI) and another study showed an increase in VPI in patients [21]. Burkart et al. [12] showed a significant correlation between MR and US PBF measurements, however this was with a limited number of subjects. Error is expected in the US measurement of flow since the area of the vessel is not directly measured but calculated from a diameter measurement using the area equation for a circle. In some cases the PV cross-section may not be a perfect circle.

In general with cirrhosis, the portal vein diameter increases [9, 20, 44]. However, other studies found no significant difference in diameter between normal subjects and patients [22, 33]. PV diameter was also correlated to liver fibrosis by Lu et al. [25]. The significant increase in PV congestion index (CI) is well supported by the literature [9, 20, 22, 43]. However, the clinical usefullness of the parameter is still unknown. Flow data for the portal vein can be found in Tables 1 and 2.

Table 1: Data for Portal Vein in Healthy Subjects

Parameter	Yin 2001 [43]	Kutlu 2002 [22]	Kayacetin 2004 [20]
Velocity (cm/s)	30.4 ± 7.2^a	19.6 ± 4.4	12.6 ± 2.9
Flow Rate (ml/min)	1040 ± 190	1109 ± 278	1208 ± 184
CI	0.03 ± 0.001	0.05 ± 0.016	0.03 ± 0.01
Method	Doppler US	Doppler US	Doppler US

[a]Cross Sectional Velocity Maximum

Table 2: Data for Portal Vein in Patients

Parameter	Yin 2001 [43]	Kutlu 2002 [22]	Kayacetin 2004 [20]	Vyas 2002 [40]
Velocity (cm/s)	14.9 ± 3.1^a	17.3 ± 9.5	7.5 ± 6.5	5.3 ± 1.1
Flow Rate (ml/min)	1361 ± 501	1361 ± 1337	755 ± 355	380 ± 103
CI	0.14 ± 0.06	0.076 ± 0.044	0.11 ± 0.6	
Method	Doppler US	Doppler US	Doppler US	Doppler US

[a]Cross Sectional Velocity Maximum

3.1.1 Streamlining of PV Flow

Physicians have hypothesized that the blood flowing from the SMV and SV preferentially distribute into the RPV and LPV, respectively. This theory developed due to the high predilection of the right lobe of the liver for disease. Since the SMV blood is coming from the digestive tract it can carry toxins such as alcohol and other infectious agents. This could explain the high incidence of cirrhosis in the right lobe.

Tsukuda et al. [39], using MR and blood tagging, matched the signal in the PV to its contributing vessel. Before a meal, the SV was the major contributor to the PV signal and flowed in the center of the PV in the majority of subjects. The SMV flow was split bilaterally. While the tagged blood was not directly imaged in the PV branches (some of the vessels were captured with the PV), in a few example subjects there was no dominant contributor to the RPV. After a meal, when the SMV flow was thought to increase, the SMV flow dominated the PV signal and pushed the SV flow to the left side. The SMV also became the clear contributor to the RPV. In both cases there was still little mixing of the two flows agreeing with the streamline effect in the PV. This study demonstrates that when toxins would be at their highest levels, after a meal, the SMV is the major contributor to the RPV. However under fasting conditions the SMV contribution to the RPV may be subject specific and could be genetic.

3.2   Right Portal Vein

Cirrhosis is located preferentially on the right side of the liver and therefore the resistance in that lobe would increase and one would expect the RPV velocity and flow to decrease. These decreases have been shown to be significant when compared with normal subjects [22,23,43]. Kutlu et al. [22] demonstrated a significant decrease in diameter and Yin et al. [43] an increase in congestion index. The ratio of RPV flow to PV flow was found to decrease possibly indicating changes in flow division or just a decreased flow in general [22]. An increase in the bluntness of the velocity profile as calculated by a velocity profile shape parameter was seen by Yin et al. [43]. Flow data for the right portal vein can be found in Table 3.

3.3   Spleen and Splenic Artery

Spleen enlargement is a hallmark of portal hypertension and cirrhosis. Shah et al. [35] related spleen volume to portal vein cross sectional area and portal vein blood flow

Table 3: Data for Right Portal Vein

Parameter	Healthy		Cirrhotic	
	Yin 2001 [43]	Kutlu 2002 [22]	Yin 2001 [43]	Kutlu 2002 [22]
Velocity (cm/s)	13.1 ± 2.8^a	20.1 ± 3.8	9 ± 2.8^b	15.7 ± 5.9
Flow Rate (ml/min)	407 ± 128	666 ± 168	365 ± 182	470 ± 473
CI	0.07 ± 0.03	0.028 ± 0.075	0.1 ± 0.5	0.033 ± 0.02
Method	Doppler US	Doppler US	Doppler US	Doppler US

[a]Cross Sectional Velocity Maximum
[b]Cross Sectional Velocity Maximum

volume. Bolognesi et al. [9] found that the splenic artery resistive index and pulsatility index significantly increased in cirrhosis.

3.4 Splenic Vein

Due to spleen enlargement, the flow from the splenic vein is usually increased. No conclusions can be drawn about the velocity since it has been found to be significantly lower, significantly higher, and not significantly different in several studies [15, 20, 22, 43]. An increase in SV diameter was found with cirrhosis [15, 20, 22, 44]. There are reports of no significant change in the SV flow rate [15, 20] and in some cases an increase in flow [22, 43]. The congestion index was also found to increase [20, 22, 43]. Yin et al. [43] saw a significant increase in phasic flow patterns perhaps due to the increase in splenic artery flow. Flow data for the splenic vein can be found in Tables 4 and 5.

3.5 Correlation with Cirrhosis Grading

Based on the Child-Pugh score (Figure 15 on page 18), the hemodynamics of different grades of cirrhosis were compared. Child's A, B and C are based on scores of 5-6, 7-9, and > 9 respectively [1]. The portal flow velocity (8.5 *cm/s*) and portal blood flow (614.9 *ml/min*) were significantly decreased in Child's C cirrhosis (and Child's B [22])

Table 4: Data for Splenic Vein in Healthy Subjects

Parameter	Yin 2001 [43]	Kutlu 2002 [22]	Kayacetin 2004 [20]
Velocity (cm/s)	14 $\pm 3.6^a$	17.9 ± 4	23.9 ± 9
Flow Rate (ml/min)	318 ± 108	353 ± 136	447 ± 107
CI	0.05 ± 0.02	0.019 ± 0.054	0.04 ± 0.02
Method	Doppler US	Doppler US	Doppler US

[a]Cross Sectional Velocity Maximum

Table 5: Data for Splenic Vein in Patients

Parameter	Yin 2001 [43]	Kutlu 2002 [22]	Kayacetin 2004 [20]
Velocity (cm/s)	15.3 $\pm 3.9^a$	18.2 ± 4.8	12.8 ± 1.4
Flow Rate (ml/min)	839 ± 507	666 ± 397	652 ± 176
CI	0.08 ± 0.04	0.034 ± 0.019	0.08 ± 0.03
Method	Doppler US	Doppler US	Doppler US

[a]Cross Sectional Velocity Maximum

as compared to Child's A (velocity: 16.2 cm/s, flow volume: 1098.5 ml/min) [20]. There was also a significant increase in congestion index in the portal (0.14) and splenic (0.08) veins in Child's C as compared to Child's A (portal CI: 0.06, splenic CI: 0.04) [20].

3.6 Correlation with Esophageal Varices

The splenic artery RI and PI were higher in patients with cirrhosis and large EV than in those with cirrhosis and no or small EV [9]. Blood flow velocity in the left gastric vein increased as EV size increased [18]. There was a shift to an anterior dominant flow pattern at the left gastric bifurcation as EV size increased [18]. A higher percentage of patients with cirrhosis with hepatofugal flow verses hepatopetal had gastro-oesophageal varices (p<0.025) [11]. In patients with large EV the portal blood velocity and portal blood flow were significantly lower than in those without varices [24]. Those with large EV had a significantly higher max inner portal vein

diameter [24]. Those with EV has significantly greater splenic blood flow volume and splenic CI [20]. Among cirrhotics, those with EV has significantly increased mean flow volume in the splenic vein, mean SV/PT, and mean spleen size [43].

3.7 Correlation with Ascites

Those with ascites had significantly lower portal flow velocity and higher portal vein and splenic CIs [20]. In those with cirrhosis, portal vein blood flow, portal flow velocity, and gastric mucosal blood flow were significantly lower in those with ascites [40]. Renal RI significantly increased in those with cirrhosis and refractory or responsive ascites (higher in refractory ascites) [10]. In fulminant hepatic failure patients, found significantly lower portal flow velocity in those with ascites compared to those without [13].

3.8 MR Classifications of Cirrhosis

Traditional diagnosis of cirrhosis is by biopsy. Martin et al. [27] have shown that MR scaling of fibrosis and inflammation from contrast enhanced MR images correlate to histological scaling of the same measures thus potentially eliminating the need for a biopsy especially if combined with other liver function results and perhaps flow parameters.

3.9 Summary of Previous Research

This previous research illustrates significant changes in portal venous system hemodynamics with cirrhosis that vary across grades of cirrhosis as well as correlations with esophageal varices and ascites. The main parameters previously investigated were portal vein velocity, portal vein flow rate, and congestion index. However, the role of these parameters in a clinical setting is not well defined. The measurement method of choice in the previous research was Doppler ultrasound. Errors associated with US measurement include measurement of cross-sectional area (calculated by diameter

measurement), angle of insonation of the doppler beam with vessel, and high inter-observer variability. The method is also technically limited by patient habitus. The modalities of Magnetic Resonance Imaging (MRI) and Phase Contrast MRI have been used limitedly. These methods have the advantage of being completely noninvasive and of providing both anatomical and hemodynamic information and thus may yield more precise evaluation for improved assessment of cirrhosis in the clinical setting. There is little detailed knowledge available for normal portal venous hemodynamics, and therefore departures in physiological hemodynamics that arise from disease are difficult to interpret. The specific aims of this research are designed to examine the use of MRI to hemodynamically investigate normal and cirrhotic portal venous blood flow, with the objective of leading to the use of hemodynamic parameters in clinical diagnoses.

CHAPTER IV

METHODOLOGY

The methodologies employed in this body of work include magnetic resonance imaging (MRI), phase contrast- magnetic resonance imaging (PC-MRI), image processing and computational fluid dynamics (CFD).

4.1 Magnetic Resonance Imaging

MR scanners available for use include a Philips 1.5T Intera system and a Siemans Avanto 1.5T system located at the Emory Hospital and the Emory Clinic, respectively. Both were equipped with a body phased array coil.

4.1.1 MR Data Acquisition

The scans were completed with the subjects in a supine position. The session began with short reconnaissance scans using balanced fast field echo in 3 planes to locate the portal vein. The vessel geometry, including the superior mesenteric vein (SMV), splenic vein (SV), complete portal vein (PV), and the right and left portal vein branches (RPV & LPV), was scanned using balanced fast field echo or steady-state free precession technique (SSFP). The scans were breath-held contiguous slices of $3mm$ thickness with a resolution of at least 1.37x$1.37mm$.

4.1.2 PC-MR Data Acquisition

PC-MRI scans were performed during the same session as the geometry acquisition. ECG leads or a Peripheral Pulse Unit (PPU) were applied for cardiac vector cardiogram gating. Velocity data were gathered from breath-hold cardiac-gated PC-MRI using a segmented gradient echo sequence obtained from the mid-portal vein with the

imaging plane placed at 90 degrees to the long axis of the vein. PC-MRI scans were also done for the SMV and SV before the PV confluence and the RPV or LPV just after the PV bifurcation. Scan parameters were as follows; slice thickness 6-8mm, resolution of 1.17x 1.17mm, TR 24.2, TE 8, number of phases 16-20, and Venc 30-60 cm/s.

4.2 Image Processing

4.2.1 Vessel Image Segmentation

4.2.1.1 Preprocessing and Image Registration

It is necessary to preprocess the original MRI data and in some cases conduct image registration. Since scanning is completed during breath-holds, more than one breath-hold may be necessary to sufficiently capture the volume of interest. The subjects may move or not hold their breath in the same position for the subsequent scans causing misalignment between the last slice of the first scan and the first slice of the second scan. The effect of misalignment can be seen in Figure 19 by overlapping two adjacent slices.

To solve this problem, rigid registration is applied to two consecutive image series

Figure 19: Misalignment Before Registration

before image segmentation is performed. Since there is no significant nonlinear deformation rigid registration was used. Mean squared difference (MSD) is used as the image similarity measure:

$$MSD = \frac{1}{N} \sum_{i=1}^{N} (f(p_i) - g(p_i))^2,$$ (6)

where f, g are the intensities of pixel p_i in the two images to be aligned [19].

A translation (t_x, t_y) and a rotation by angle θ are applied to the second image in order to minimize the MSD between the first image (the last image in the first breath-hold series) and the second image (the first image in the second breathhold series). A gradient decent approach is used to solve for the parameters (t_x, t_y, θ) that minimize MSD. Figure 20 shows the result after registration, notice the overlapping has disappeared.

After the registration, another preprocessing step is performed on the data. Since the slice thickness is generally larger than the in-plane pixel spacing, the data was linearly interpolated in the third direction (z-direction) to create near-isotropic voxels. This helps to create a smoother 3D model of the veins.

Figure 20: After Registration

4.2.1.2 Bayesian Voxel Classification

With the data properly aligned and interpolated, 3D image segmentation is performed to segment the portal vein and its branches. A 3D voxel classification is performed on the data using the intensity distributions of the MR images. We assume that blood filled regions (i.e. the veins) have higher intensities as compared to the background tissue. Each voxel is labeled as either "blood" or "background" by taking the highest probability that the voxel belongs to its respective group. The probability of a voxel belonging to the blood or background classification is calculated using Bayes' rule [16, 42]:

$$Pr(x \in c_k \mid V(x) = v) = \frac{Pr(V(x) = v \mid x \in c_k)Pr(x_k)}{\sum \gamma Pr(V(x) = v \mid x \in \gamma)Pr(x \in \gamma)}, \quad (7)$$

which means that given the probability density function $p(V(x) \mid c_k)$ of each class c_k (blood or background) and the prior probability $Pr(x \in c_k)$ of each class, posterior probabilities can be calculated via the Bayes rule Equation 7 to give the probabilities of a single voxel at position $x = (x, y, z)$ belonging to different classes. $V(x)$ is the intensity of voxel x, and v is any possible value within the range of the intensity in the images.

To determine the probability density functions for both blood and background, we analyze the histogram of the images to determine the mean (μ_c), standard deviation (σ_c) of each class. Then the probability density function can be approximated using Gaussian functions with the learned mean and standard deviation in each class, thus the likelihood of a particular voxel having a certain intensity value v given that it is in class $c \in \{blood, background\}$ is:

$$Pr(V(x) = v \mid x \in c) = \frac{1}{\sqrt{2\pi}}\sigma_c exp(-\frac{(v - \mu_c)^2}{2\sigma_c^2}, \quad (8)$$

The voxels can then be labeled according to the *maximum a posteriori* (MAP)

rule:

$$C(x) = \underset{c \in \{blood, background\}}{\arg \max} \ Pr^*(x \in c \mid V(x) = v), \qquad (9)$$

where $C(x)$ is the class that voxel x belongs to, and Pr^* is a smoothed version of the posterior probability obtained using the anisotropic smoothing [34] described by the following affine invariant flow:

$$\frac{\partial Pr}{\partial t} = sign(H)\kappa_+^{\frac{1}{4}}\vec{N}, \qquad (10)$$

where H and κ are the mean curvature and Gaussian curvature of Pr, and $\kappa_+ \colon= max\{\kappa_+, 0\}$. $\vec{N}$ is the inward unit normal.

The voxel labeling result is seen in Figure 21. All blood regions are shown as white, while the background region is the same as the original images.

Figure 21: Voxel Labeling Result

4.2.1.3   Isolating Portal Veins

Since the voxel labeling results identify all blood filled regions, the portal vein and it's inlets and outlets needed to be isolated. An in-house program was developed for

this application that labeled all connected veins thus allowing the portal vein to be selected.

4.2.2 Velocity Data Segmentation and Processing

4.2.2.1 Preprocessing

Image preprocessing was performed using a MATLAB program written for this purpose. PC-MR data consists of both magnitude and phase images. The magnitude images were cropped to isolate the vein of interest. The phase images were filtered using a median filter:

$$y[m,n] = median\{x[i,j], (i,j) \in w\}, \tag{11}$$

where w is a neighborhood centered around the location (m,n). Then the intensity images were also cropped to isolate the vein of interest.

4.2.2.2 Threshold Segmentation

Image segmentation was performed using a MATLAB program written for this purpose. The processed magnitude images were segmented based on a threshold criteria:

$$g(i,j) = 1 \, for f(i,j) \geq T \tag{12}$$

$$= 0 \, for f(i,j) > T, \tag{13}$$

where T is the intensity threshold. Next, the segmented magnitude images were used as a mask to multiply the phase images, leaving only the phase intensity information of interest. An example can be seen in Figure 22 showing the original cropped image and the mask.

4.2.2.3 Velocity Calculations

The segmented velocity intensities were converted to actual velocity values using a MATLAB program we developed for this application and the relationships:

(a) Original Magnitude Image   (b) Mask
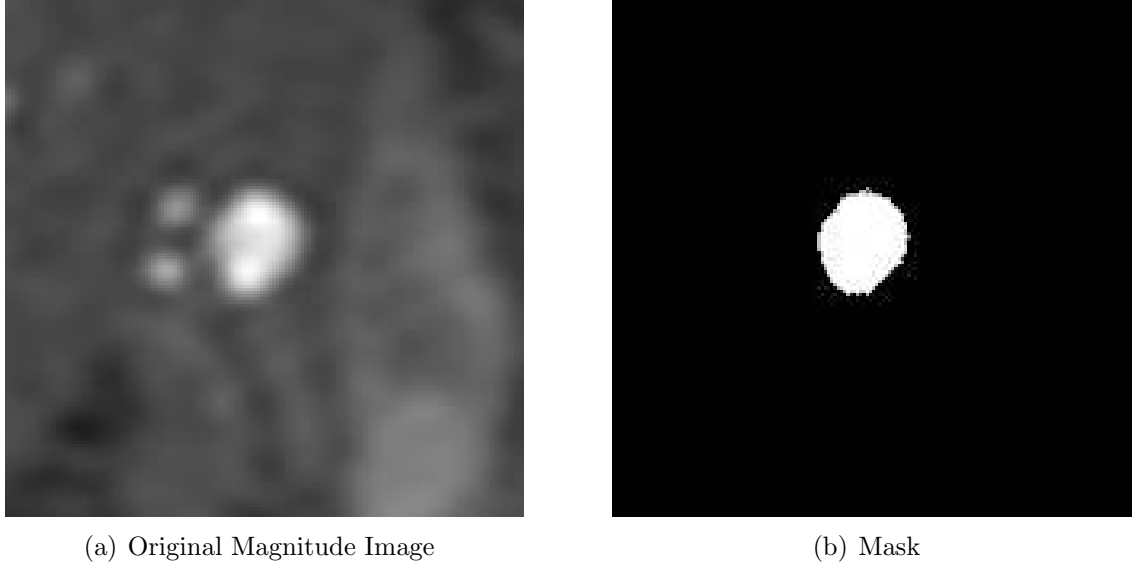
Figure 22: PC-MR Processing Example

$$a = \frac{2V_{enc}}{4096} \tag{14}$$

$$b = V_{enc} \tag{15}$$

$$Velocity(i,j) = a \times Intensity(i,j) + b \tag{16}$$

The V_{enc} number is a parameter defined by the user and is the velocity of protons that will produce a phase shift of 180°. It is the maximum velocity that can be measured without aliasing. These calculations provide 2D cross-sectional velocity images (Figure 23).

In addition the average, maximum and minimum velocities, the flow rate, and the area were calculated for each cross-section.

$$FlowRate = \sum Velocity_{(i,j)} \times PixelArea \tag{17}$$

$$Area = NumberofPixels \times PixelArea \tag{18}$$

The above values were calculated for the entire cardiac cycle by taking the average of the cross-sectional averages. The diameter and Reynolds Number were also
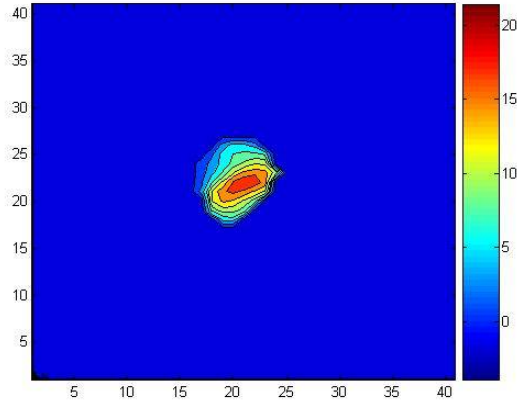
Figure 23: 2D Velocity Cross-Section Example (cm/s)

calculated.

$$Diameter = \sqrt{\frac{4 \times AverageArea}{\pi}} \qquad (19)$$

$$ReynoldsNumber = \frac{\rho \times AverageVelocity \times Diameter}{\mu}, \qquad (20)$$

where ρ is blood density (1060 kg/m^3) and μ is blood viscosity (0.0035 kg/ms).

4.3   Computational Fluid Dynamics

Computational fluid dynamics obtains numerical solutions to fluid flow problems using computers. The governing equations are the Navier-Stokes equations which are shown in Equation 21 for an incompressible fluid. The first equation is the continuity equation which is basically the conservation of mass. The second equations represent the conservation of momentum. On the left side is density multiplied by acceleration which is the material derivative of velocity. On the right side is the sum of the forces acting on the fluid, the pressure gradient, the viscous forces, and the body forces such as gravity [41].

$$\frac{\partial u}{\partial x} + \frac{\partial v}{\partial y} + \frac{\partial w}{\partial z} = 0 \tag{21}$$

$$\rho \left(\frac{\partial u}{\partial t} + u\frac{\partial u}{\partial x} + v\frac{\partial u}{\partial y} + w\frac{\partial u}{\partial z} \right) = -\frac{\partial P}{\partial x} + \eta \left(\frac{\partial^2 u}{\partial x^2} + \frac{\partial^2 u}{\partial y^2} + \frac{\partial^2 u}{\partial z^2} \right) + F_x \tag{22}$$

$$\rho \left(\frac{\partial v}{\partial t} + u\frac{\partial v}{\partial x} + v\frac{\partial v}{\partial y} + w\frac{\partial v}{\partial z} \right) = -\frac{\partial P}{\partial y} + \eta \left(\frac{\partial^2 v}{\partial x^2} + \frac{\partial^2 v}{\partial y^2} + \frac{\partial^2 v}{\partial z^2} \right) + F_y \tag{23}$$

$$\rho \left(\frac{\partial w}{\partial t} + u\frac{\partial w}{\partial x} + v\frac{\partial w}{\partial y} + w\frac{\partial w}{\partial z} \right) = -\frac{\partial P}{\partial z} + \eta \left(\frac{\partial^2 w}{\partial x^2} + \frac{\partial^2 w}{\partial y^2} + \frac{\partial^2 w}{\partial z^2} \right) + F_z, \tag{24}$$

These equations contain coupled non-linear partial differential equations. Analytical solutions can be found if the non-linear terms drop out or are very small in comparison to other terms and thus can be neglected. In most fluid flows, especially blood flow, the non-linear terms can not be neglected and numerical methods must be used to solve these equations. In CFD, the governing equations are discretized and can be solved with the help of a computer to find approximate solutions. These methods involve developing a numerical grid of the anatomy of the region of interest, as obtained from the MRI scans. It is necessary to provide velocity or flow boundary conditions for the inflow and outflow of the region of interest. These data will be obtained from the PC-MRI results. At the interior grid points, the governing equations are replaced by discretized approximations.

4.3.1 Grid Generation

The first step in creating a grid for the geometry is making sure that the geometry is in the correct form. After isolating the portal vein, we are left with a series of 2D cross-sections. These cross-sections are imported into MIMICS which creates a smooth surface.

This smooth surface is then trimmed down. Next contour lines are manually drawn on the geometry, this divides the geometry into panels which are then subdivided into patches. It is ideal for the patches to be equilateral. These patches are then

the containers for grids. The resolution of the grid is set and the grid automatically generated. A Non-Uniform Rational B-Spline (NURBS) Surface is created based on the grids that lie in the patches on the panels. NURBS is a set of smoothly connected curves imposed on a surface to make the surface smooth. The surface is saved in IGES format which can be imported into GAMBIT.

GAMBIT is the grid generation component of the FLUENT package. The IGES geometry file was imported into GAMBIT. The faces of the outlets and inlets were created from the edges. Then a volume was created by stitching all faces together. Both the inlets and outlets needed to be extended so local coordinate systems were established and a line created perpendicular to the face being extended. Then the face was swept along the line forming the extension. Once all extensions were completed they were added to the original volume. Next the volume was automatically meshed with the following specified; meshing scheme and mesh node spacing. The meshing scheme is composed of the elements and type. The elements' parameter defines the shape of the elements used to mesh. The elements selected were Tet/Hybrid which specifies that the mesh is primarily composed of tetrahedral elements and where appropriate may include hexagonal, pyramidal, and wedge elements. The type parameter defines the meshing algorithm which in our case was Map, creating a regular structured grid of hexahedral mesh elements. The mesh node spacing was also set based upon the geometry. After the geometry is successfully meshed, the zone types are specified. The boundary types such as wall, inlet velocity and outflows are set as well as the continuum type which is fluid. A mesh file is exported for use in FLUENT.

4.3.2 Computations

The meshed geometry was imported into FLUENT where it was scaled and the grid points were smoothed and swapped for a minimum skewness of 0.7. Blood was specified in the materials database with a density of 1060 kg/m^3 and viscosity of 0.0035

kg/ms. The next steps are divided into Steady and Unsteady Flow Calculations.

4.3.2.1 Steady Flow Calculations

The boundary conditions were for the inlets and outlets. The SMV and SV inlets were classified as velocity inlets and the velocity was taken from literature or MR data. All outlets were classified as outflow in which the flow split was again taken from literature or MR data. The outflow boundary condition is treated as a zero diffusion flux for all flow variables and an overall mass balance correction.

The solver parameters were as follows. The pressure based solver was chosen due to the modeling of low-speed incompressible flow. FLUENT solves the governing equations for mass and momentum in order to obtain the velocity field. To do this a control volume based technique is used. The domain is divided into discrete control volumes based on the computational grid. The governing equations are integrated over the individual control volumes to construct algebraic equations. The discretized equations are linearized and solved to yield values for unknown variables. The formulation for the solver was implicit. The velocity formulation was absolute and porous formulation was superficial velocity. The Green-Gauss Cell based gradient option was used. For the pressure-velocity coupling the SIMPLE algorithm was selected which uses the relationship between velocity and pressure correction to enforce mass conservation and obtain the pressure field. Convergence was assumed when all scaled residuals decrease to 10^{-3}.

4.3.2.2 Unsteady Flow Calculations

The boundary conditions for the inlets were User-Defined functions of the velocity waveform from MR data. The outlet conditions were the same as above for the steady calculations.

The solver parameters were as follows: implicit pressure based solver, absolute velocity, 1st order implicit, superficial velocity, and green-gauss node based gradient

41

option. The pressure-velocity coupling selected was the PISO algorithm part of the SIMPLE family but based on the higher degree of the approximate relation between the corrections for pressure and velocity.

4.3.2.3 Visualization

Visualization was done using TECPLOT 360 which displayed results, calculated additional variables, and performed integrations.

4.4 Flow Contribution Calculations

Physicians have noted that liver disease is located preferentially on the right side of the liver. One hypothesis is that the right side of the liver is predominately fed by SMV blood which is coming from the digestive system and carries toxins. Therefore a protocol was developed to calculate the contributions of one inlet to all outlets. First a slice perpendicular to the inlet was created. Next a grid was overlaid on the slice. This information was used to create a macro that added streamtraces at all of the grid points inside the vessel. The streamtraces were then extracted and run through a separate C program that calculated to which outlet they went based on input $x, y, and\, z$ criteria. Once the streamtraces were separated by outlets, the flow to each outlets was calculated by taking the sum of the velocities at the grid points on the inlet multiplied by the individual grid area.

$$FlowRate\,per\,outlet = \sum Velocity_{(i,j)} \times Individual\,Grid\,Area \qquad (25)$$

4.5 Liver Volume

The liver volumes were calculated based on manual segmentation and program calculation of the volume by summing the volumes of the voxels. An example liver segmentation for a normal subject and patient can be seen in Figure 24.

(a) Normal   (b) Patient

Figure 24: Subject Liver Segmentation Example

CHAPTER V

IDEALIZED MODELS

Specific Aim 1: Develop an idealized, but physically representative model of the portal venous system to preliminarily investigate portal venous flow and study the effect of boundary conditions and geometric shape on flow patterns.

5.1   Model Development

The model consists of the Superior Mesenteric Vein (SMV) and Splenic Vein (SV) joining to form the Portal Vein (PV), which then divides into the left and right portal vein branches (LPV and RPV). The vessel parameters and average velocity were obtained from literature results of which can be seen in Table 6. The model parameters can be found in Table 7. Four variations of the geometry were investigated; a planar model, 90-degree model, 45-degree model and an Altered 90-degree model. The models can be seen in Figure 25. These models were created using GAMBIT 2.4.6.

Table 6: Literature Portal Vein Parameters

Vein	Average Velocity (cm/s)	Diameter (mm)	Length (cm)
Portal Vein	12.6-22	9-14.5	5-8
RPV	20.1	8.3	
LPV	16.8	7.3	
SMV	21	6.2-12	
SV	17.9-23.9	5.6-8.8	

Table 7: Idealized Model Geometry Parameters

Vein	Diameter (mm)	Length (cm)
Portal Vein	10	8
RPV	8	2.4
LPV	7	2.1
SMV	10	3
SV	6	2.4

(a) Planar

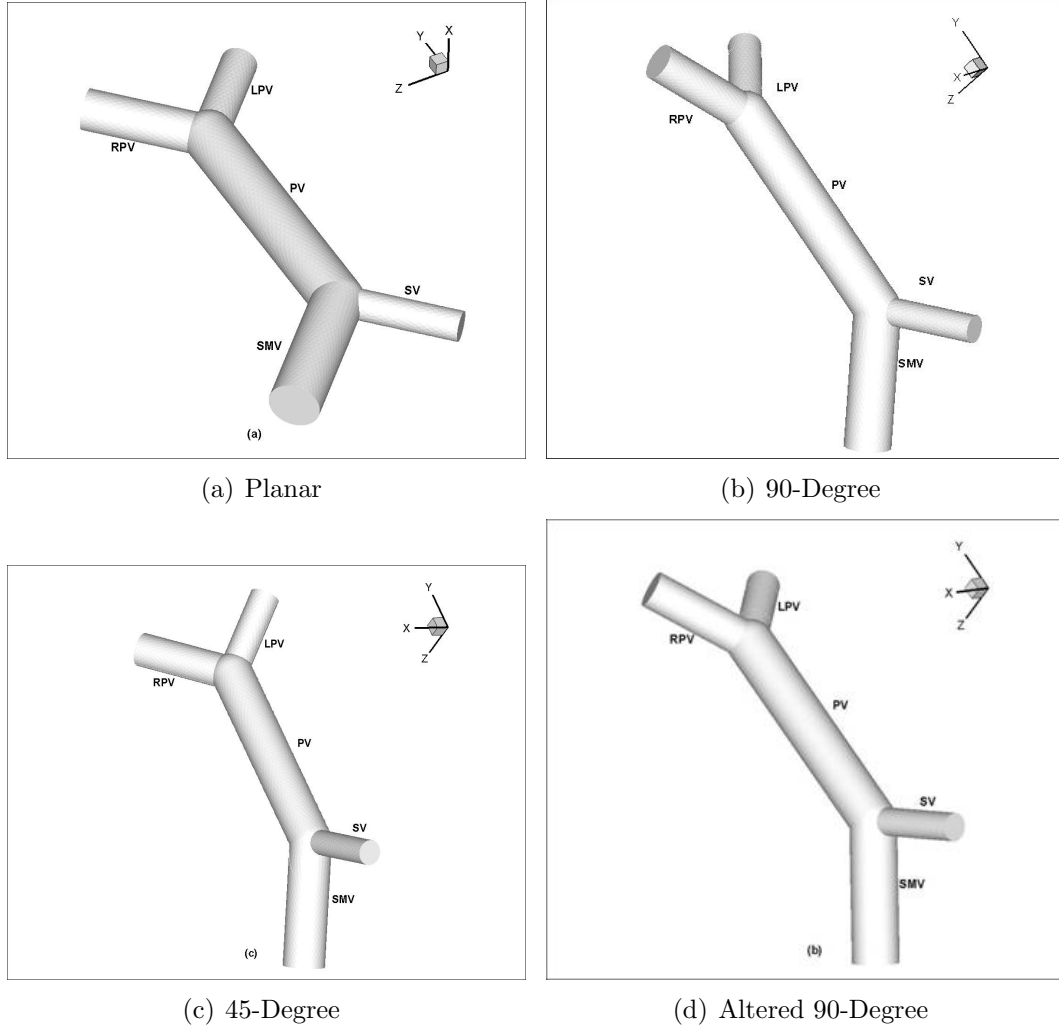(b) 90-Degree

(c) 45-Degree

(d) Altered 90-Degree

Figure 25: Idealized Model Geometries

5.2   Computational Analysis

5.2.1   Mesh Generation

GAMBIT 2.4.6 was used to generate a mesh for all models, the meshing parameters
are located in Table 8 and an example mesh for the Altered 90-degree Model is found

in Figure 26

Table 8: Mesh Generation Parameters

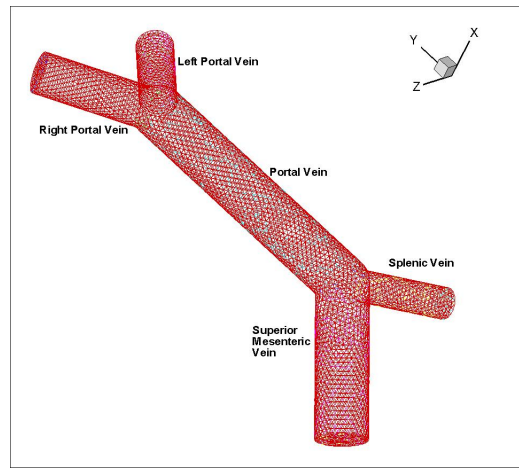| Model	Mesh Type	Mesh Size	Mesh Volume
Planar	Tet/Hybrid	0.1	55,599
90-Degree	Tet/Hybrid	0.1	53,205
45-Degree	Tet/Hybrid	0.1	53,270
Altered 90-Degree	Tet/Hybrid	0.1	60,172

Figure 26: Altered 90-Degree Model Mesh

5.2.2 Boundary Conditions

The boundary conditions used in all 4 models were a constant flat profile inlet velocity for the SMV (0.21 m/s) and SV (0.18 m/s) and a flow split for the RPV (0.6) and LPV (0.4), all taken from the literature.

5.2.3 Computations

The commercial code FLUENT was used to solve this 3D laminar, steady flow field. All solutions reached convergence criteria within 81 iterations. In order to determine that the outlets were of sufficient length as not to have an effect on the flow field, an extended planar model was developed for comparison. This extended model showed

little difference between the flow fields in the outlets and thus the extensions were not necessary.

5.3 Planar Model

The computational results showed that the velocity along the portal vein is parabolic-like with slight skewing to the posterior side of the PV closest to the confluence (Figure 27). There is also little mixing of the blood from the SV and SMV based upon close to zero secondary velocities in the cross-sectional plane and streamtraces (Figures 28, 29 & 30). Both the LPV and RPV illustrate skewing of the velocity profile to the inner walls which is consistent with bifurcating vessels (Figures 31 & 32).
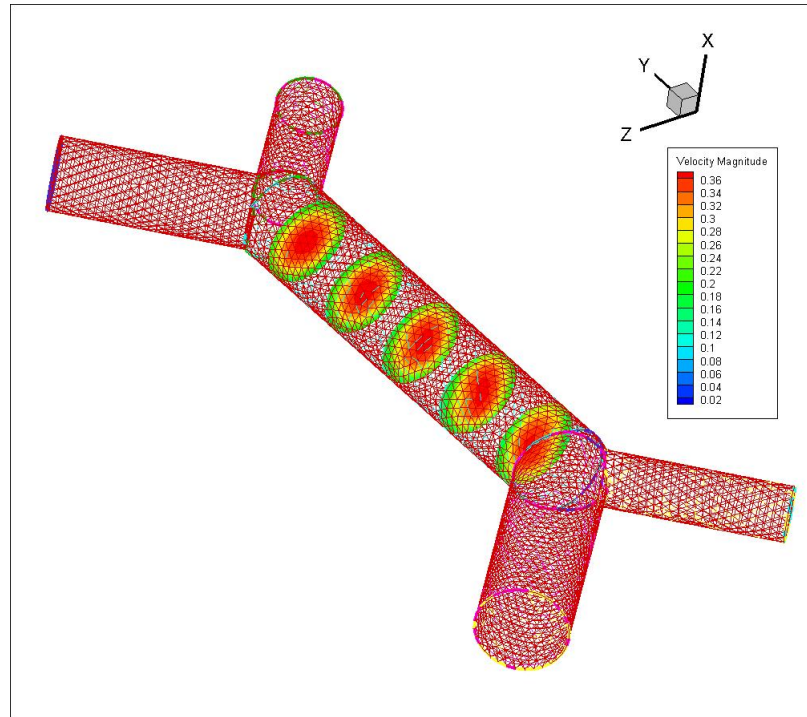
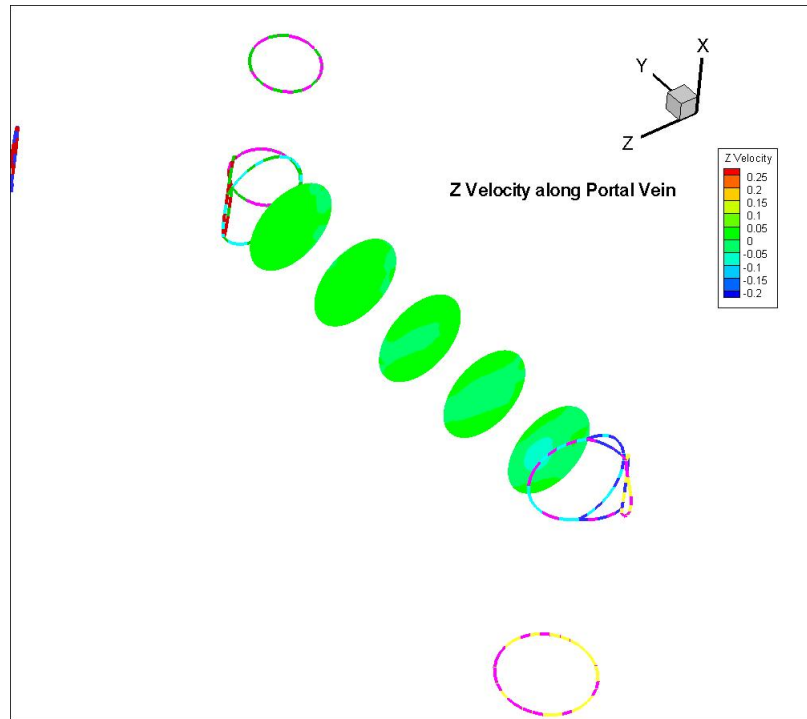Figure 27: Planar Model PV Cross-Sections; Velocity Magnitude m/s

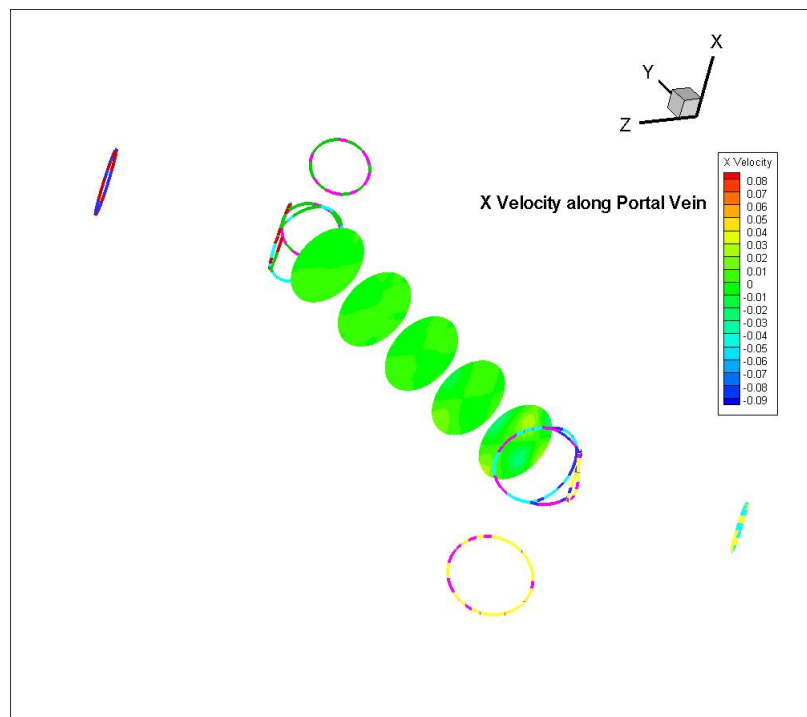Figure 28: Planar Model PV Z-direction Velocity Magnitude m/s

Figure 29: Planar Model PV X-direction Velocity Magnitude m/s
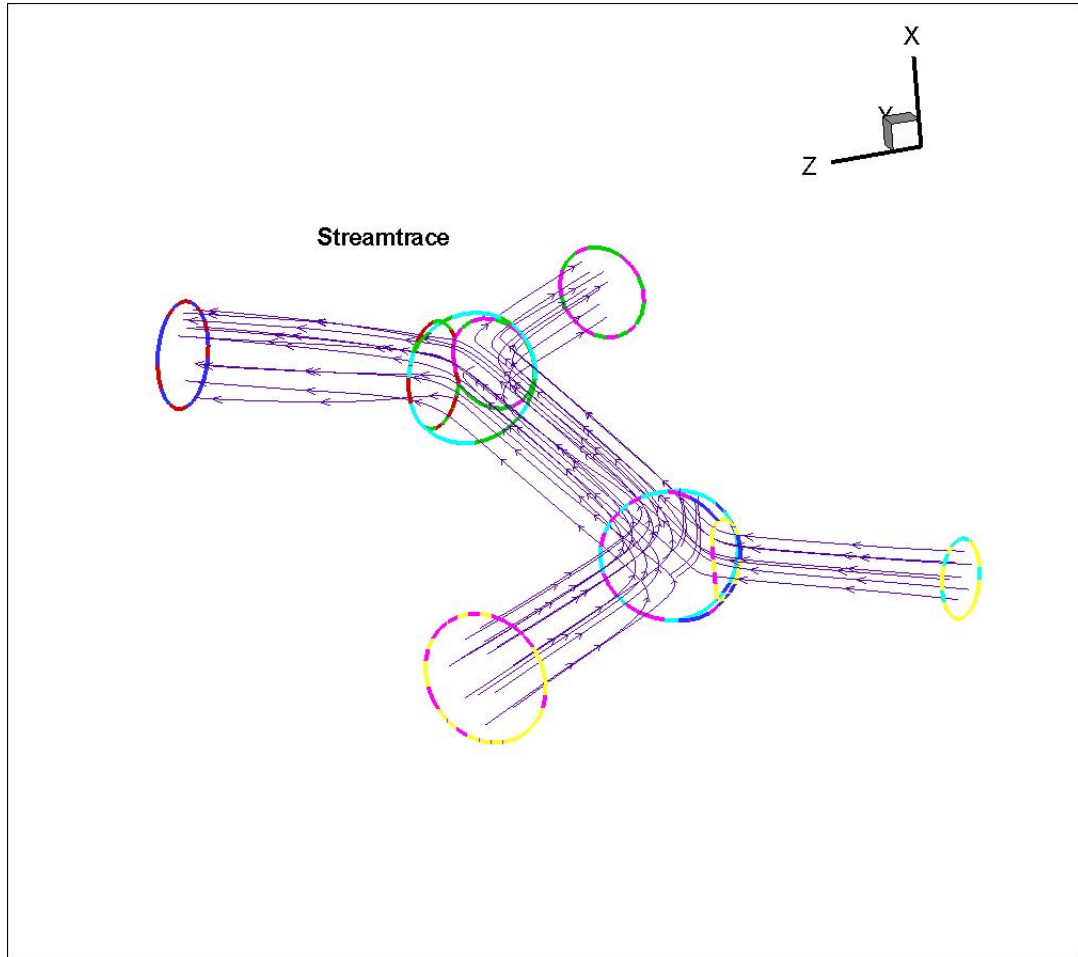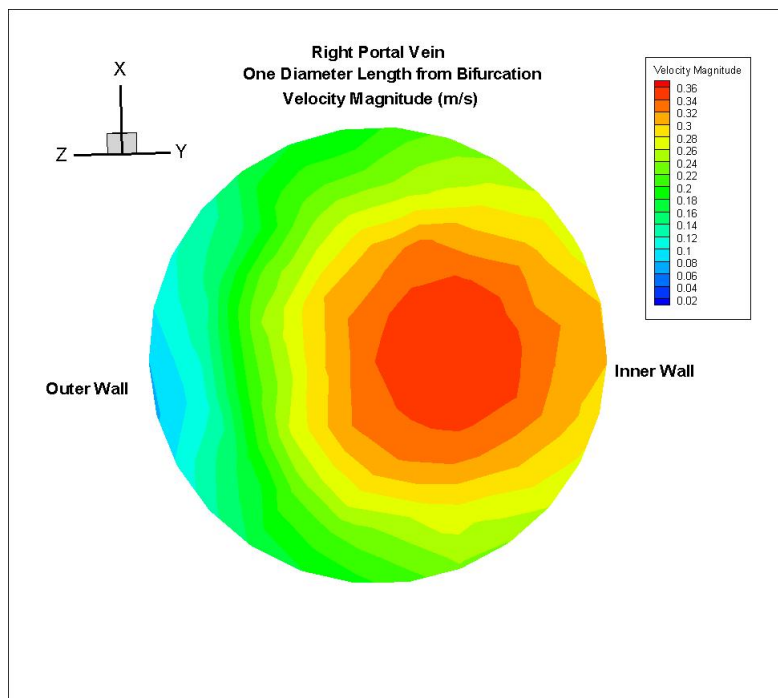
Figure 30: Planar Model Streamtraces

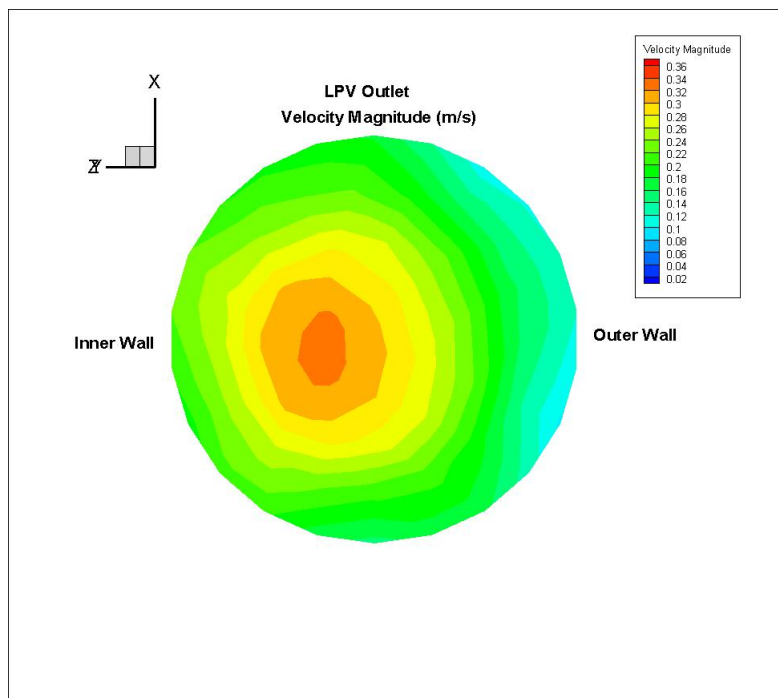Figure 31: Planar Model RPV Outlet Velocity Magnitude m/s

Figure 32: Planar Model LPV Outlet Velocity Magnitude m/s

5.4   90-Degree Model

In this model, the outlets were rotated 90-degrees from the planar model. This geometrical change did not affect the velocity profile within the portal vein (Figure 33). Little mixing of the SMV and SV blood is seen in the streamtraces (Figure 34). The LPV and RPV velocity profiles also remain unchanged.
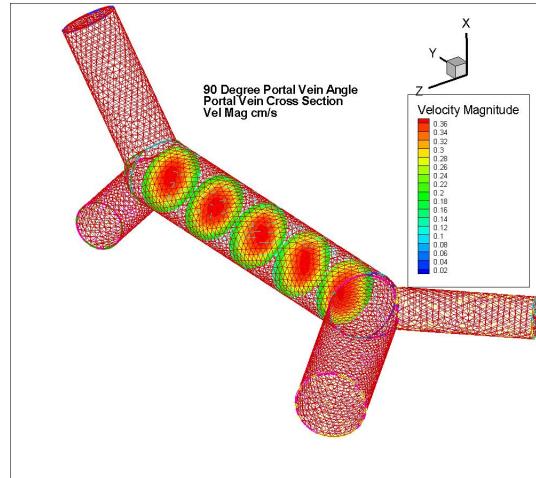

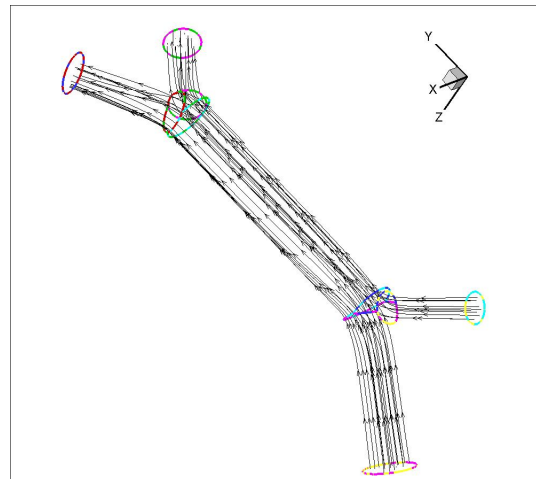Figure 33: 90-Degree Model PV Cross-Sectional Velocity Magnitude m/s

Figure 34: 90-Degree Model PV Streamtraces

5.5   45-Degree Model

In this model the outlets were rotated 45-degrees from the planar model. Again this geometrical change did not affect the velocity profile within the portal vein (Figure 35). And again little mixing of the SMV and SV blood is seen with the streamtraces (Figure 36). The LPV and RPV profiles also remain unchanged.
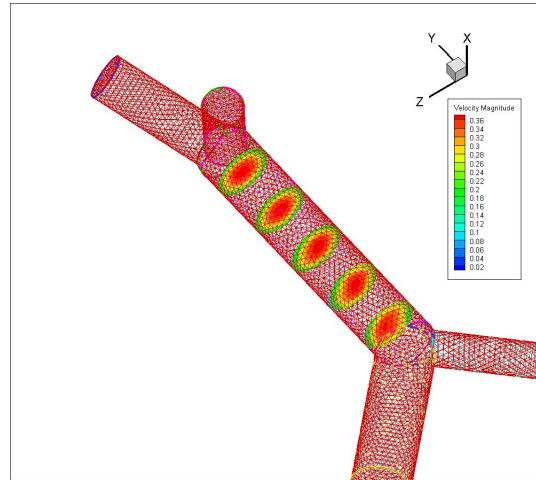

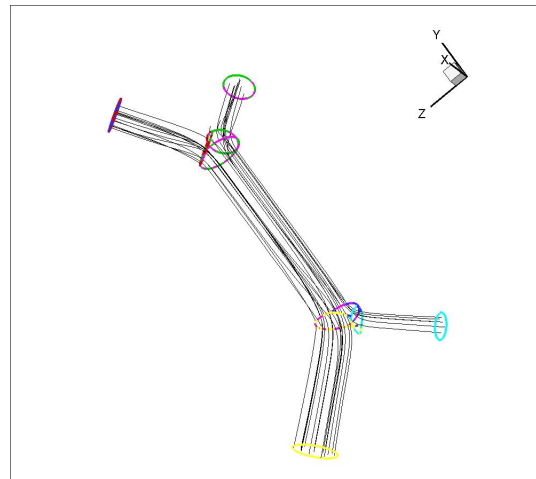Figure 35: 45-Degree Model PV Cross-Sectional Velocity Magnitude m/s

Figure 36: 45-Degree Model PV Streamtraces

5.6   Altered 90-Degree Model

For this model the angle between the PV and SMV was increased from that of the previous 90-degree model. This geometrical change resulted in changes in the PV cross-sectional velocity profile (Figure 37). However these changes disappeared by the bifurcation allowing for similar RPV and LPV profiles as compared to the previous models. At the center of the PV, the velocity profile is skewed to the superior wall of the PV (Figure 38). Streamtraces again indicate little mixing of the blood (Figure 39).
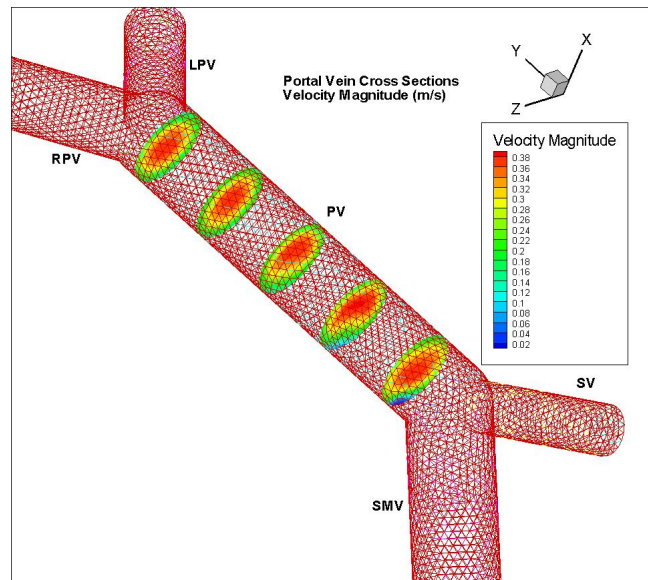

Figure 37: Altered 90-Degree Model PV Cross-Sectional Velocity Magnitude m/s
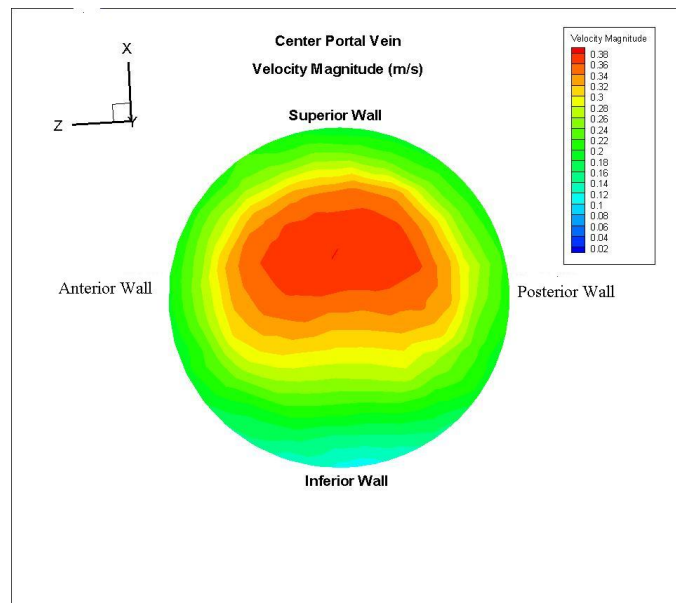
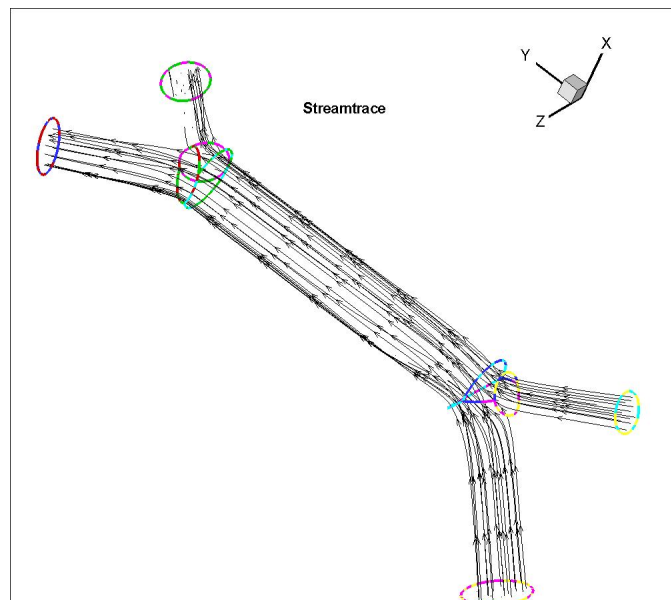Figure 38: Altered 90-Degree Model Center PV Velocity Magnitude m/s

Figure 39: Altered 90-Degree Model Streamtraces

5.7 Model Comparisons

The center PV cross-sectional velocity profile cross-sections for each model can be seen in Figure 40. The first three are similar but the altered 90-degree model is skewed a little more to the superior wall of the portal vein.

(a) Planar

(b) 90-Degree

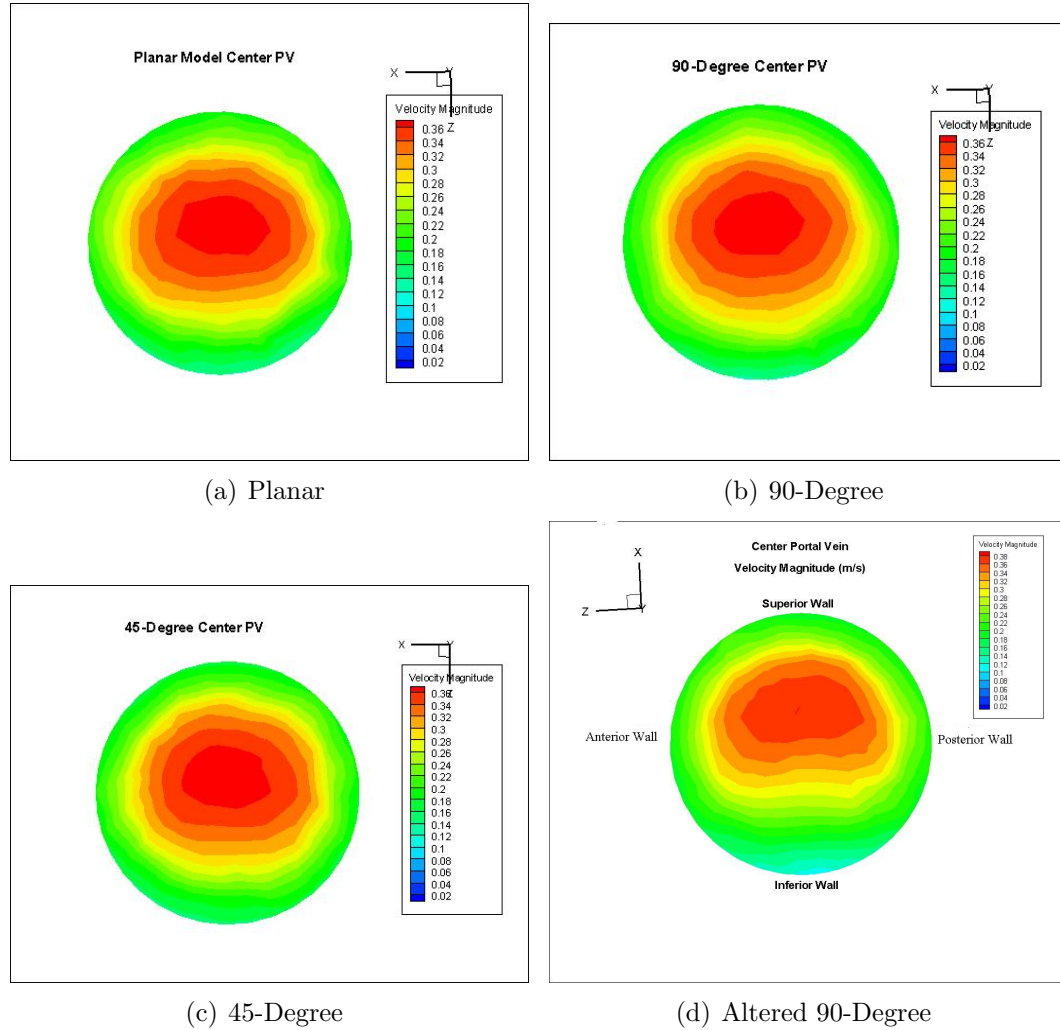(c) 45-Degree

(d) Altered 90-Degree

Figure 40: Idealized Model Center PV Cross-Sections Velocity Magnitude m/s

5.8 Flow Contribution Calculation

A protocol was developed to calculate the flow contributions of the SV to the right and left PV and therefore the the contribution of the SMV to the RPV. This was done for the altered 90-degree model. The results show 41% of splenic flow going to

the LPV and 59% going to the RPV. However, the splenic flow accounts for 25% of both the RPV and LPV flow. Thus the SMV flow contributes 75% to both the RPV and LPV. The streamtraces show that the splenic flow is pushed towards the superior wall of the PV. Results can be seen in Tables 9, 10 & 11 and Figures 41 & 42.

Table 9: Idealized Theoretical Flow Rate (ml/min)

SMV	989.60
SV	305.36
PV	1294.95
RPV	770.98
LPV	517.99

Table 10: Idealized CFD Calculated Flow Rate (ml/min)

SV to LPV	126.64
SV to RPV	179.54
Total SV	306.18

Table 11: Idealized Altered 90-Degree Model Flow Ratios

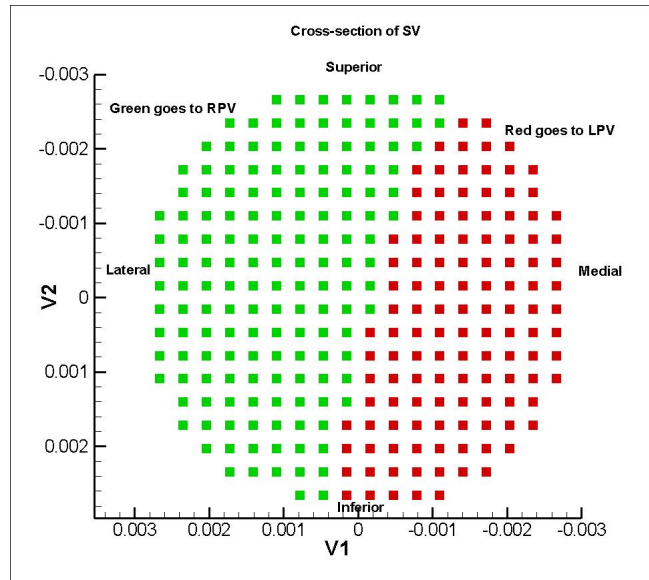|	
SV/LPV	0.24
SV/RPV	0.23
SMV/LPV	0.76
SMV/RPV	0.77

Figure 41: Idealized Model: Splenic vein cross-section showing which particles went to the RPV (green) and LPV (red)
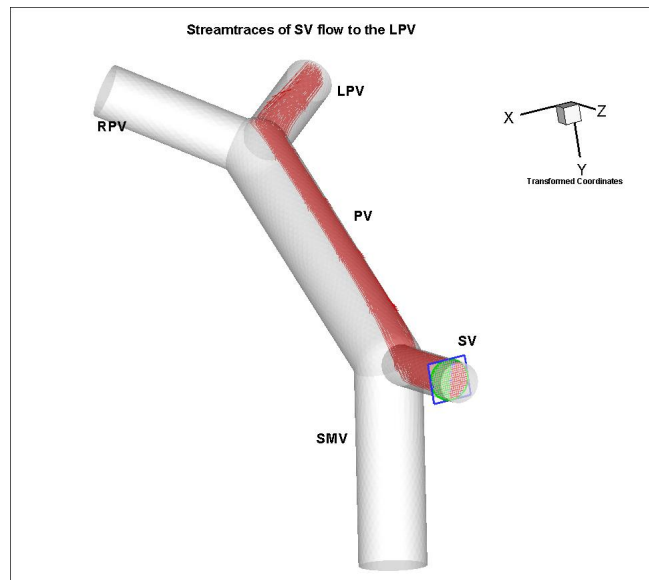

Figure 42: Idealized Model: Streamtraces for particles going to the LPV

5.9 Unsteady Calculations

Although preliminary data and the literature show that the PV flow has little variation and is basically steady, unsteady calculations were run to determine whether the flow could be treated as quasisteady. Unsteady calculations were run using the altered 90-degree model. In order for the unsteady calculations to converge it was necessary to add 3 *cm* to each outlet. A user defined function was created from PCMRI data for the SV and SMV boundary conditions. Waveforms measured in subject N6 can be seen in Figure 43.

Normal Subject MR Data SMV & SV Velocity Waveform
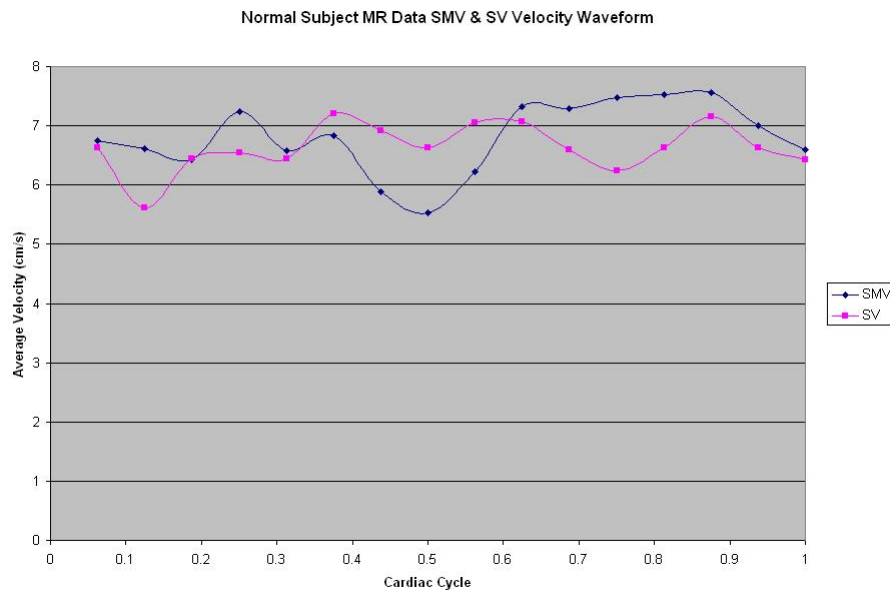
Figure 43: Average Velocity SMV and SV Inlet Boundary Conditions from MR data for subject N6

In the center of the PV the velocity remained slightly skewed to the superior side of the PV throughout the cardiac cycle. The area of highest velocity increased and decreased during the cardiac cycle. A sampling of center PV cross-sections at various time points is found in Figure 44.

(a) t=0.063s   (b) t=0.189s

(c) t=0.315s   (d) t=0.441s

(e) t=0.567s   (f) t=0.693s
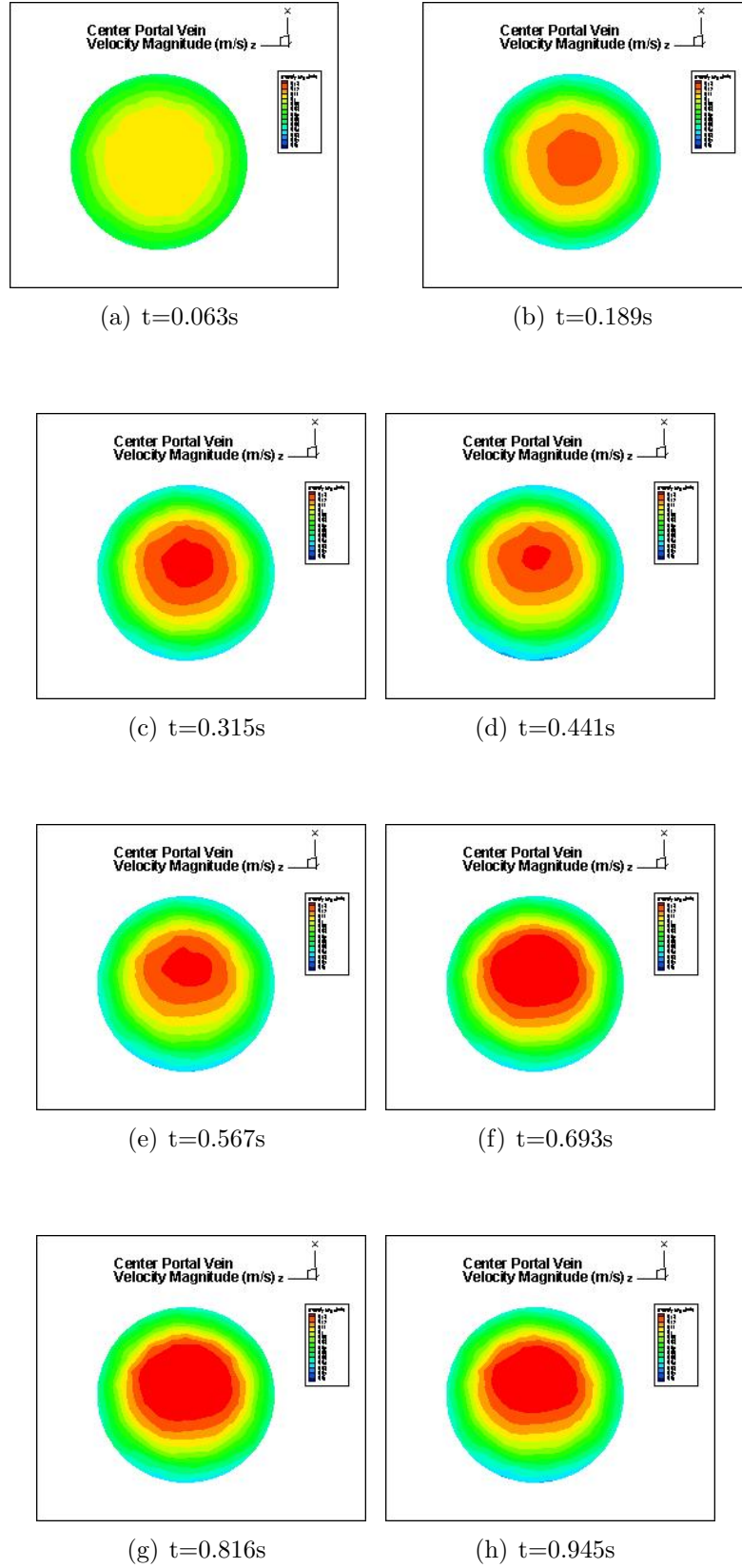
(g) t=0.816s   (h) t=0.945s

Figure 44: Idealized Unsteady Calculations: Center PV Cross-Sectional Velocity Magnitude (m/s) at various time points; Color scale goes from $0.01\ m/s$ to $0.13\ m/s$

5.9.1 Quasisteady Check

Since there was little fluctuation in the inlet velocity boundary conditions a quasi-steady check was performed. A comparison of the center PV cross-sectional velocity magnitude profiles for steady and unsteady calculations at the same inlet velocities was completed. As seen in Figure 45, there is little difference between the steady and unsteady calculations, so that a quasisteady approach is applicable.
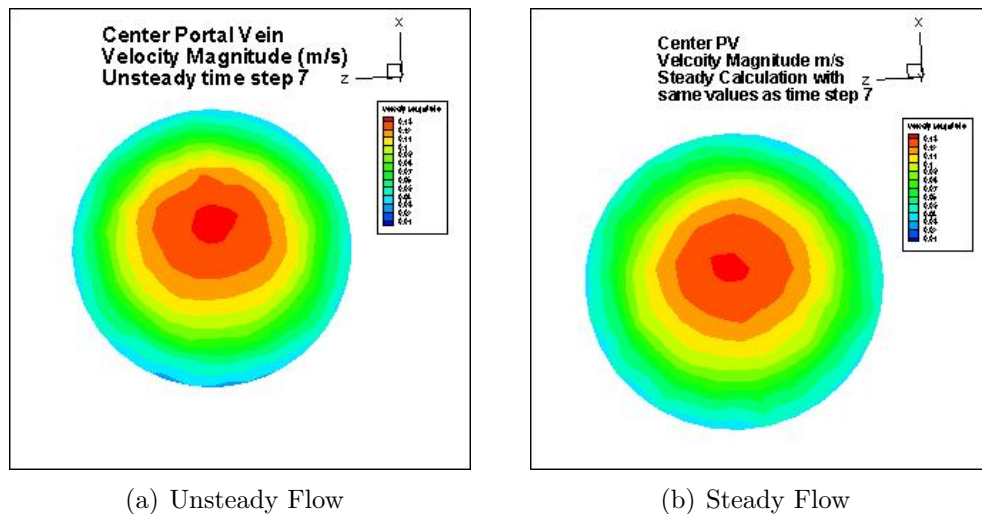

(a) Unsteady Flow   (b) Steady Flow

Figure 45: Center PV Cross-Sectional Velocity Magnitude 7th time step m/s

5.10 Idealized Model Summary

The purpose of creating the idealized models was to become familiar with the characteristics of portal venous flow and CFD starting with simplified models. The goal was also to gain some insight into the affects of geometry and boundary conditions on the CFD results. For all models, the flow in the PV was approximately parabolic and there was little mixing of the blood from the two inlets. In the altered 90-degree, the center PV velocity profile was also approximately parabolic but it was skewed slightly more to the superior wall of the PV; however, this effect disappeared by the bifurcation. The flow contribution protocol was developed and tested on the altered 90-degree model which illustrated that the SMV contributes to roughly 75% of both

the RPV and LPV flows. This did not confirm the hypothesis that the SMV primarily feeds the RPV. The quasisteady assumption was also assessed for the altered 90-degree model which showed some variation with time but when compared to the steady counterpart there was minimal difference. Moving forward, these techniques will be applied to both the normal subjects and the patients with more complex geometries. We postulate that the quasisteady assumption will also be valid for the subject specific CFD models.

CHAPTER VI

NORMAL PORTAL VENOUS HEMODYNAMICS

Specific Aim 2: Characterize hemodynamics in the normal adult portal venous system.

6.1 MR Data Acquisition

The data set consisted of 9 normal volunteers, 4 males and 5 females, all ages 25-30 with no previously diagnosed liver disease.

6.1.1 Vessel Geometry

The geometry was successfully obtained in 7 subjects. General characteristics include a straight PV, winding SV, and PV branch variations which can be seen in Figures 46, 47, and 48. There was generally a narrowing of the SMV before the PV confluence due to the pancreas and the supine position of the subject. In addition in Figure 47 an SMV branch variation is also seen.
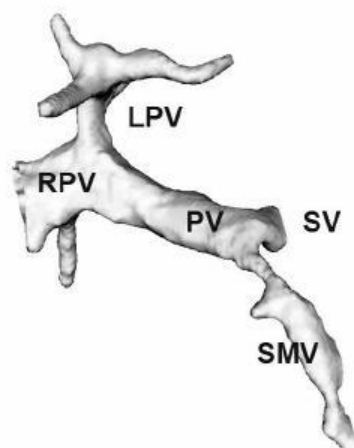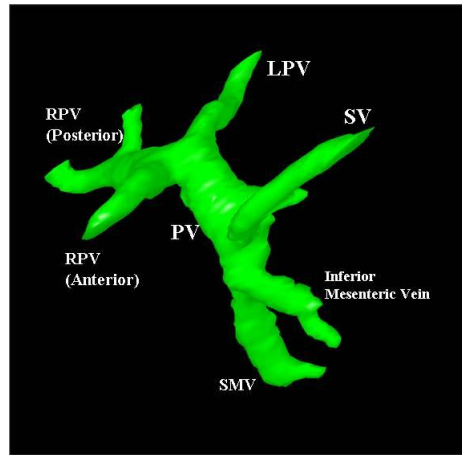

Figure 46: N1 Portal Vein Geometry
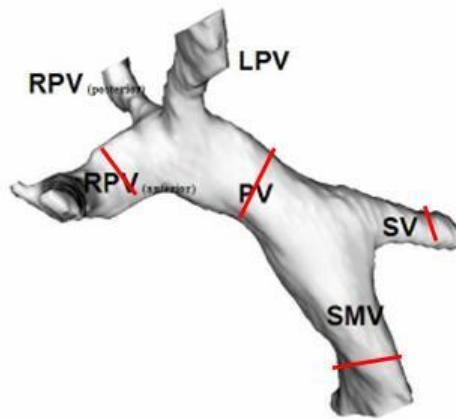
Figure 47: N6 Portal Vein Geometry

Figure 48: N3 Portal Vein Geometry

6.1.2 Velocity Measurements

Velocity measurements were taken at the center cross-section of the PV, the SMV and SV before the confluence, and either the RPV or LPV after the bifurcation but before any branches, if possible. The measurement locations are marked by red lines on Figure 48.

6.1.2.1 Portal Vein

The velocity was successfully obtained in 7 subjects. The velocity profiles were parabolic-like although skewed. The direction of the skewing was dependent on the subject. Center PV cross-sectional velocity profiles at time of maximum velocity can

be seen in Figure 49.

PV area ranged from 0.879 - 1.1 cm^2. There were little velocity and flow rate changes over the cardiac cycle as seen in Figures 86 & 87. The average velocity was 12.74 cm/s and the average flow rate was 783 ml/min. Results for the PV can be found in Table 12.

Table 12: Normal PV Results

	Average Velocity (cm/s)	Velocity Range	Average Flow rate (ml/min)	Flow Rate Range	Area (cm^2)
N0	14.4	4.16	848.8	227.9	0.924
N1	9.43	7.38	528.8	413.7	0.935
N3	9.55	2.99	558.3	180.6	0.919
N5	10.9	2.93	597.2	186.7	0.879
N6	16.4	4.67	1126.8	446.6	1.1
N8	17.03	5.15	1057.8	269.6	0.994
N9	11.5	3.61	766	178.2	1.07
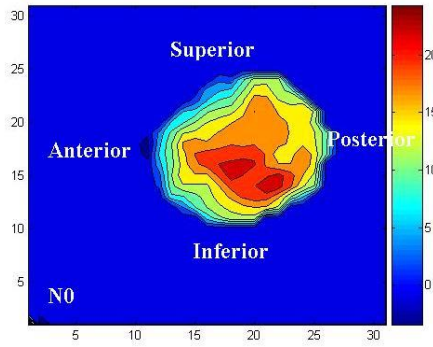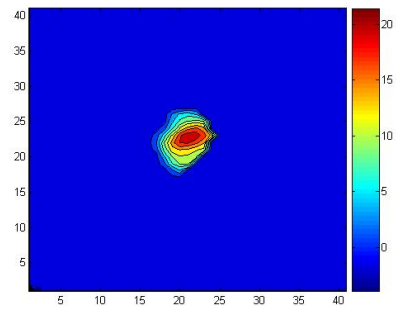
(a) N0   (b) N1
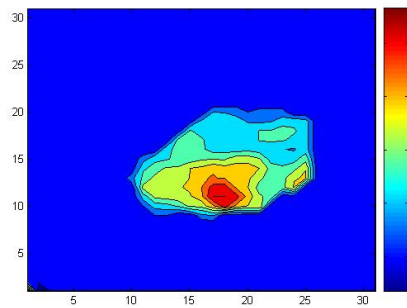
(c) N3   (d) N5
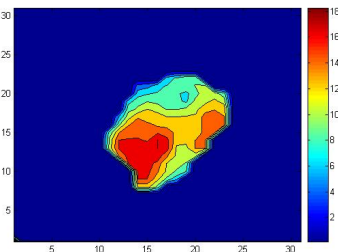
(e) N6   (f) N8

(g) N9

Figure 49: Normal Center PV Cross-sections displaying Velocity Magnitude (cm/s) at maximum velocity and at the same anatomical orientation. Note that the spatial and velocity scales differ among the figures.

**CENTER PV
AVERAGE VELOCITY**
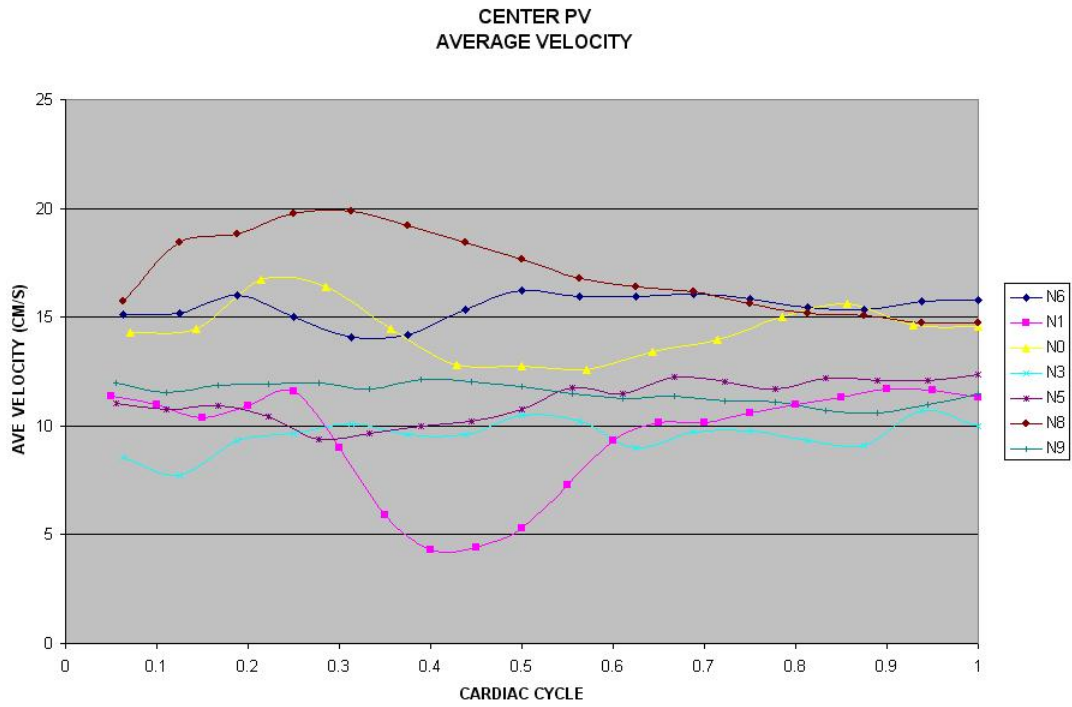
Figure 50: Normal Subject Average PV Cross-Sectional Velocity (cm/s)

CENTER PV FLOWRATE

Figure 51: Normal Subject Average PV Cross-Sectional Flow Rate (ml/min)

6.1.2.2 Superior Mesenteric Vein

Velocity was successfully obtained in 6 subjects. Generally multiple jets were observed, potentially due to SMV branches upstream. SMV cross-sectional velocity profiles at the time of maximum velocity can be seen in Figure 52.

SMV area ranged from 0.361 - 0.966 cm^2. The multiple jets can also be seen in the SMV average velocity and flow rate waveforms (Figures 53 & 54). The average velocity was 9.8 cm/s and the average flow rate was 386 ml/min. Note that subject N8 had a high velocity but also a small area so that the flow was only slightly higher than the other subjects. Continuity was maintained for this subject, therefore these measurements are potentially reasonable. Results for the SMV can be found in Table 13.

Table 13: Normal SMV Results

	Average Velocity (cm/s)	Velocity Range	Average Flow rate (ml/min)	Flow Rate Range	Area (cm^2)
N3	6.23	2.65	231	123.8	0.584
N4	6.46	2.71	332.3	143.9	0.855
N5	6.61	3.1	385.1	181.1	0.966
N6	6.8	2.03	394.2	123.1	0.902
N8	25.05	7.6	506.2	204.4	0.361
N9	7.64	2.85	410.1	223.2	0.791

(a) N3
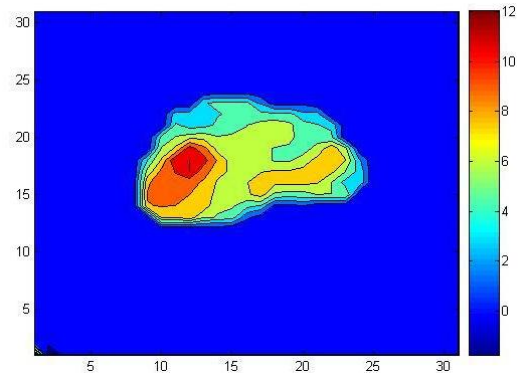
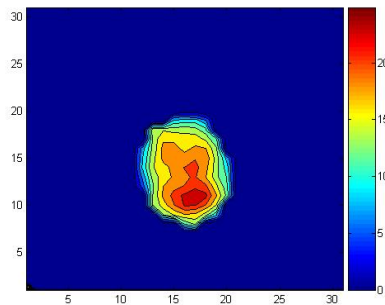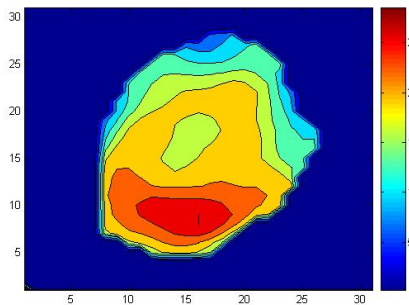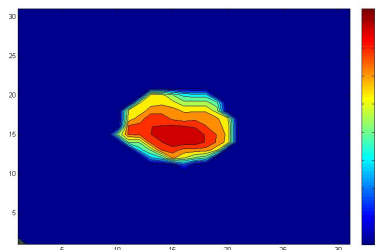(b) N4
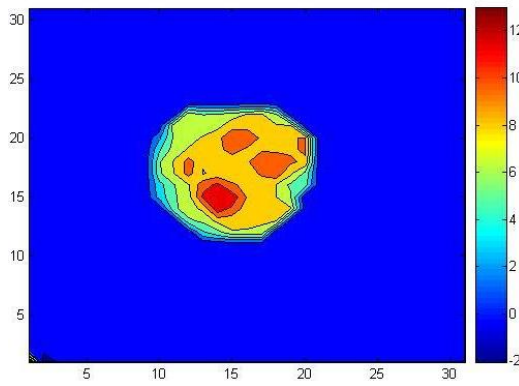
(c) N5
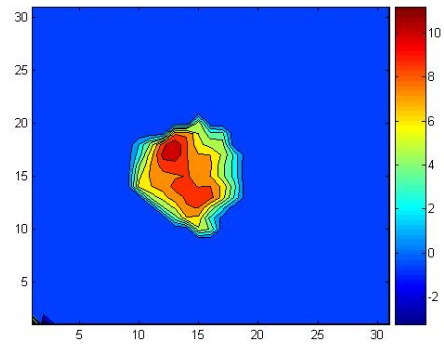
(d) N6
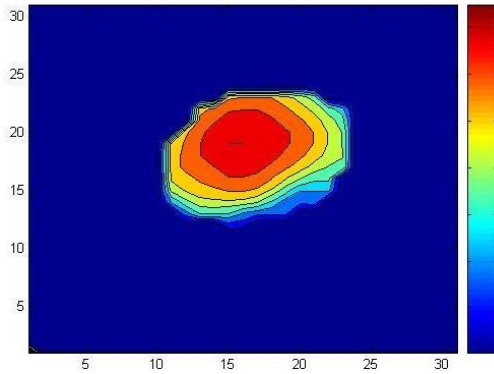
(e) N8
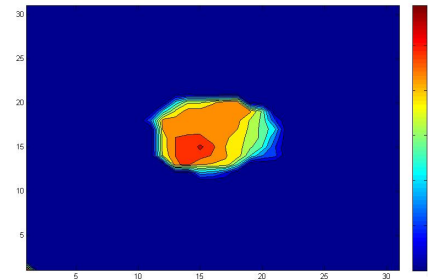
(f) N9

Figure 52: Normal SMV Cross-sections displaying Velocity Magnitude (cm/s) at time of maximum velocity and at the same anatomical orientation. Note that the spatial and velocity scales differ among the figures.

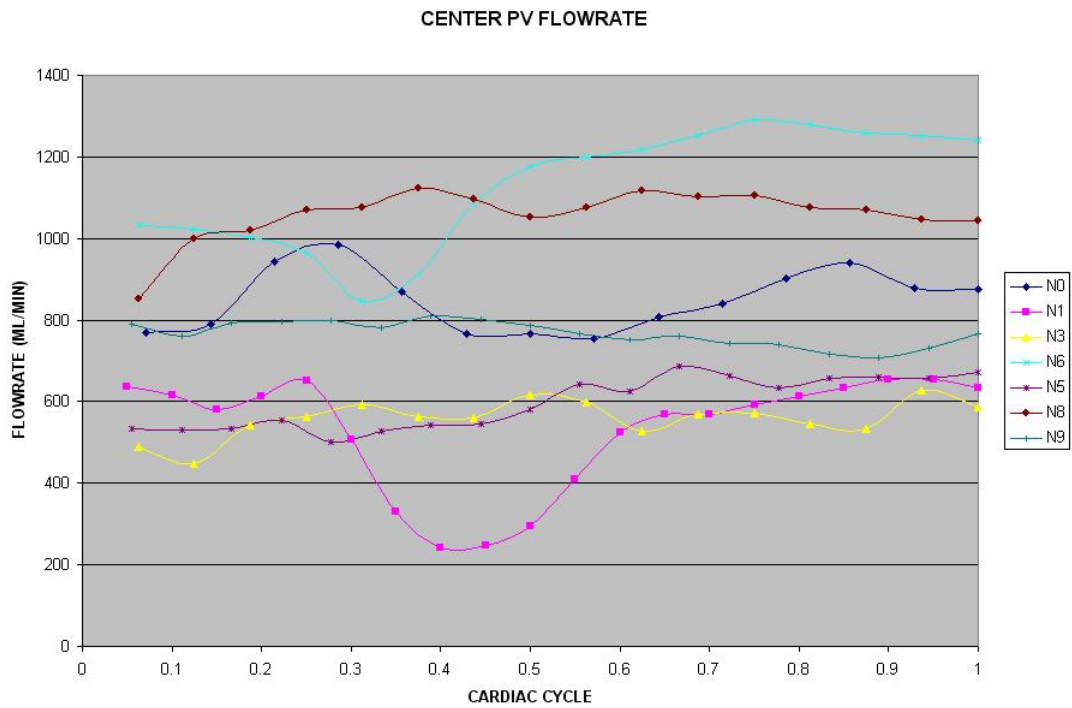Figure 53: Normal Subject Average SMV Cross-Sectional Velocity (cm/s)

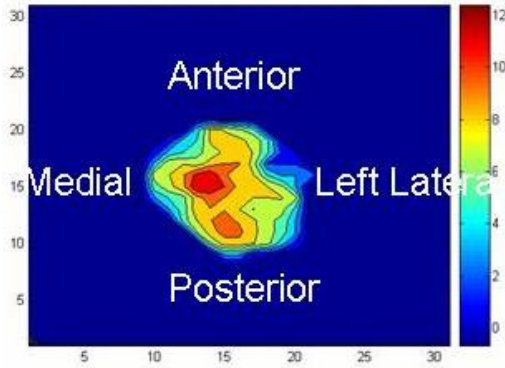Figure 54: Normal Subject Average SMV Cross-Sectional Flow Rate (ml/min)

Velocity was successfully obtained in 7 subjects. Due to the winding nature of the SV, skewed velocity profiles were seen. SV cross-sectional velocity profiles at the time of maximum velocity can be seen in Figure 55.

SV area ranged from 0.443 - 0.742 cm^2. Generally, only small variations were seen in the velocity and flow rate waveforms (Figures 56 & 57). N8 had the largest variation in waveforms. The average velocity was 7.93 cm/s and the average flow rate was 300 ml/min. Results for the SV can be found in Table 14.

Table 14: Normal SV Results

|	Average Velocity (cm/s)	Velocity Range	Average Flow rate (ml/min)	Flow Rate Range	Area (cm^2)
N1	6.19	3.16	203.5	159.5	0.548
N3	7.21	2.57	232.9	84.67	0.488
N4	10.53	1.48	477	64.88	0.742
N5	6.73	1.84	217.1	110.5	0.443
N6	6.64	1.59	269.5	80.97	0.626
N8	9.0	3.72	247.2	157	0.658
N9	8.65	3.61	329	178	0.553
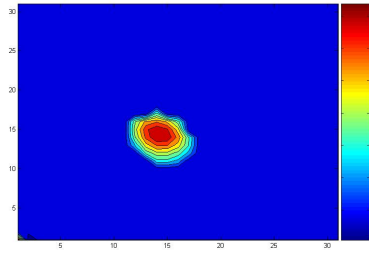
(a) N1
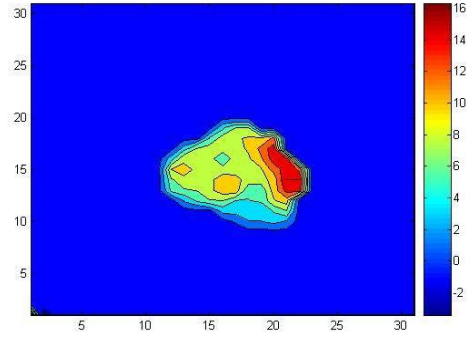
(b) N3
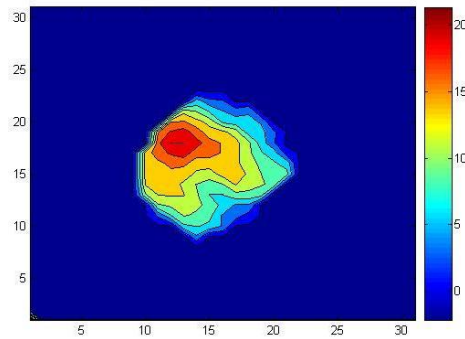
(c) N4

(d) N5
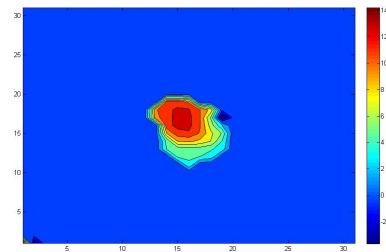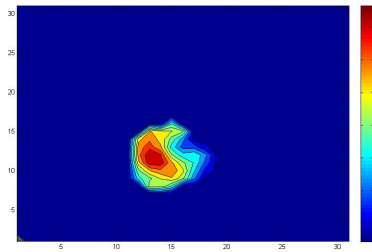
(e) N6
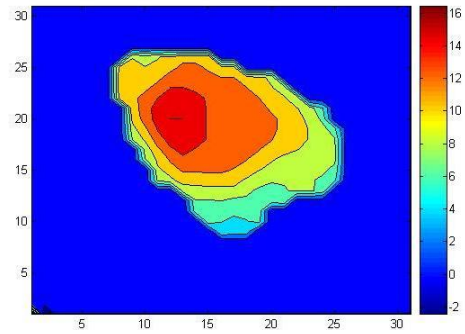
(f) N8
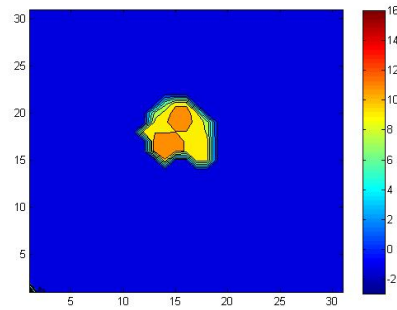
(g) N9

Figure 55: Normal SV Cross-sections displaying Velocity Magnitude (cm/s) at time of maximum velocity and at the same anatomical orientation. Note that the spatial and velocity scales differ among the figures.

SV AVERAGE VELOCITY
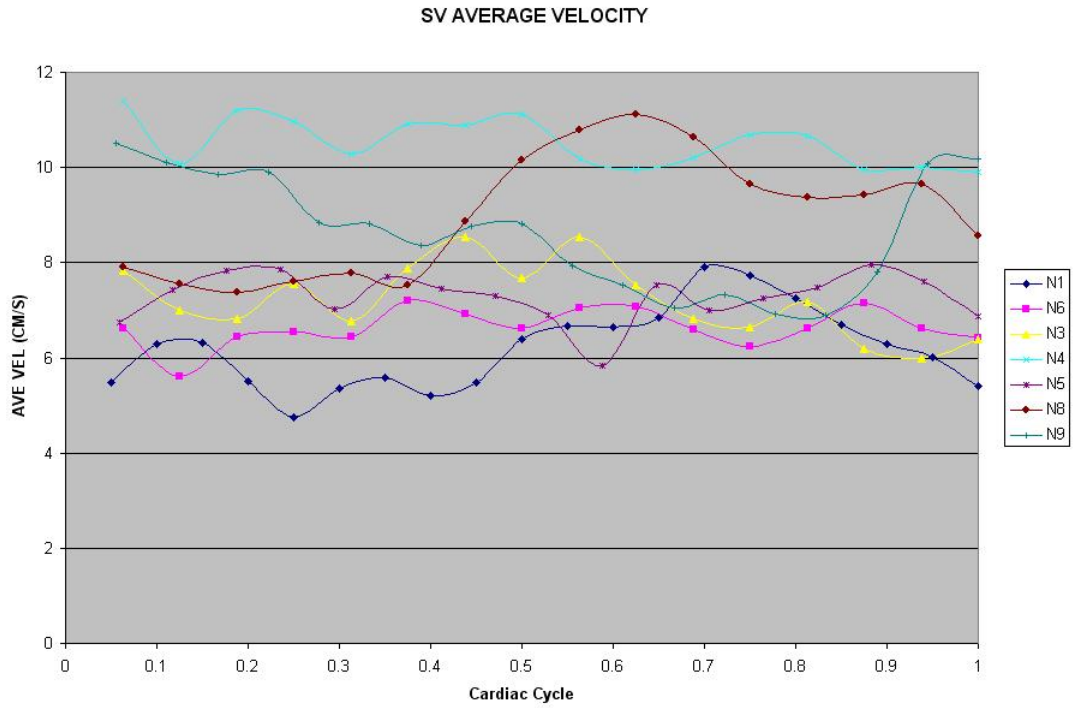
Figure 56: Normal Subject Average SV Cross-Sectional Velocity (cm/s)
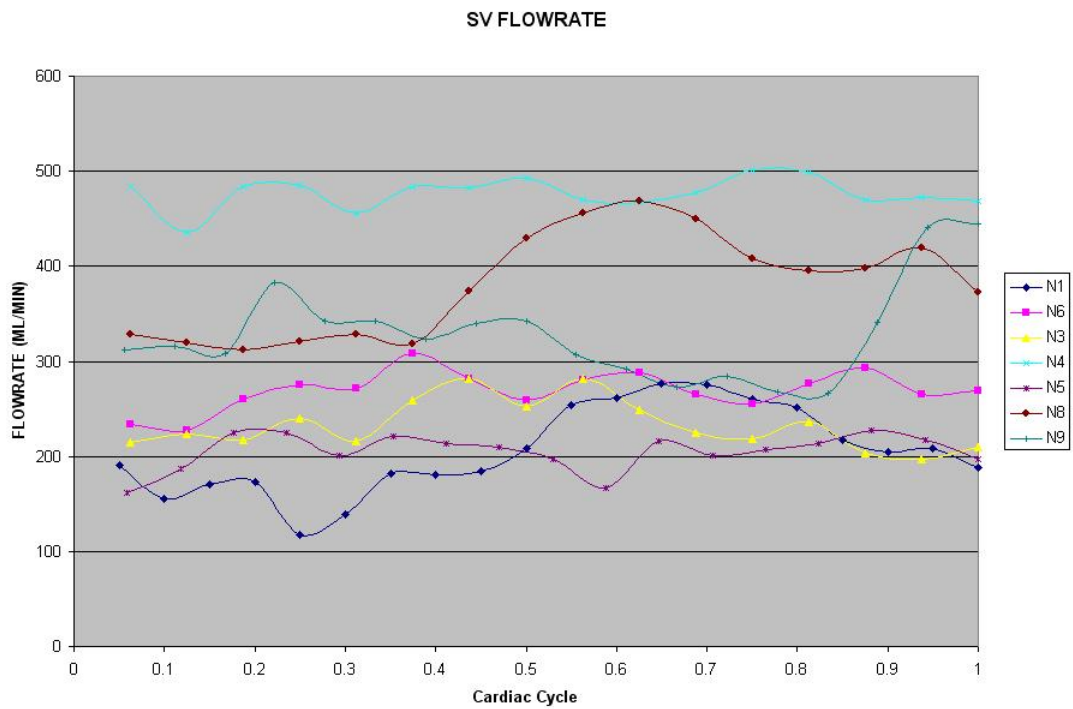
SV FLOWRATE

Figure 57: Normal Subject Average SV Cross-Sectional Flow Rate (ml/min)

Velocity was successfully obtained in 4 subjects. The cross-sectional velocity profiles were skewed as expected at a bifurcation. RPV cross-sectional velocity profiles at the time of maximum velocity can be seen in Figure 58.

(a) N3

(b) N4

(c) N5

(d) N9
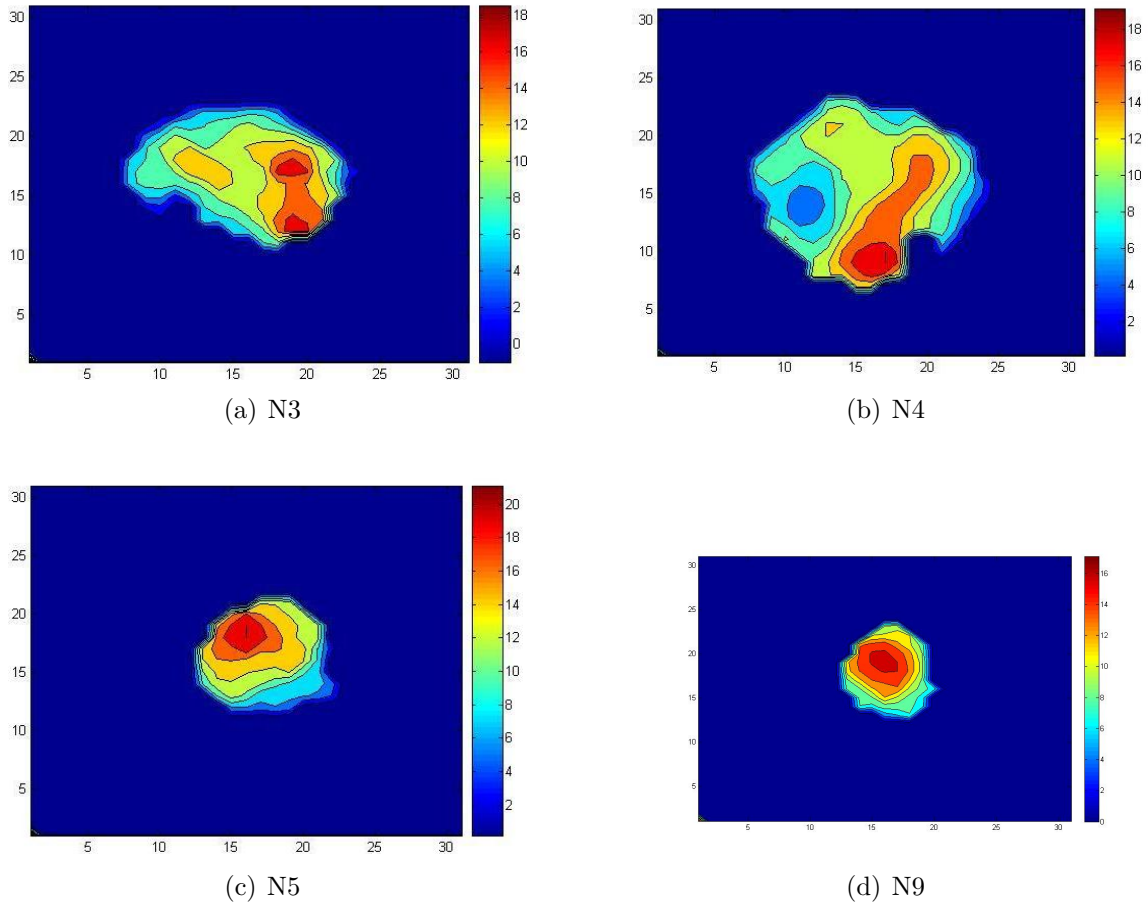
Figure 58: Normal RPV Cross-sections displaying Velocity Magnitude (cm/s) at time of maximum velocity and at the same anatomical orientation. Note that the spatial and velocity scales differ among the figures.
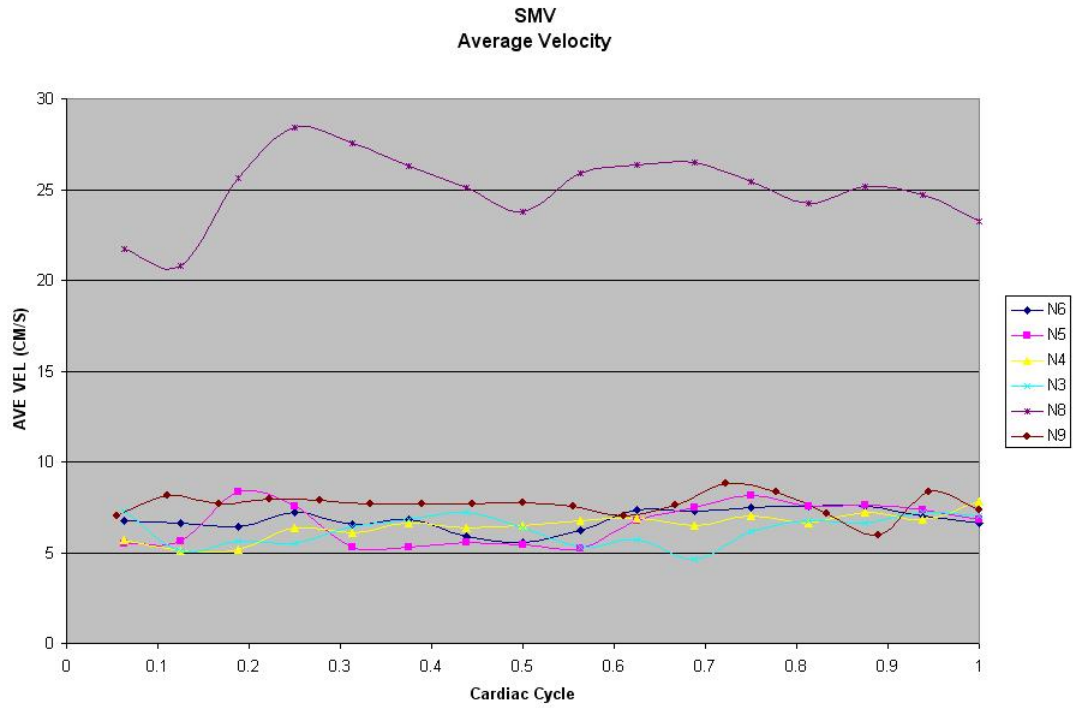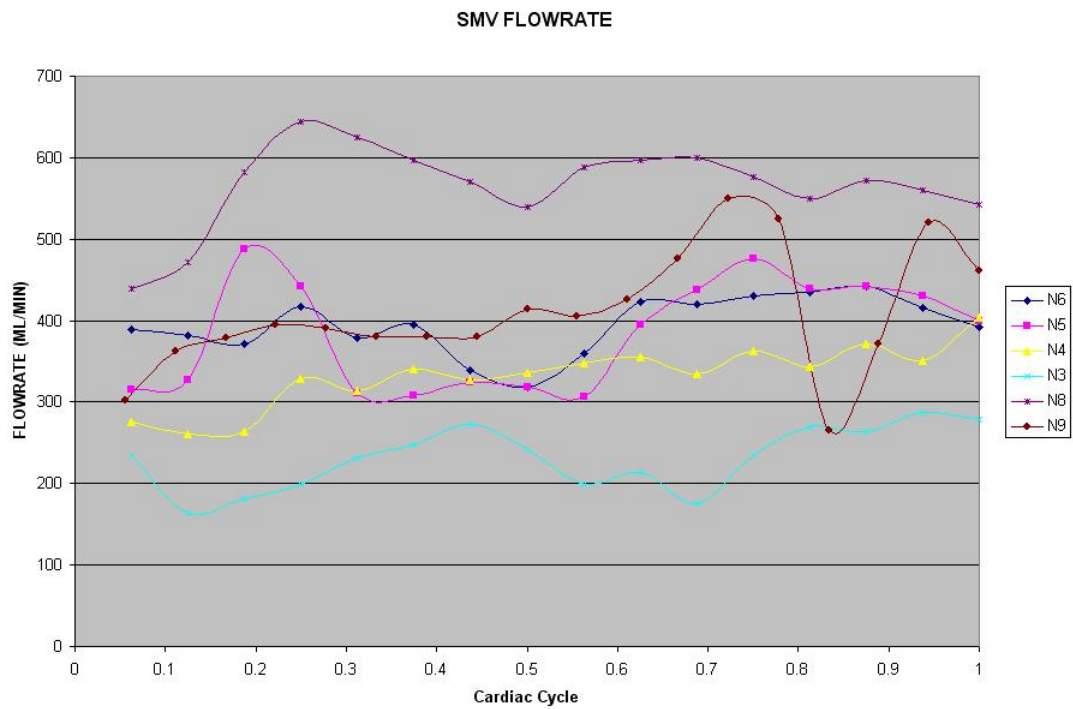
RPV area ranged from 0.684 - 1.23 cm^2. Generally, very small variations were seen in the velocity and flow rate waveforms (Figures 59 & 60). The average velocity was 10.4 cm/s and the average flow rate was 606 ml/min. Results for the RPV can be found in Table 15.
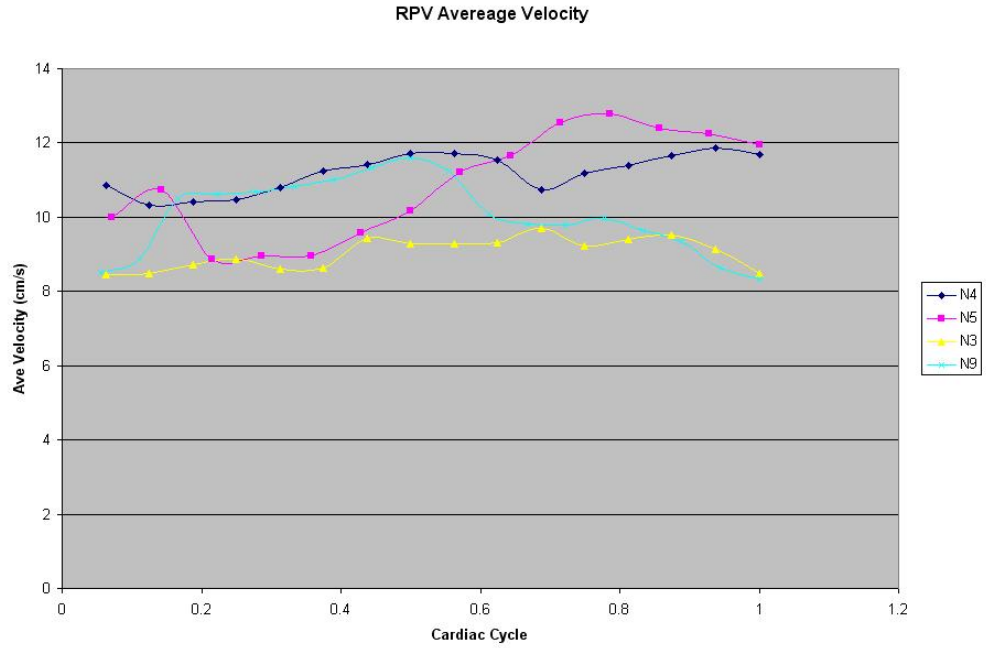
Figure 59: Normal Subject Average RPV Cross-Sectional Velocity (cm/s)
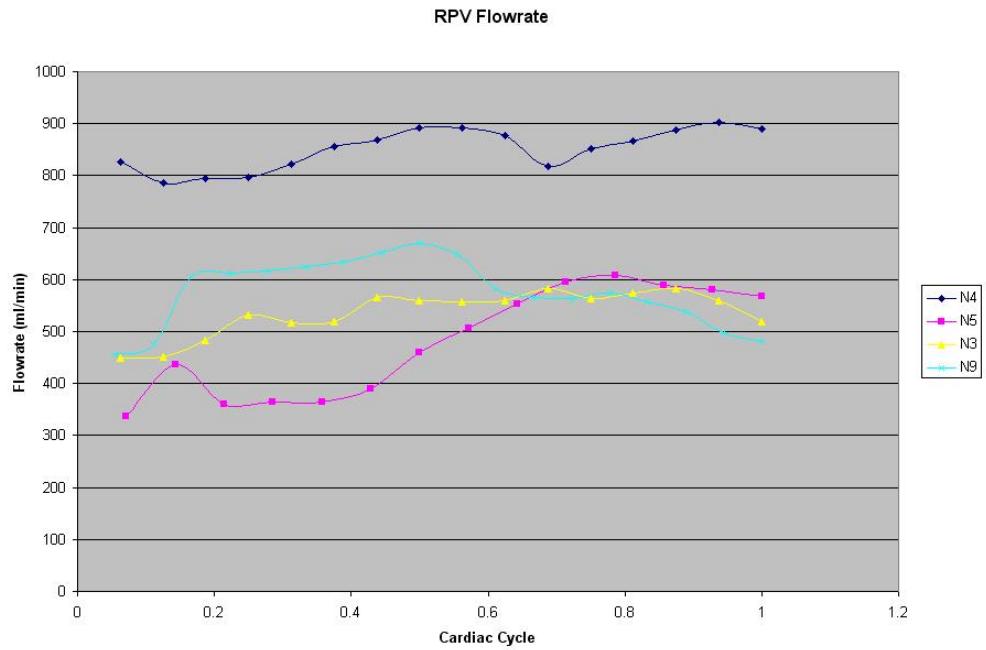
Figure 60: Normal Subject Average RPV Cross-Sectional Flow Rate (ml/min)

Table 15: Normal RPV Results

	Average Velocity (cm/s)	Velocity Range	Average Flow rate (ml/min)	Flow Rate Range	Area (cm²)
N3	9.67	1.53	518.7	114.9	0.87
N4	11.1	1.85	881.3	185.2	1.23
N5	10.86	3.92	479.5	269.7	0.684
N9	10	2.27	575	151.4	0.875

6.1.2.5 Portal Vein Flow Split

The flow split between the left and right portal vein branches was calculated and the results are given in Table 16. This calculation was done by taking the ratio of average RPV flow over the average PV flow the LPV flow was then the difference. The trend in two of the three was for a greater percentage of blood to go to the RPV.

Table 16: Normal Flow Split

Subject	Flow Split (RPV/LPV)
N3	0.9/0.1
N5	0.77/0.23
N9	0.75/0.25

6.1.2.6 Portal Flow Compositions

The composition of portal vein flow was determined and the results can be seen in Table 17. In all cases the results are consistent and the SMV blood composed a majority of the PV blood.

6.2 Computational Models

In order to understand portal venous flow in greater detail, CFD was employed to calculate the flow field for two of the normal subjects.

Table 17: Normal PV Contributions

Subject	PV Flow Contributions (SMV/SV)
N1	0.62/0.38
N3	0.58/0.42
N5	0.66/0.34
N6	0.76/0.24
N8	0.64/0.36
N9	0.57/0.43

6.2.1 Normal Subject 3

In order to impose a parabolic velocity profile for the SMV and SV inlets, the inlets were extended to allow the flow to develop. The outlets were also extended due to the outflow impositions. Table 18 provides the extension and mesh details.

Table 18: N3 Mesh Parameters

SV	40 cm
SMV	100 cm
RPV	30 cm
ARPV	20 cm
LPV	20 cm
Mesh Interval	1 mm
No. Volumes	687237

6.2.1.1 Steady Flow Calculations

The boundary conditions were taken from the PC-MR data collected and can be found in Table 19. Three different steady flow calculations were performed, one using the average inlet velocities over the cardiac cycle, one using the inlet velocities at maximum flow and one using the inlet velocities at minimum flow. The outflows are prescribed as flow splits and remained constant. In this case, there were two unknown outlets. Since they appeared to have roughly the same area, the flow was split evenly

between them.

Table 19: N3 Steady Boundary Conditions (Velocities and Flow Divisions)

	Average Values	Max Flow	Min Flow
SV (cm/s)	6.92	8.55	7
SMV (cm/s)	5.88	7.24	5.07
RPV	0.8	0.8	0.8
PRPV	0.1	0.1	0.1
LPV	0.1	0.1	0.1

For the average velocity case, the flow at the center of the PV was approximately parabolic although slightly skewed to the anterior side. The maximum and minimum flow cases illustrated the same skewing. Center PV cross-sectional velocity profiles at the time of maximum velocity can be seen in Figure 61.

There was evidence of modest mixing of the blood from the SMV and SV, as evidenced by plots of streamlines (Figure 62).
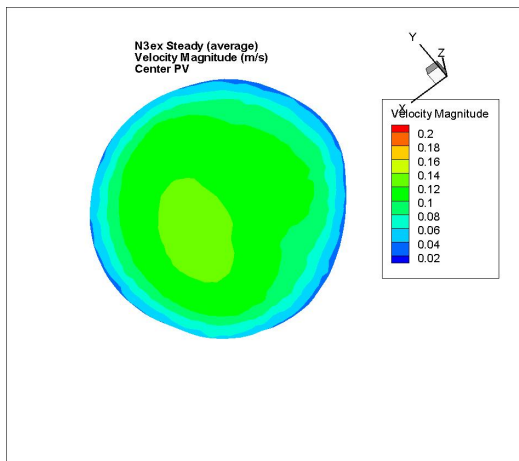
(a) Average
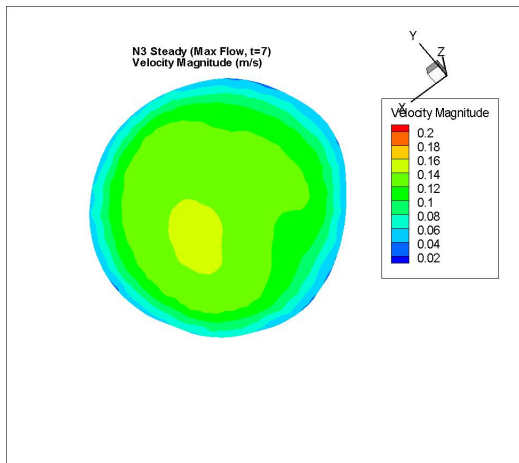
(b) Max Flow
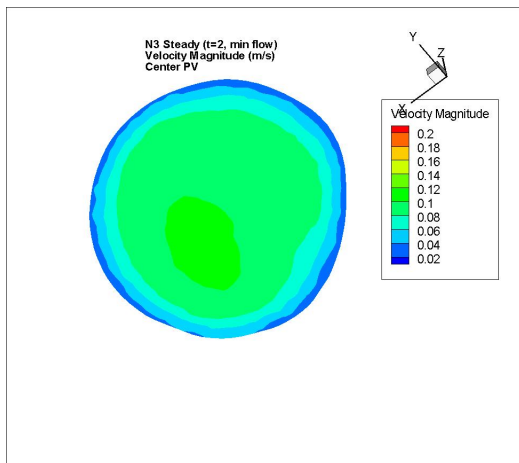
(c) Min Flow

Figure 61: N3 Steady CFD PV Cross-sections displaying Velocity Magnitude (m/s) at the same anatomical orientation
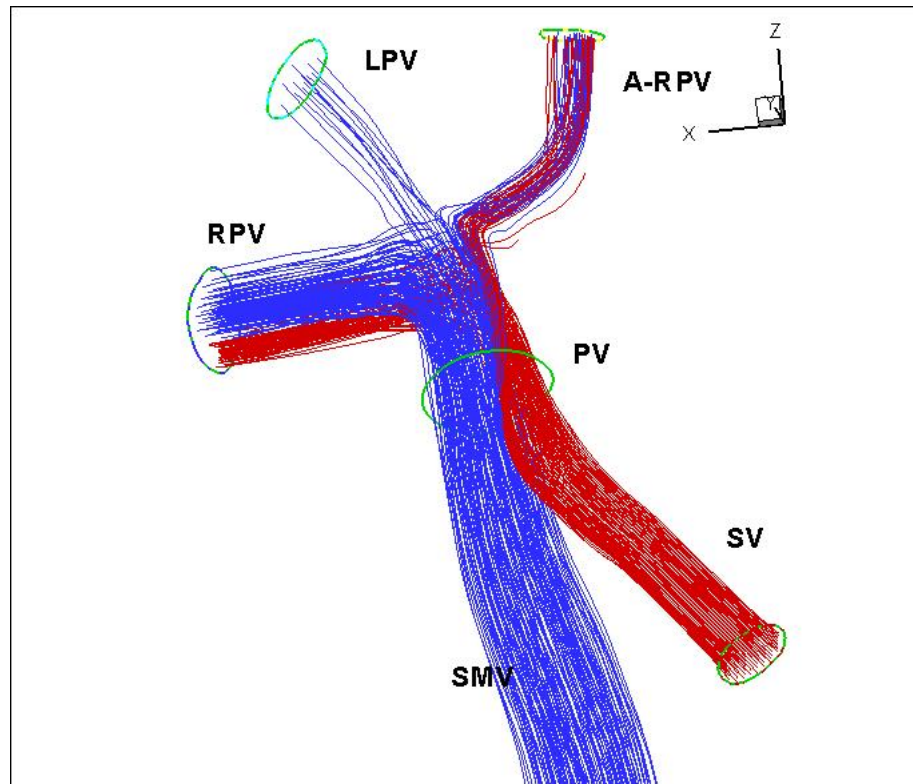
Figure 62: N3 Steady CFD Average Streamtraces; SMV (blue) and SV (red).

6.2.1.2 Flow Contribution Calculations

The flow contribution of blood from the SMV to the right and left portal veins was calculated and results can be found in Table 20. The streamtraces show the movement of the fluid towards the outlets (Figure 63). A visual representation of the SMV cross-section shows which streamlines went to which corresponding outlet (Figure 64). SMV blood is the major contributor to the RPV and LPV contributing to 91% of the RPV flow, 96% to the LPV and 21% to the Posterior-RPV. A total of 95% of the SMV blood went to a RPV branch.

Table 20: N3 Flow Contributions

Vessel	Flow Rate (ml/min) (% composed of SMV blood)
Inlets	
SMV	470
Outlets	
RPV	475
PRPV	59
LPV	59
SMV to Outlets	
SMV/RPV	434 (0.91)
SMV/PRPV	12 (0.21)
SMV/LPV	56 (0.96)

Figure 63: N3 Flow Contribution Streamtraces; RPV (red), PRPV (yellow) and LPV (Green)
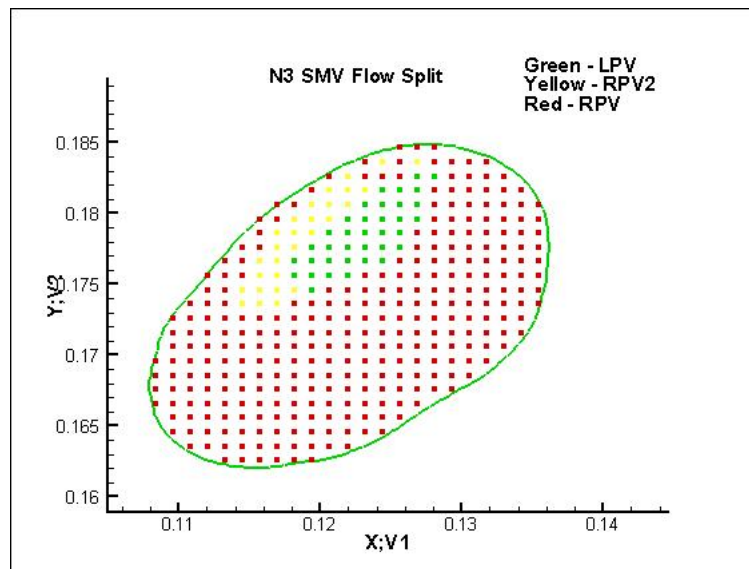
Figure 64: N3 SMV Cross-Section illustrating Flow Contributions

6.2.1.3   Unsteady Flow Calculations

Although there were slight variations in the velocity and flow over the cardiac cycle, unsteady calculations were performed to assess the validity of assuming quasisteady flow. The velocity and flow for N3 from the MR data are found in Figures 65 and 66.
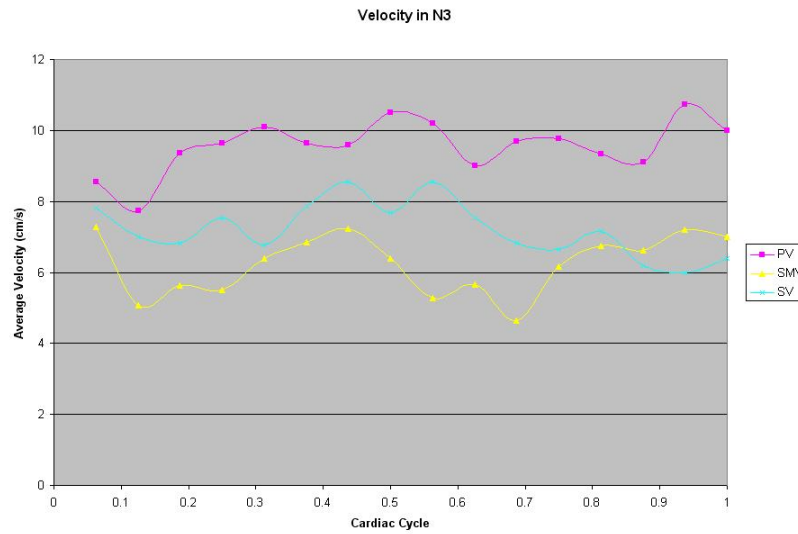
Figure 65: N3 Inlet Velocities (cm/s)
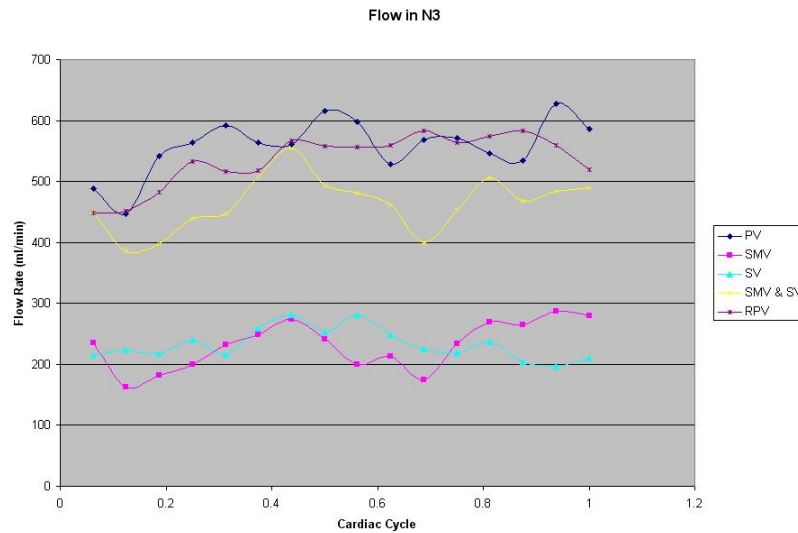
Figure 66: N3 Flow Rate (ml/min)

The inlet velocities for the SMV and SV were used as the boundary conditions

for the unsteady calculations. The center PV velocity magnitude cross-sections were similar to the steady flow calculations done at maximum and minimum flow. A comparison of the cross-sections can be found in Figures 67 & 68. The maximum unsteady case had a similar magnitude and profile as the steady case. The minimum unsteady case had slightly lower velocity magnitudes and a different skewing pattern.

(a) Unsteady Max Flow

(b) Steady Max Flow
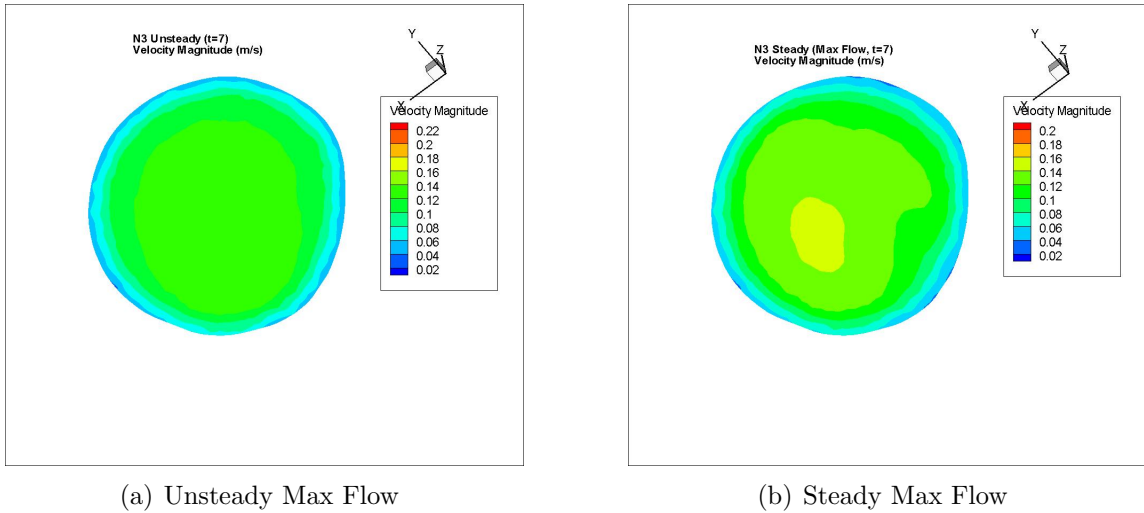
Figure 67: Unsteady Calculations Comparison: PV Cross-sections displaying Velocity Magnitude (m/s)Note: Different Color Scale

(a) Unsteady Min Flow

(b) Steady Min Flow
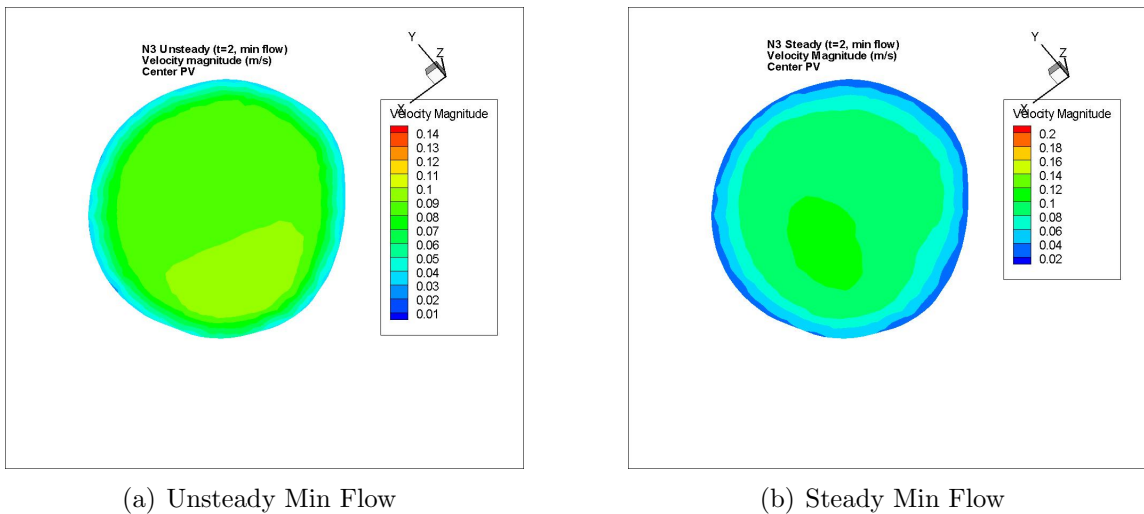
Figure 68: Unsteady Calculations Comparison: PV Cross-sections displaying Velocity Magnitude (m/s)Note: Different Color Scale

6.2.1.4 N3 Validation

To validate the model the CFD results were compared to the MR results. Although the MR images were not taken exactly perpendicular to the vessel axis, the skewing, area of high velocity, and magnitude are similar as evidenced by Figure 69.

(a) Average Steady Flow

(b) Average MR
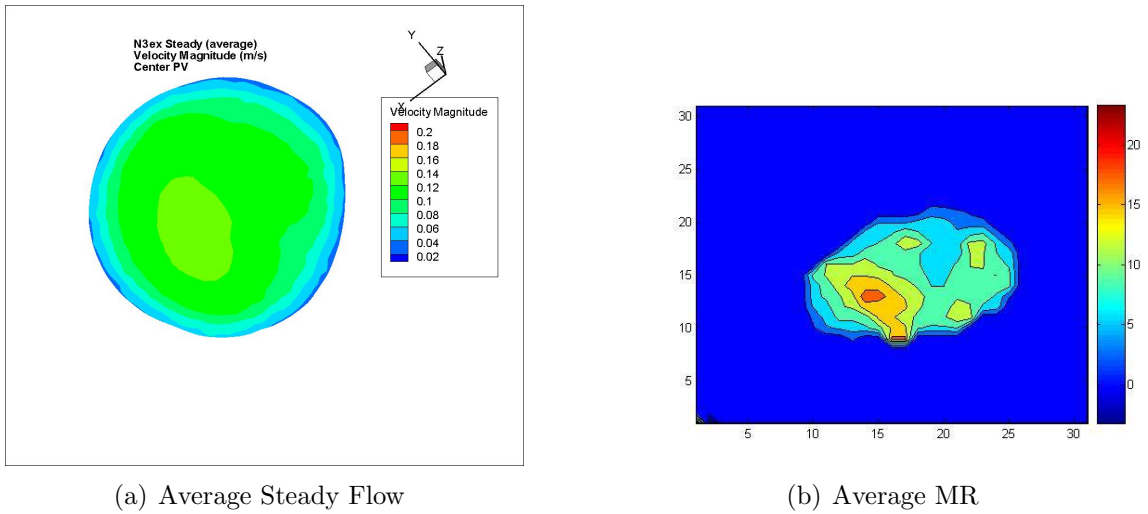
Figure 69: N3 PV Cross-Sections comparing Average CFD Result to MR Data

The results for maximum flow and minimum flow were also compared with their MR counterparts, and again the velocity profile and magnitude compared favorably. The comparisons can be seen in Figures 70 and 71.
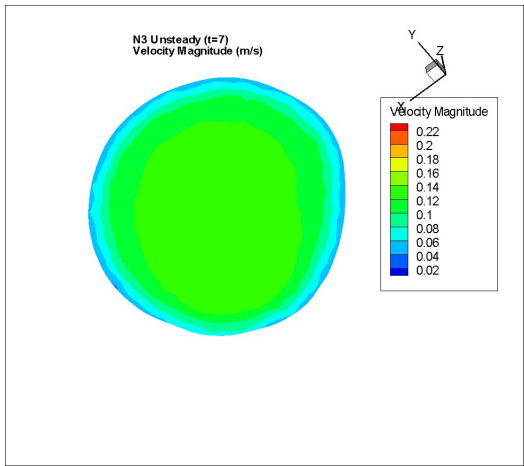
(a) Max Flow
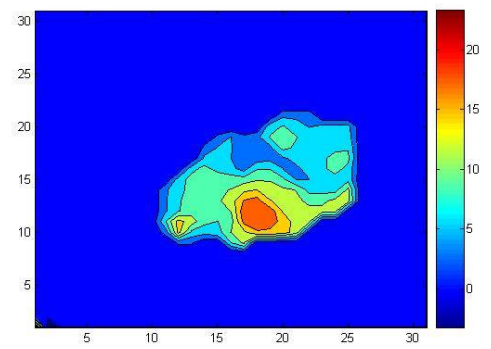
(b) MR Data Time Point 7

Figure 70: N3 PV Cross-Sections comparing Max Flow Unsteady CFD Result to MR Data
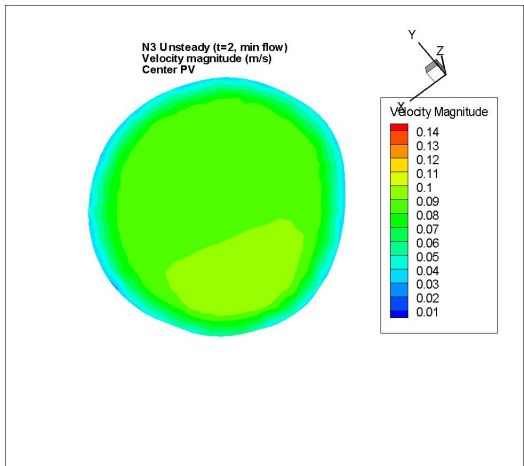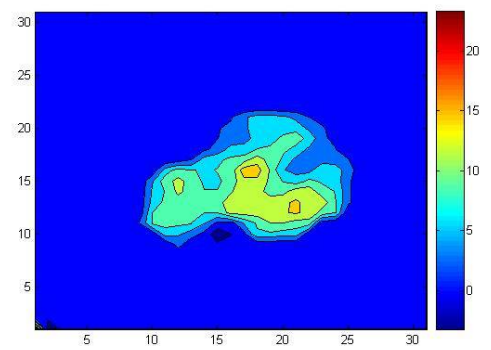
(a) Min Flow

(b) MR Data Time Point 2

Figure 71: N3 PV Cross-Sections comparing Min Flow Unsteady CFD Result to MR Data

6.2.2 Normal Subject 9

The SMV and SV inlets were again extended to allow the flow to develop. The outlets were also extended due to the outflow impositions. Table 21 provides the extension and mesh details.

Table 21: N9 Mesh Parameters

SV	20 cm
SMV	30 cm
RPV	30 cm
LPV	20 cm
Mesh Interval	1 mm
No. Volumes	727225

6.2.2.1 Steady Flow Calculations

The boundary conditions were taken from the PC-MR data collected and can be found in Table 22. The inlet velocities were the average velocities over the cardiac cycle. The outflows are prescribed as flow splits and remained constant.

Table 22: N9 Steady Boundary Conditions (Velocities and Flow Division)

	Average Values
SV (cm/s)	8.7
SMV (cm/s)	7.64
RPV	0.75
LPV	0.25

The velocity at the center of the PV was skewed to the posterior side. A center PV cross-sectional profile of velocity magnitude can be seen in Figure 72. The stream-traces showed greater mixing of the blood than N3 and also some rotation (Figure 73).
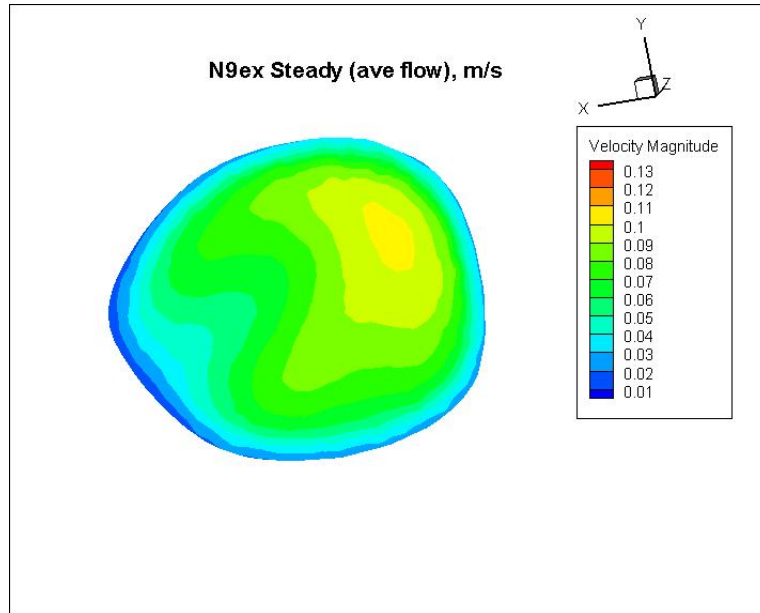
Figure 72: N9 Center PV Cross-Sections Velocity Magnitude (m/s)
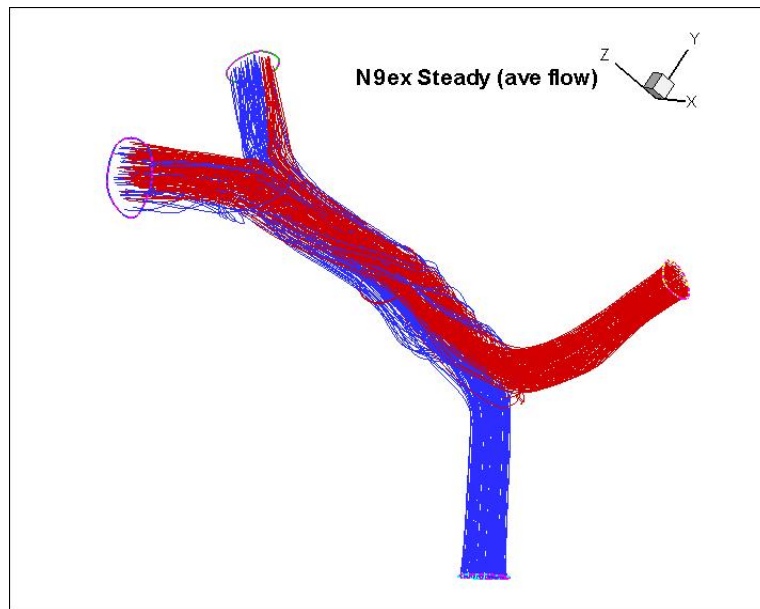
Figure 73: N9 Streamtraces; SMV (blue), SV (red).

6.2.2.2 Flow Contribution Calculations

The flow contribution of blood from the SMV to the right and left portal veins was calculated and results can be found in Table 23. 26% of the SMV blood went to the

LPV and 63% went to the RPV thus the majority of the SMV flow did go to the RPV. LPV blood is composed of 94% SMV blood and RPV blood is composed of 48% SMV blood. Even though the majority of the SMV flow supplies the RPV, the SMV is the major contributor to the LPV. The streamtraces show the movement of the fluid towards the outlets (Figure 74). A visual representation of the SMV cross-section shows which streamlines went to which corresponding outlet (Figure 75).

Table 23: N9 Flow Contributions

Vessel	Flow Rate (ml/min) (% composed of SMV blood)
Inlets	
SMV	262
Outlets	
RPV	347
LPV	72
SMV to Outlets	
SMV/RPV	166 (0.48)
SMV/LPV	67 (0.94)

6.2.2.3   Unsteady Flow Calculations

Again, quasisteady flow was assessed and unsteady calculations run. The velocity and flow for N9 from the MR data are found in Figures 76 and 77.

The inlet velocities for the SMV and SV were used as the boundary conditions for the unsteady calculations. The unsteady cross-sectional velocity profile at a time point (time point 8) with similar inlet velocities to the average steady case was compared to the steady case (Figure 78). The magnitude was similar to the steady calculations but the skewing was a little more inferior. Even with these differences, quasisteady flow may still be applicable.
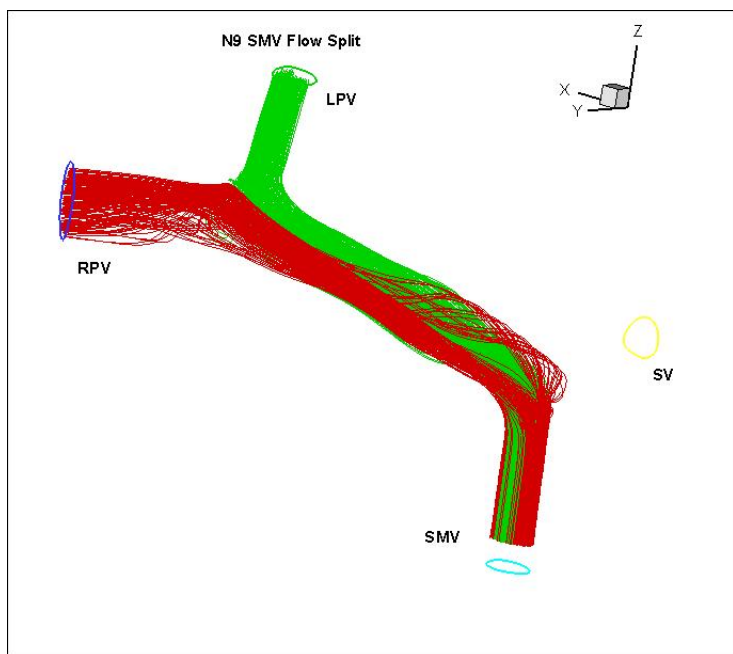
Figure 74: N9 Flow Contribution Streamtraces; RPV (red) and LPV (green).
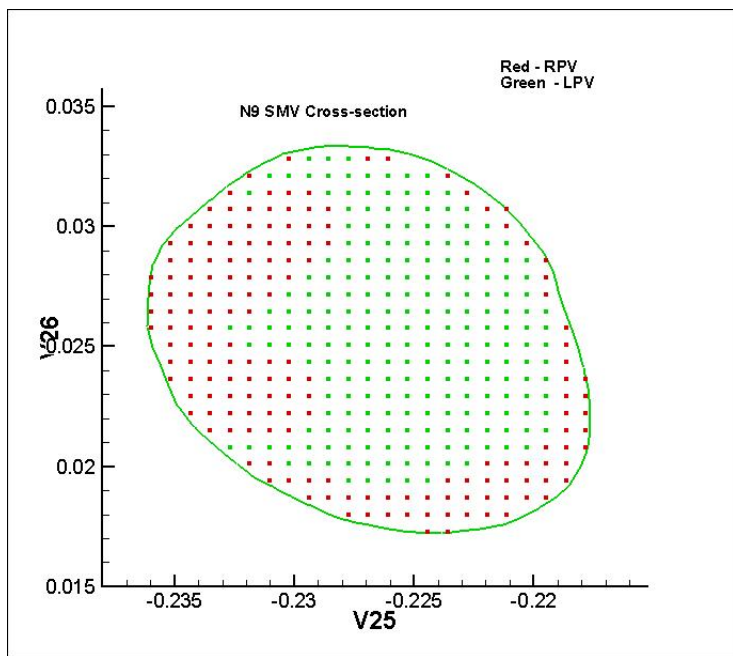
Figure 75: N9 SMV Cross-Section illustrating Flow Contributions
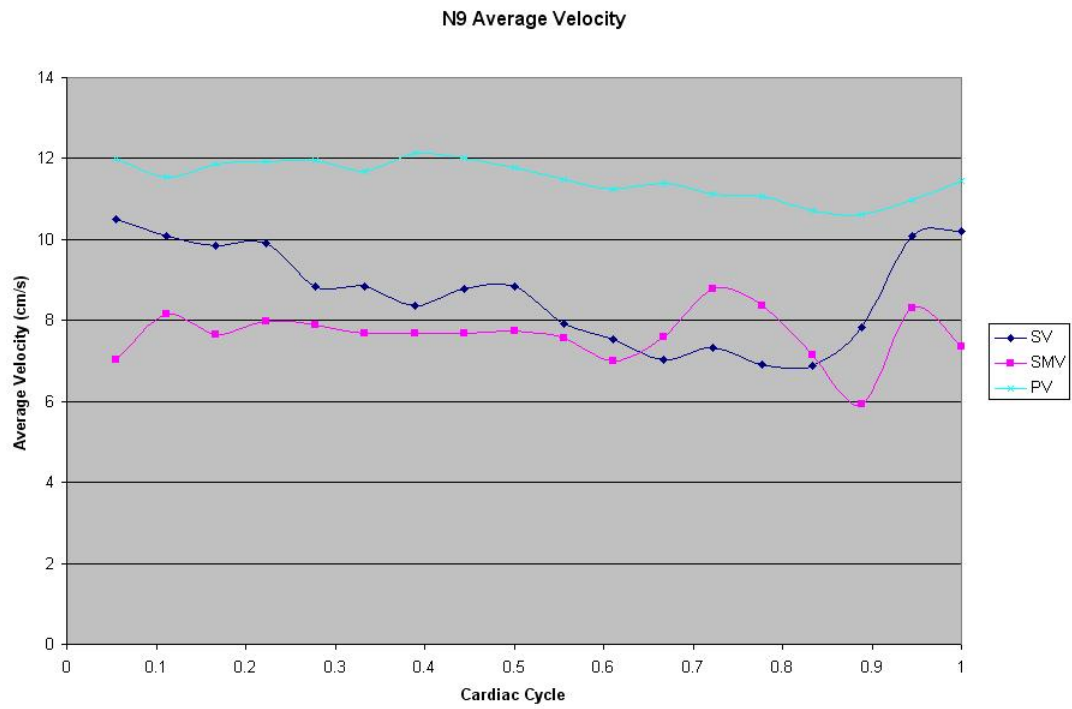
Figure 76: N9 Inlet Velocities (cm/s)
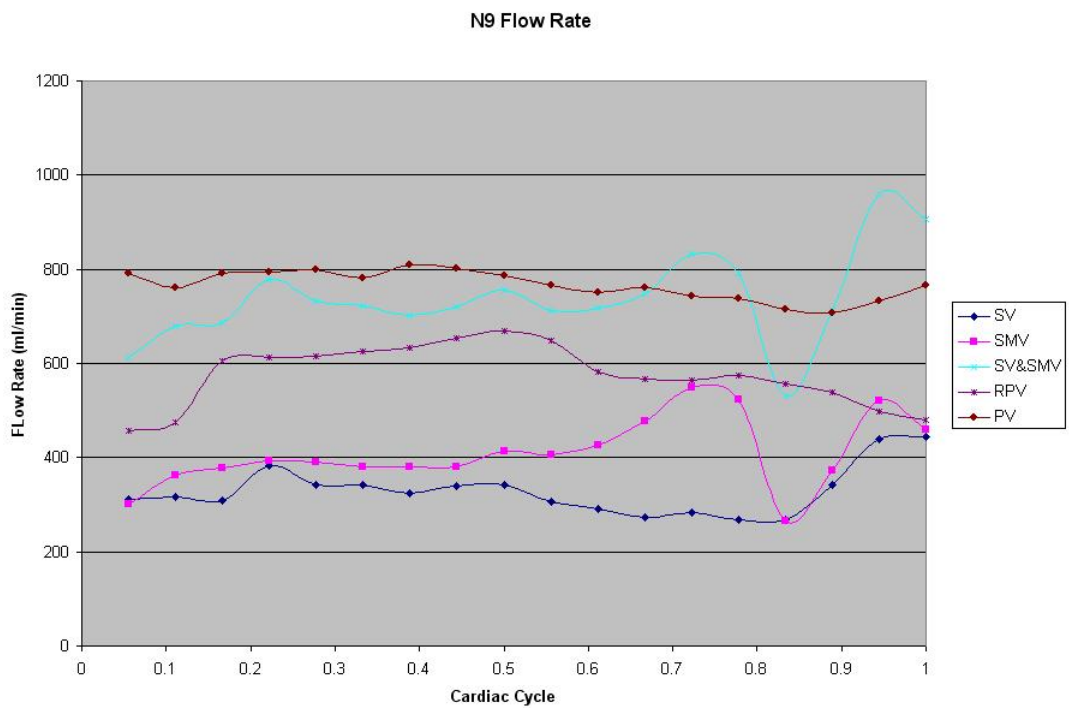
Figure 77: N9 Flow Rate (ml/min)
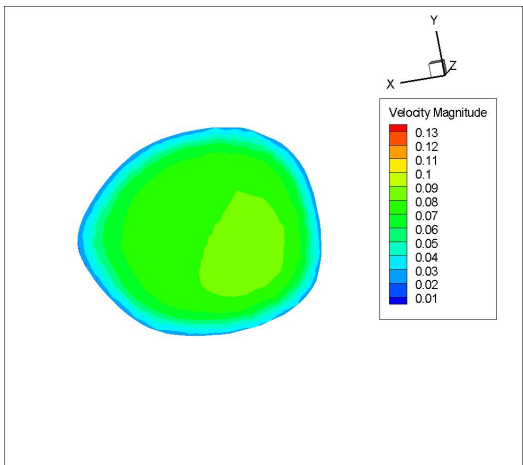
(a) Unsteady Time Point 8   (b) Average Steady Flow
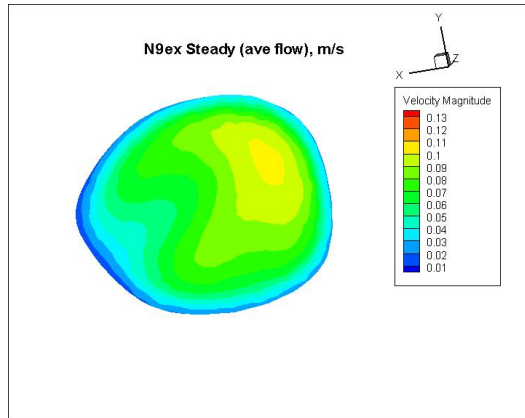
Figure 78: N9 Unsteady PV Cross-Section Velocity Magnitude (m/s)

6.2.2.4 Validation

To validate the model the CFD results were compared to the MR results. The MR data shows a more centered parabolic-like profile while the CFD data shows a slight skewing to the posterior side. The velocity magnitudes are slightly lower in the CFD results for all cases. Unsteady CFD results were compared with the MR data from the same time step, including average, maximum, and minimum flow. These comparisons can be seen in Figures 79, 80, and 81.

(a) Average Unsteady Flow Time Step 8   (b) Average MR Time Step 8
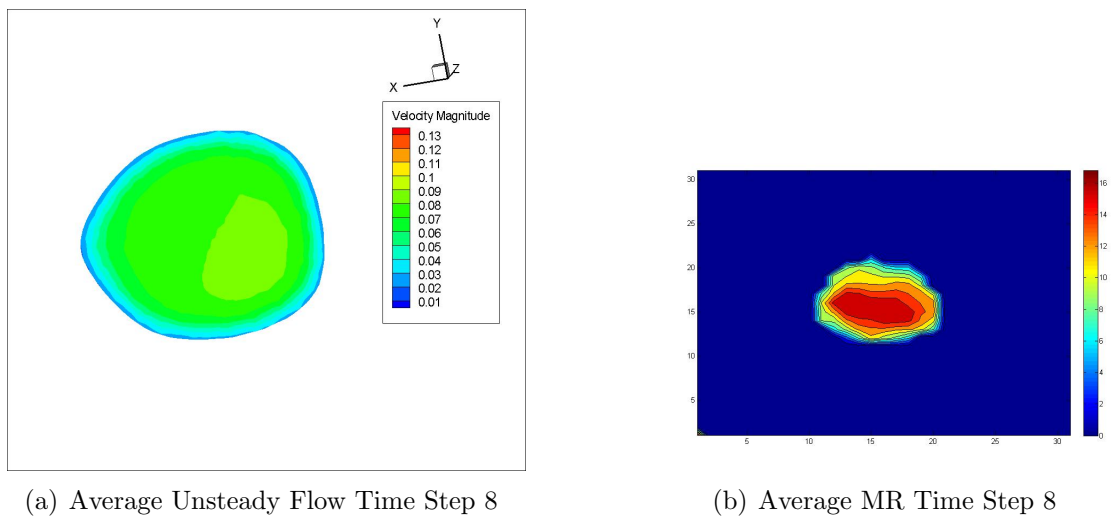
Figure 79: N9 PV Cross-Sections comparing Unsteady Average CFD Result to MR Data; Note: Different Scales
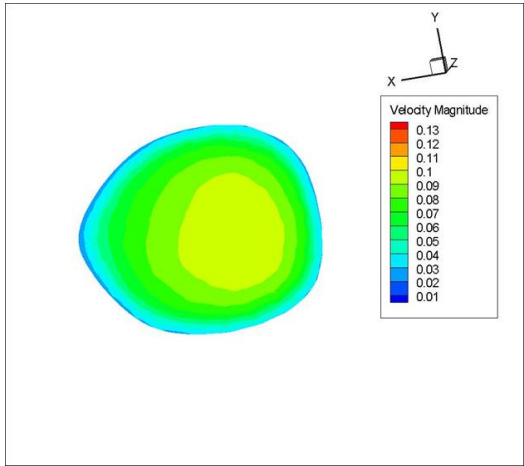
(a) Unsteady Max Flow Time Step 17
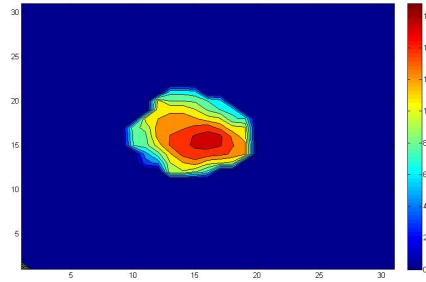
(b) MR Data Time Point 17

Figure 80: N9 PV Cross-Sections comparing Max Flow Unsteady CFD Result to MR Data; Note: Different Scales
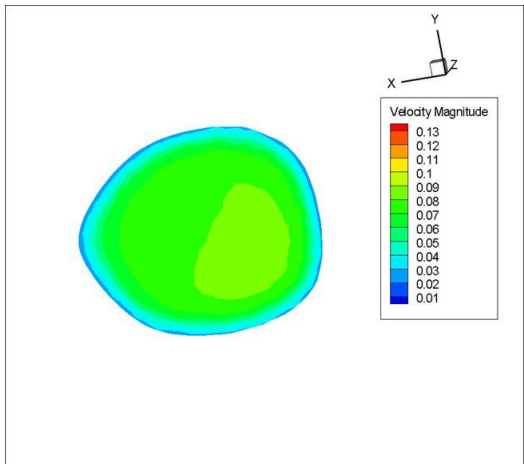
(a) Unsteady Min Flow Time Step 7
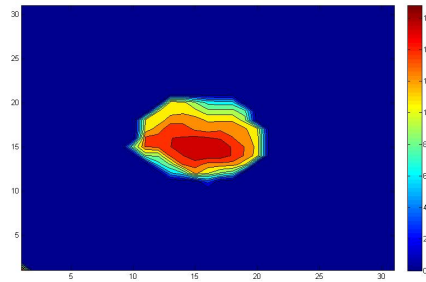
(b) MR Data Time Point 7

Figure 81: N9 PV Cross-Sections comparing Min Flow Unsteady CFD Result to MR Data; Note: Different Scales

CHAPTER VII

PATIENT PORTAL VENOUS HEMODYNAMICS

Specific Aim 3: Characterize hemodynamics in the portal venous system in patients with cirrhosis and portal hypertension.

7.1   MR Data Acquisition

The data set includes 4 patients who were already scheduled for an abdominal MRI with a diagnosis of cirrhosis. All subjects had more advanced cirrhosis. A summary of cirrhosis indicators for each patient can be found in Table 24

Table 24: Patient Cirrhosis Characteristics from MR

Parameter	D2	D4	D5	D6
Sex	M	M	F	F
Fibrosis	Moderate	Mod-Severe Diffuse	Moderate	Mode-Severe Diffuse
Inflammation	Moderate	Minimal	Moderate	Moderate
Varices	Mild	Mild	Moderate (no SV)	Moderate
Acites	No	No	No	Trace
Tumor	No	No	No	No
PV Thrombosis	No	No	No	No
Spleen Enlargement	Severe	Marked	Mild	Severe

7.1.1   Vessel Geometry

The geometry was successfully obtained in 3 subjects. Again the PV is fairly straight and different PV branch variations are seen, including a trifurcation in Figure 82. In D5 the splenic vein no longer exists, it has been replaced by a varice or shunt (Figure 83).
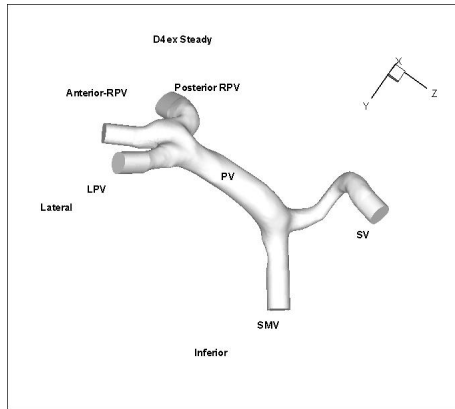
Figure 82: D4 Portal Vein Geometry
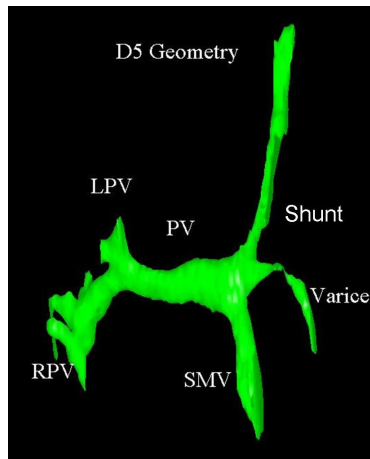
Figure 83: D5 Portal Vein Geometry
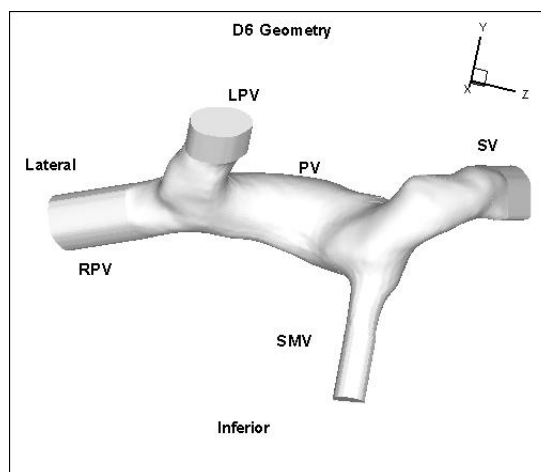
Figure 84: D6 Portal Vein Geometry

7.1.2 Velocity Measurements

The velocity measurements were taken at the same location as for the normal subjects-please refer to Figure 48 on page 63.

7.1.2.1 Portal Vein

The velocity was successfully obtained in 4 subjects. Some patients had skewed parabolic-like profiles while others showed multiple jets. The direction of the skewing was always to the posterior inferior side of the PV. Center PV cross-sectional velocity profiles at the time of maximum velocity can be seen in Figure 85.

(a) D2

(b) D4

(c) D5

(d) D6
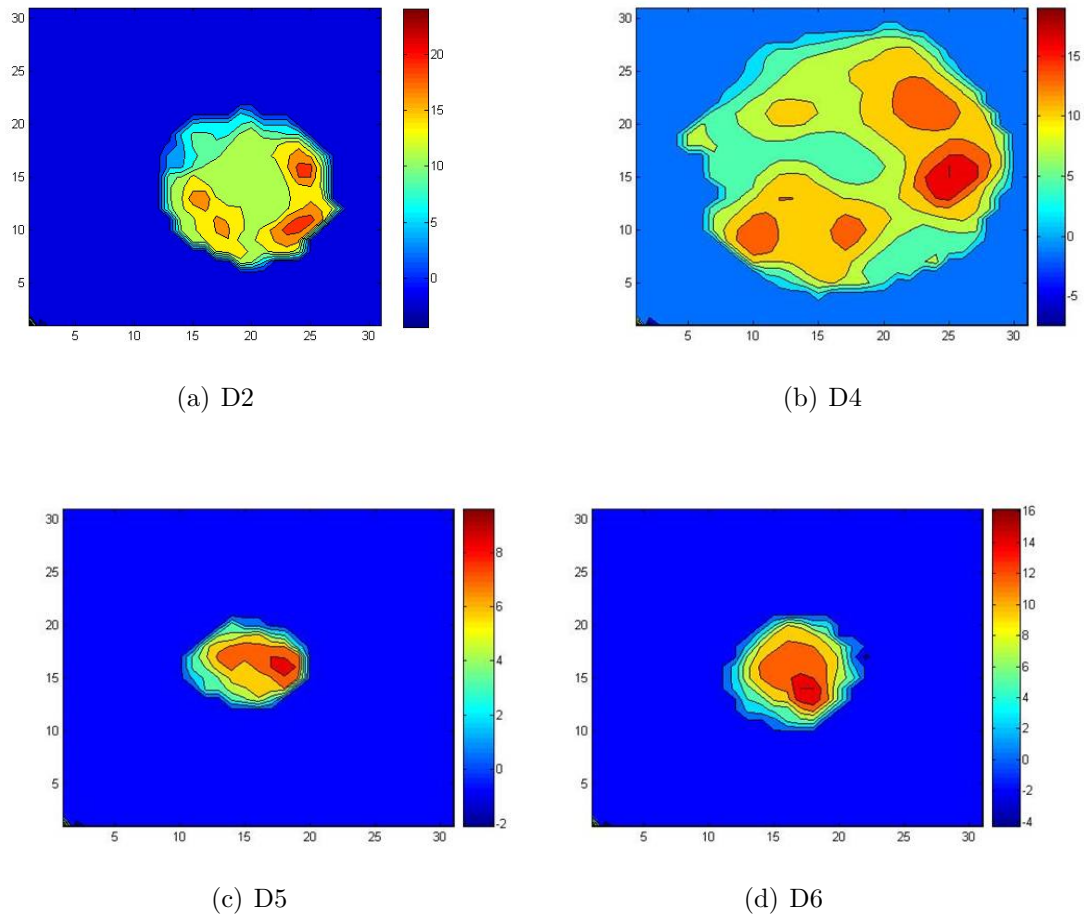
Figure 85: Patient PV Cross-sections displaying Velocity Magnitude (cm/s) at time of maximum velocity and at the same anatomical orientation. Note that the spatial and velocity scales differ among the figures.

PV area ranged from 1.35 - 2.41 cm^2. There were little velocity and flow rate changes over the cardiac cycle as seen in Figures 86 and 87. Note the lower velocity and flow in D5 which had no SV and a small SMV. The average velocity was 8.45 cm/s and the average flow rate was 1048 ml/min. Results for the PV can be found in Table 25.
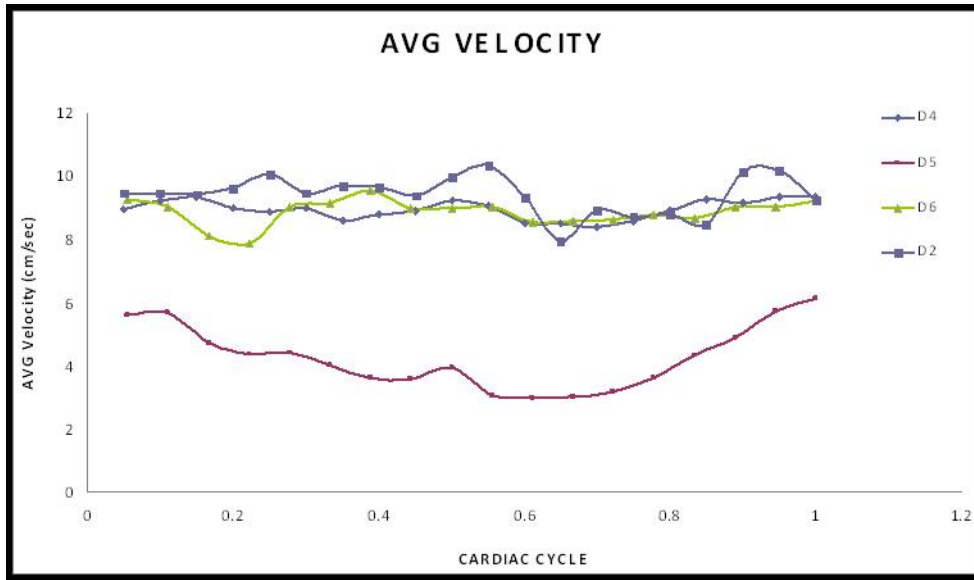
Figure 86: Patient Average PV Cross-Sectional Velocity (cm/s)
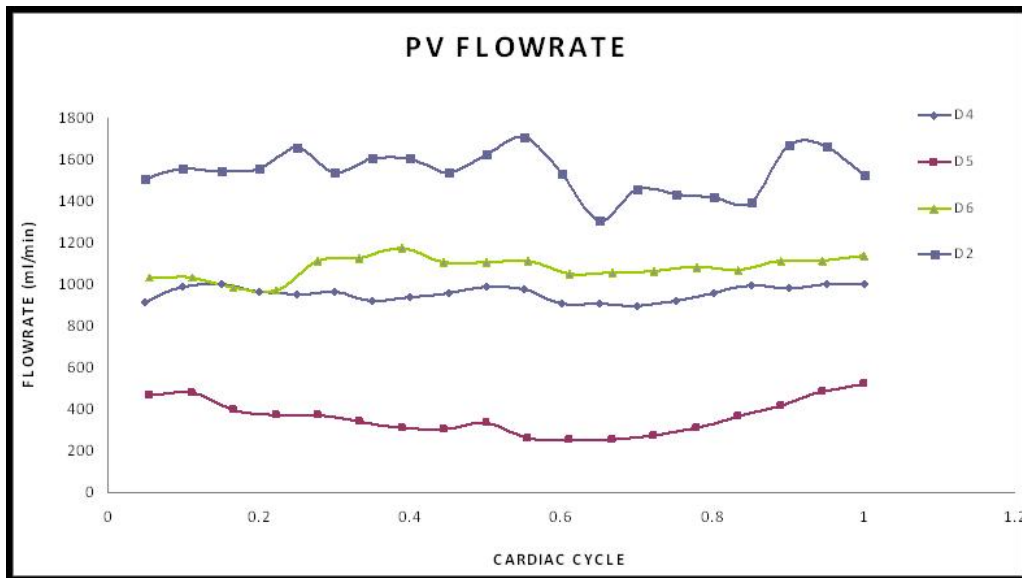
Figure 87: Patient Average PV Cross-Sectional Flow Rate (ml/min)

Table 25: Patient PV Results

	Average Velocity (cm/s)	Velocity Range	Average Flow rate (ml/min)	Flow Rate Range	Area (cm²)
D2	11.68	2.54	1788	424	2.41
D4	8.97	0.99	959	106	1.7
D5	4.28	3.12	363	265	1.35
D6	8.45	1.66	1080	204	1.88

7.1.2.2 Superior Mesenteric Vein

Velocity was successfully obtained in 3 subjects. The velocity profile was mainly centered and parabolic-like but reverse velocities were seen in one subject perhaps due to upstream varices. SMV cross-sectional velocity profiles at the time of maximum velocity can be seen in Figures 88.

SMV area ranged from 0.8 - 1.83 cm^2. There was some variation in the SMV average velocity and flow rate waveforms (Figures 89 & 90). The average velocity was 4.97 cm/s and the average flow rate was 394 ml/min. Results for the SMV can be found in Table 26.

Table 26: Patient SMV Results

	Average Velocity (cm/s)	Velocity Range	Average Flow rate (ml/min)	Flow Rate Range	Area (cm²)
D4	7.89	1.76	620	141	1.21
D5	4.18	2.76	263	174	0.8
D6	2.98	1.81	327	198	1.83
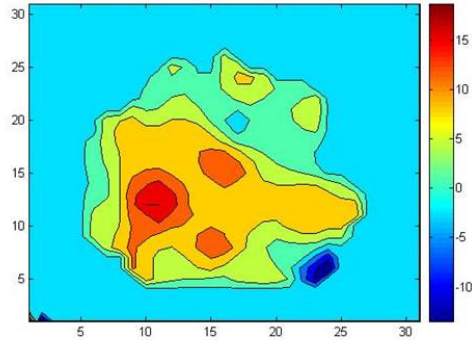
(a) D4
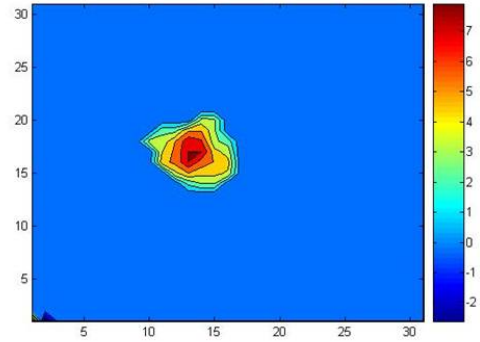
(b) D5
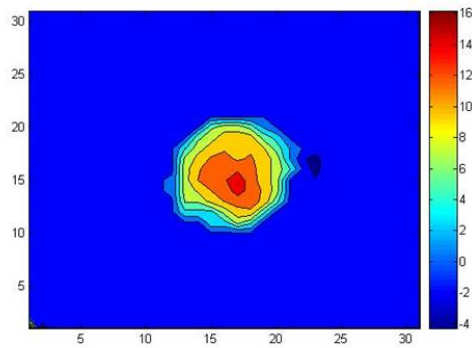
(c) D6

Figure 88: Patient SMV Cross-sections displaying Velocity Magnitude (cm/s) at time of maximum velocity and at the same anatomical orientation. Note that the spatial and velocity scales differ among the figures.
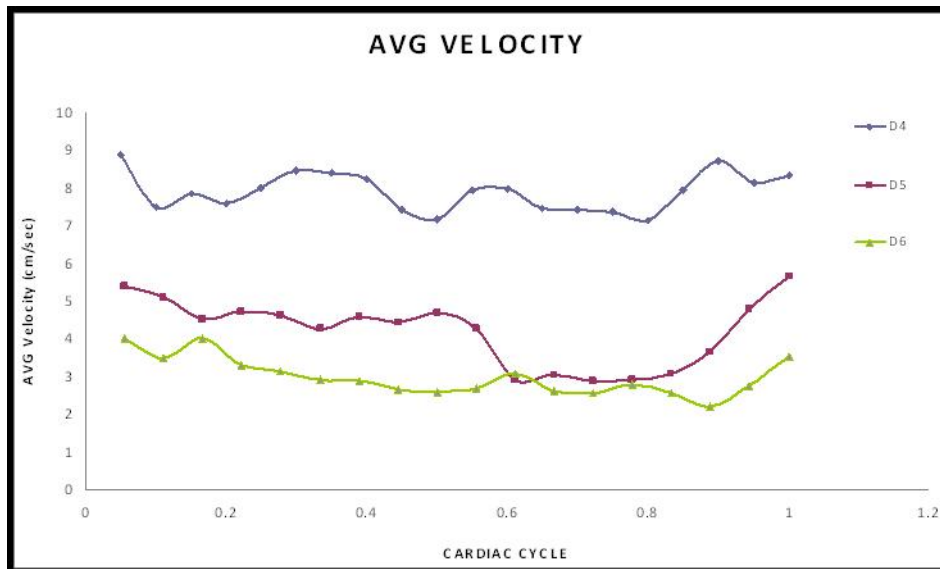
Figure 89: Patient Average SMV Cross-Sectional Velocity (cm/s)
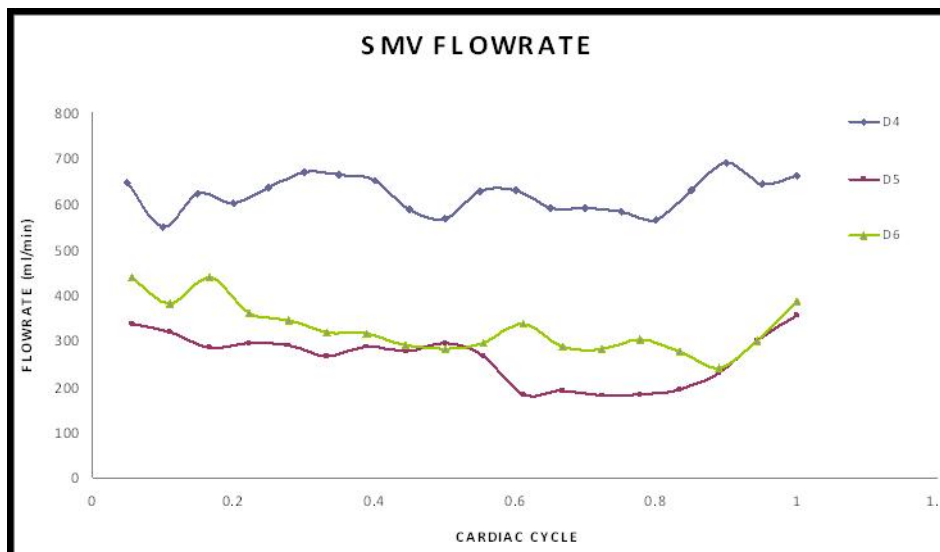
Figure 90: Patient Average SMV Cross-Sectional Flow Rate (ml/min)

100

Velocity was successfully obtained in 4 subjects. Due to the winding nature of the SV, skewed velocity profiles were seen. SV cross-sectional velocity profiles at the time of maximum velocity can be seen in Figure 91. Subjects D2 and D4 had areas of low velocity and contained some noise that could not be filtered out. The D5 SV profile represents the shunt.

(a) D2

(b) D4

(c) D5

(d) D6
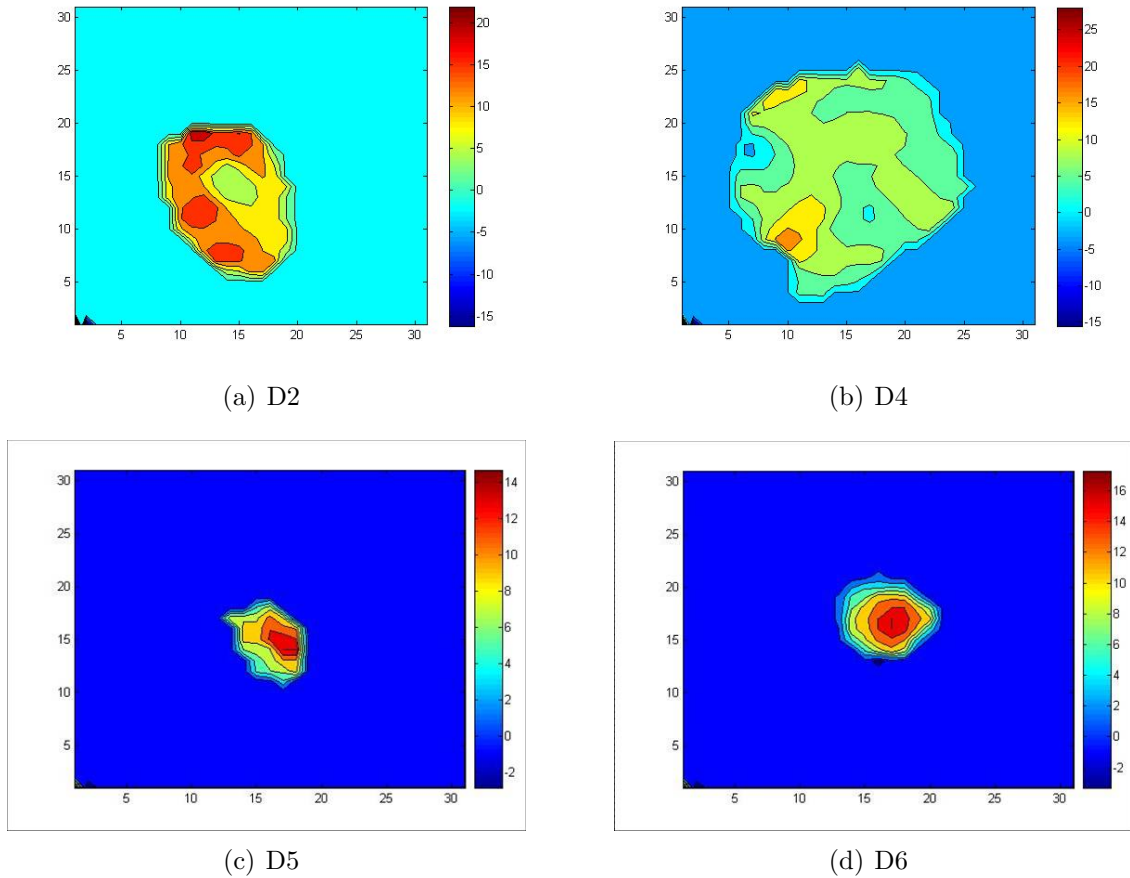
Figure 91: Patient SV Cross-sections displaying Velocity Magnitude (cm/s) at time of maximum velocity and at the same anatomical orientation. Note that the spatial and velocity scales differ among the figures.

SV area ranged from 0.834 - 1.7 cm^2. Generally little variations were seen in the velocity and flow rate waveforms (Figures 92 & 93). D2 had the largest variation in waveforms. The average velocity was 8.88 cm/s and the average flow rate was 666

ml/min. Results for the SV can be found in Table 27.
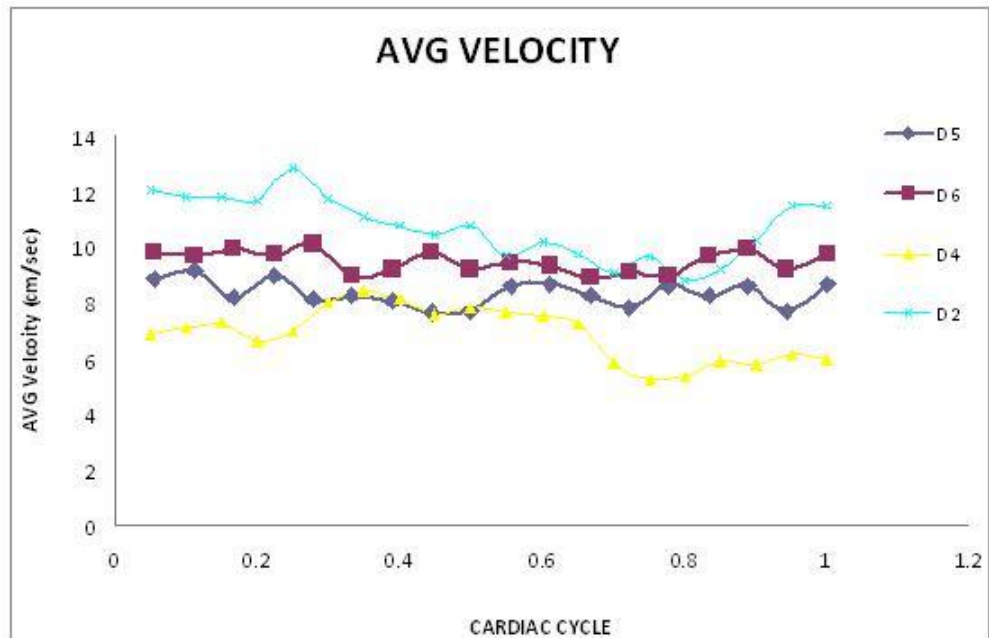
Figure 92: Patient Average SV Cross-Sectional Velocity (*cm/s*)
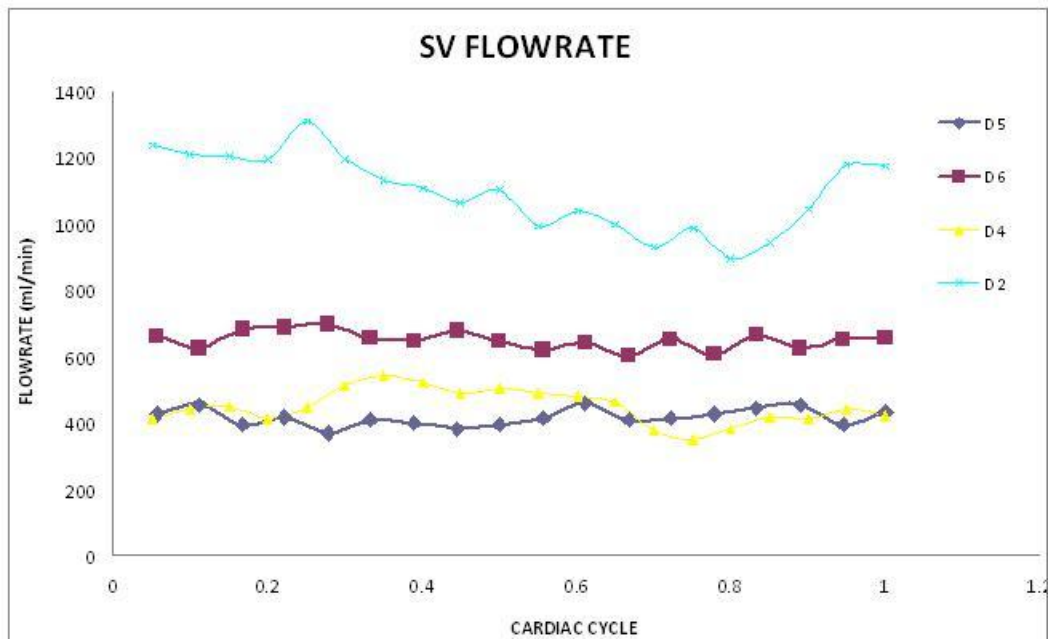
Figure 93: Patient Average SV Cross-Sectional Flow Rate (*ml/min*)

Table 27: Patient SV Results

	Average Velocity (cm/s)	Velocity Range	Average Flow rate (ml/min)	Flow Rate Range	Area (cm^2)
D2	10.8	3.7	1108	378	1.7
D4	6.89	3.21	449	193	1.06
D5	8.35	1.47	430	88	0.834
D6	9.52	1.17	685	75	1.14

Velocity was successfully obtained in one subject for the RPV and in one other subject for the LPV. The cross-sectional velocity profiles were skewed as expected at a bifurcation. RPV cross-sectional velocity profile at the time of maximum velocity can be seen in Figure 94 and LPV cross-sectional velocity profile at the time of maximum velocity can be seen in Figure 95.
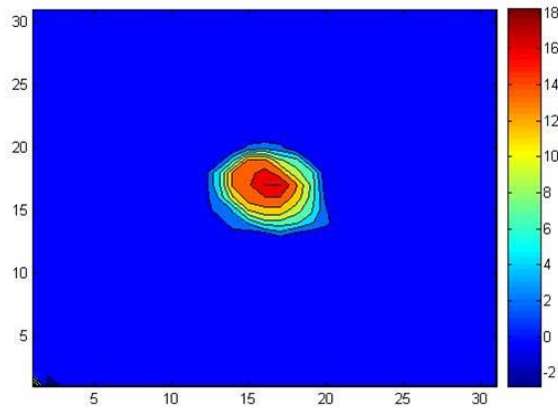
Figure 94: Patient (D6) Average RPV Cross-Sectional Velocity (cm/s)
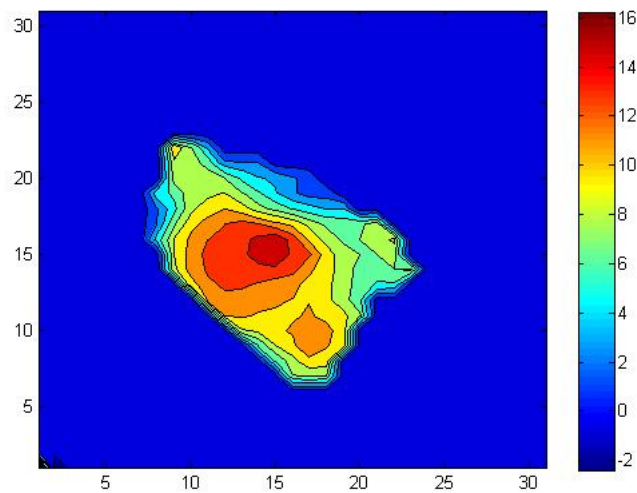
Figure 95: Patient (D4) Average LPV Cross-Sectional Velocity (cm/s)

The RPV area was 1.15 cm^2 and the LPV area was 0.5 cm^2. Generally, little variations were seen in the velocity and flow rate waveforms (Figures 96 & 97). The average velocity was 8.32 cm/s and the average flow rate was 603 ml/min for the RPV and 8.56 cm/s and 267 ml/min for the LPV. Results for the R/LPV can be found in Table 28.
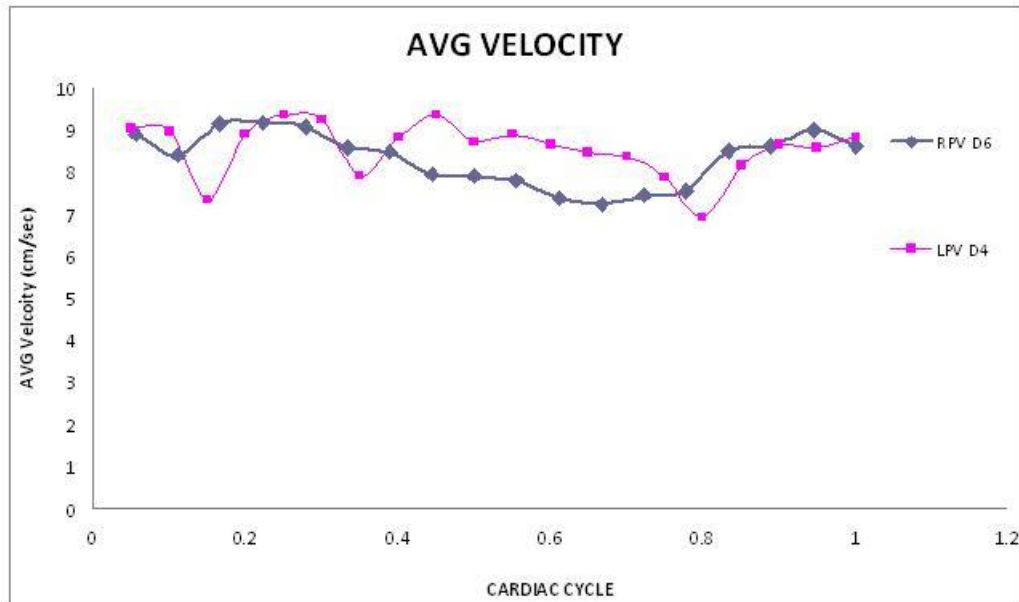
Figure 96: Patient Average R/LPV Cross-Sectional Velocity (cm/s)

Table 28: Patient R/LPV Results

	Average Velocity (cm/s)	Velocity Range	Average Flow rate (ml/min)	Flow Rate Range	Area (cm^2)
D4 (LPV)	8.56	2.45	267	75	0.5
D6 (RPV)	8.32	1.93	603	128	1.15
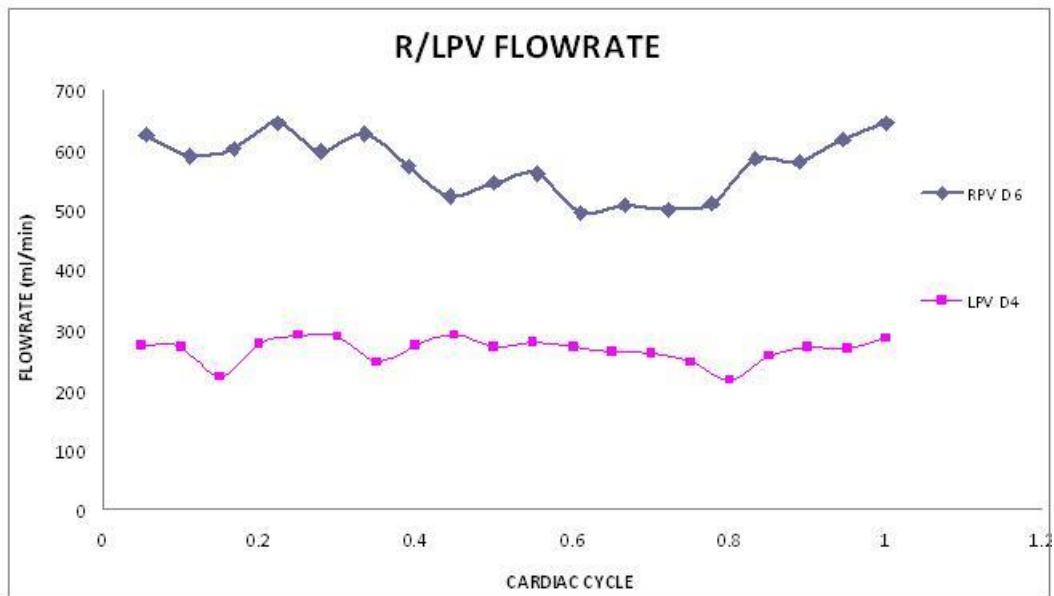
Figure 97: patient average R/LPV Cross-Sectional Flow Rate (ml/min)

7.1.2.5 Portal Vein Flow Split

The flow split between the left and right portal vein branches was calculated and the results are in Table 29. The flow to the RPV was greater than the flow to the LPV.

Table 29: Patient Flow Split

Subject	Flow Split (RPV/LPV)
D4	0.72/0.28
D6	0.56/0.44

7.1.2.6 Portal Flow Compositions

The composition of portal vein flow was determined and the results can be seen in Table 30. In two out of the three subjects the SMV contributed more than the SV.

Table 30: Patient PV Contributions

Subject	Flow Contributions (SMV/SV)
D2	0.61/0.39
D4	0.60/0.40
D6	0.32/0.68

7.2 Computational Models

In order to understand cirrhotic portal venous flow in greater detail, CFD was employed to calculate the flow field for two of the patients.

7.2.1 Patient 4

In order to impose a parabolic flow profile for the SMV and SV inlets, the inlets were extended to allow the flow to develop. The outlets were also extended due to the outflow impositions. Table 31 provides the extension and mesh details.

Table 31: D4 Mesh Parameters

SV	20 cm
SMV	40 cm
RPVA	30 cm
RPV	20 cm
LPV	30 cm
Mesh Interval	1 mm
No. Volumes	1,717,255

Table 32: D4 Steady Boundary Conditions (Velocities and Flow Division)

	Average Values	Max Flow	Min Flow
SV (cm/s)	6.89	8.01	5.26
SMV (cm/s)	7.76	8.21	6.98
RPV	0.36	0.36	0.36
ARPV	0.36	0.36	0.36
LPV	0.28	0.28	0.28

7.2.1.1   Steady Flow Calculations

The boundary conditions were taken from the PC-MR data collected and can be found in Table 32. Three different steady flow calculations were performed, one using the average inlet velocities over the cardiac cycle, one using the inlet velocities at maximum flow and one using the inlet velocities at minimum flow. The outflows are prescribed as flow splits and remained constant.

For the average case, the flow at the center of the PV was parabolic-like with skewing towards the inferior posterior side. There was evidence of modest mixing of the blood from the SMV and SV, as evidenced by plots of streamlines (Figure 98). The maximum and minimum flow cases illustrated the same skewing. Center PV cross-sectional velocity profiles can be seen in Figure 99.

Figure 98: D4 Average Streamtraces; SMV (blue) and SV (red).
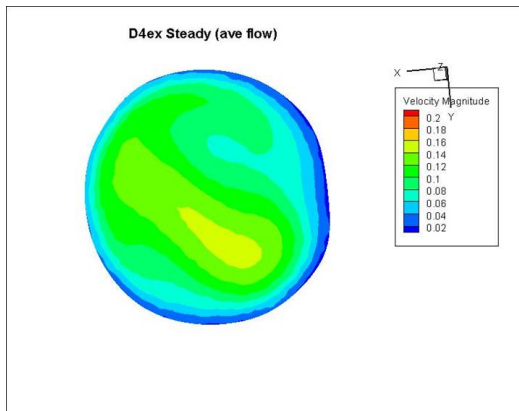
(a) Average
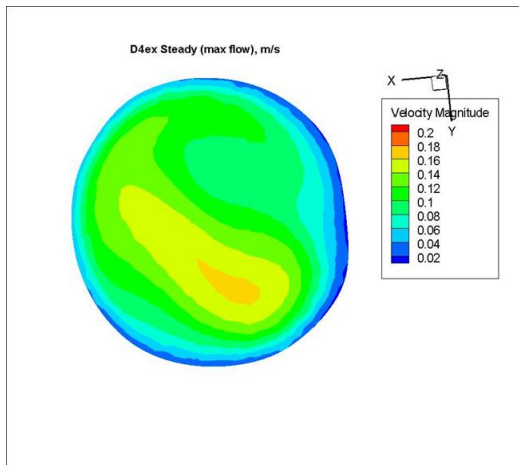
(b) Max Flow
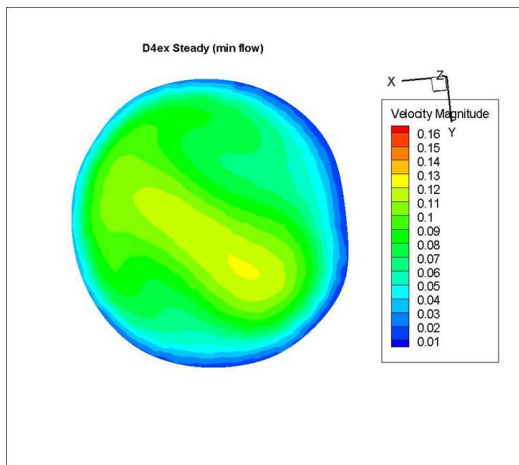
(c) Min Flow

Figure 99: D4 Steady CFD PV Cross-sections displaying Velocity Magnitude (m/s)

7.2.1.2   Flow Contribution Calculations

The flow contribution of blood from the SMV to the right and left portal veins was calculated and results can be found in Table 33. SMV blood composes 37% of the RPV flow and 99% of the LPV flow. 53% of the SMV blood went to the LPV. The streamtraces show the movement of the fluid towards the outlets (Figure 100). A visual representation of the SMV cross-section shows which streamlines went to which corresponding outlet (Figure 101).

Table 33: D4 Flow Contributions

Vessel	Flow Rate (ml/min) (% composed of SMV)
Inlets	
SMV	564
Outlets	
ARPV	327
PRPV	389
LPV	301
SMV to Outlets	
SMV/RPV(Total)	268 (0.37)
SMV/LPV	300 (0.99)
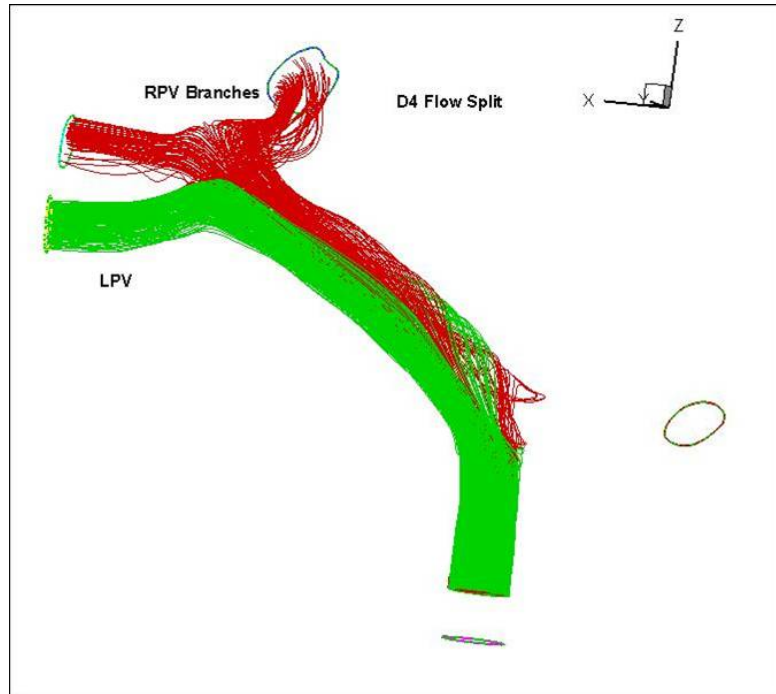
Figure 100: D4 Flow Contribution Streamtraces: LPV (green) and RPV (red).
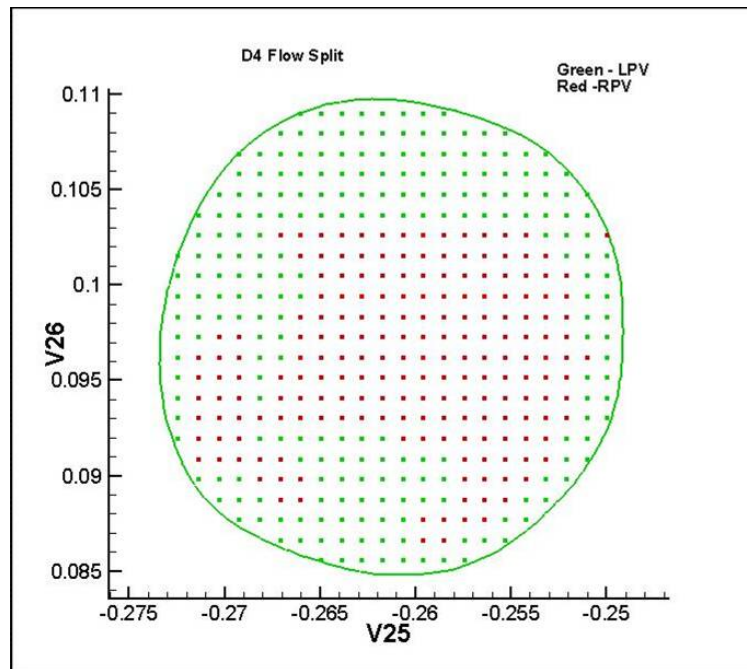
Figure 101: D4 SMV Cross-Section illustrating Flow Contributions

7.2.1.3 Unsteady Flow Calculations

Unsteady calculations were not performed for this subject.

7.2.1.4 D4 Validation

To validate the model the CFD results were compared to the MR results. Although there was noise present in the MR images, the areas of high velocity and magnitude are approximately similar as evidence by Figure 102. The CFD result was also compared to the cross-sectionally averaged MR PV image and again compared favorably although in the MR images the area of high velocity extends towards the posterior superior side verses the anterior superior side.

(a) Average Steady Flow

(b) Average MR Time Point 2

(c) Cross-Sectionally Averaged MR

Figure 102: D4 PV Cross-Sections comparing Average CFD Result to MR Data

The results for maximum flow and minimum flow were also compared with their

MR counterparts, and again the magnitude compares favorably although for the maximum flow, one area of high velocity was not captured in the CFD model. The comparisons can be seen in Figures 103 and 104.

(a) Max Flow

(b) MR Data Time Point 6
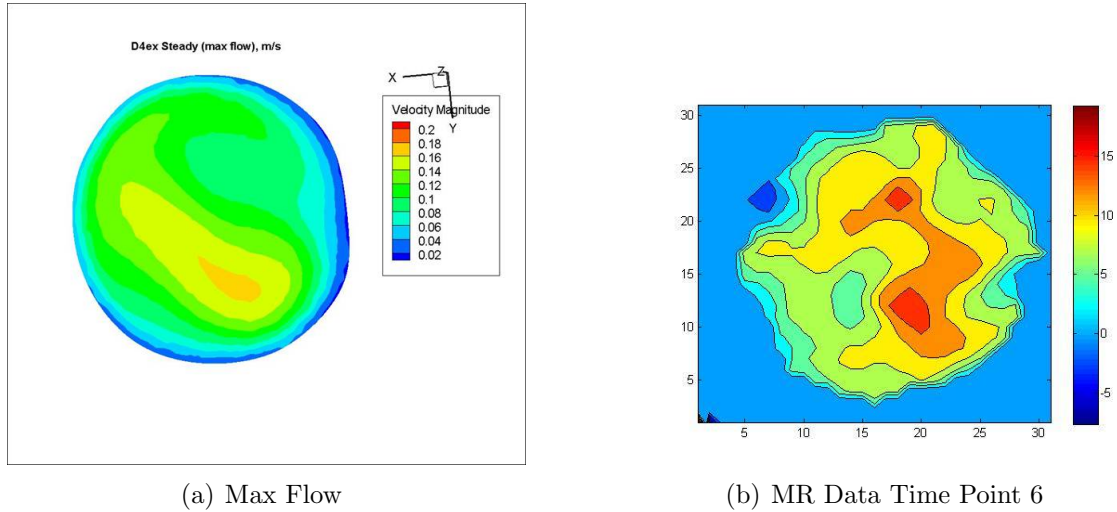
Figure 103: D4 PV Cross-Sections comparing Max Flow Steady CFD Result to MR Data

(a) Min Flow

(b) MR Data Time Point 15
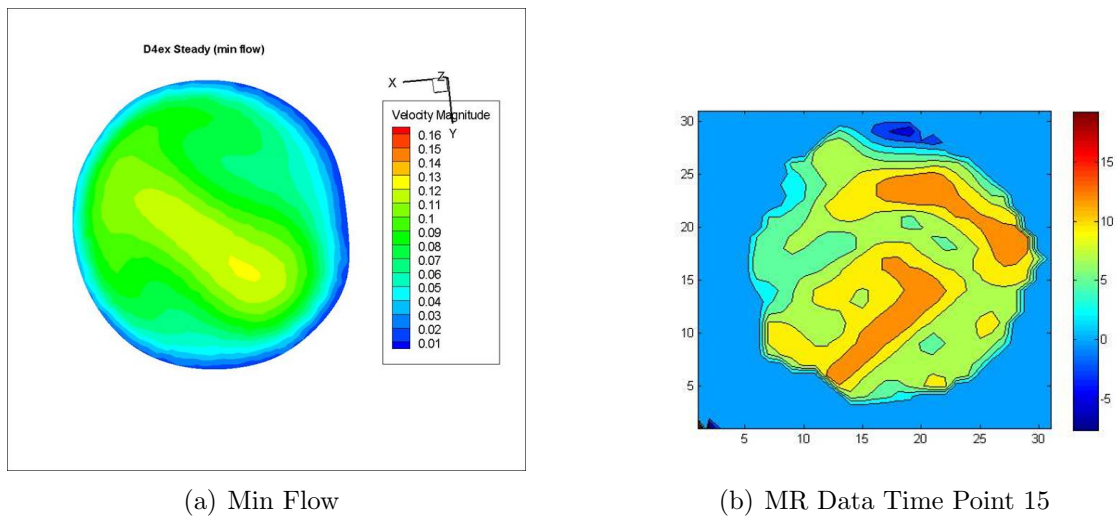
Figure 104: D4 PV Cross-Sections comparing Min Flow Steady CFD Result to MR Data

7.2.2 Patient 6

In order to impose a parabolic flow profile for the SMV and SV inlets, the inlets were extended to allow the flow to develop. The outlets were also extended due to the

outflow impositions. Table 34 provides the extension and mesh details.

Table 34: D6 Mesh Parameters

SV	20 cm
SMV	30 cm
RPV	20 cm
LPV	20 cm
Mesh Interval	1 mm
No. Volumes	1,158,591

7.2.2.1 Steady Flow Calculations

The boundary condition were taken from the PC-MR data collected and can be found in Table 35. Three different steady flow calculations were performed, one using the average inlet velocities over the cardiac cycle, one using the inlet velocities at maximum flow and one using the inlet velocities at minimum flow. The outflows are prescribed as flow splits and remained constant.

Table 35: D6 Steady Boundary Conditions (Velocities and Flow Division)

	Average Values	Max Flow	Min Flow
SV (cm/s)	9.52	9.76	8.96
SMV (cm/s)	2.98	3.53	2.62
RPV	0.56	0.56	0.56
LPV	0.44	0.44	0.44

For the average case, the flow at the center of the PV was heavily skewed towards the inferior anterior side. There was evidence of mixing of the blood from the SMV and SV, as evidenced by plots of streamlines (Figure 105). Also note the rotation in the flow. The maximum and minimum flow cases illustrated the same skewing. Center PV cross-sections of Velocity Magnitude can be seen in Figure 106.
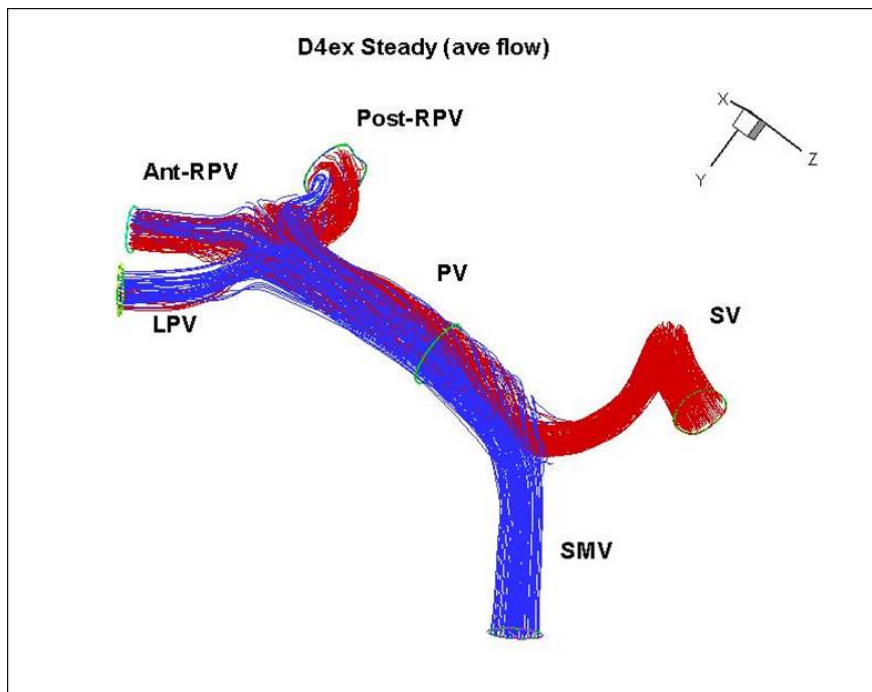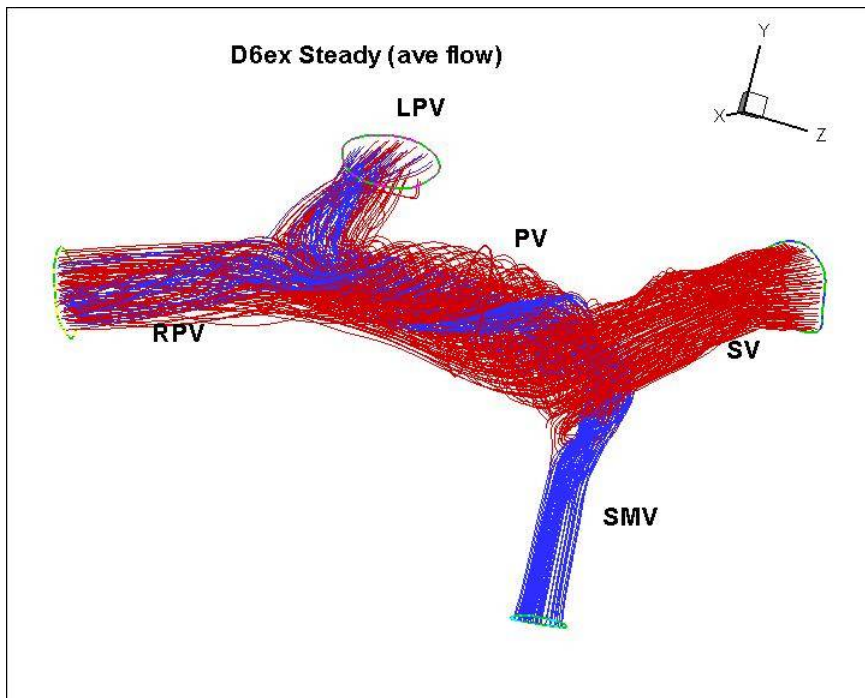
Figure 105: D6 Average Streamtraces: SMV (blue) and SV (red).
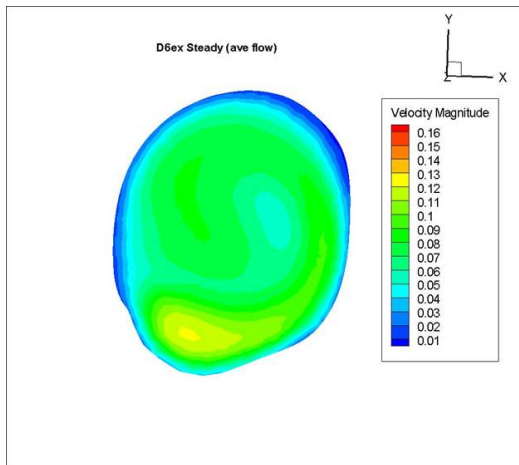
(a) Average
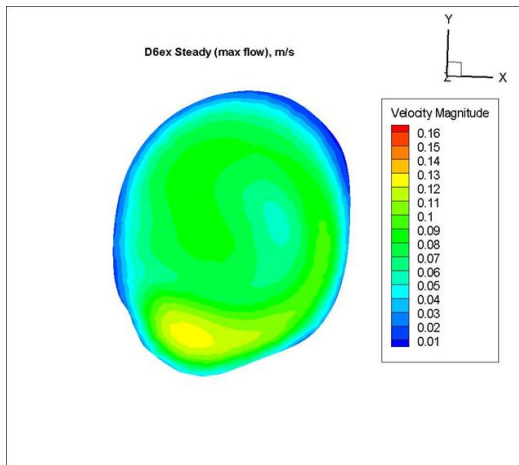
(b) Max Flow
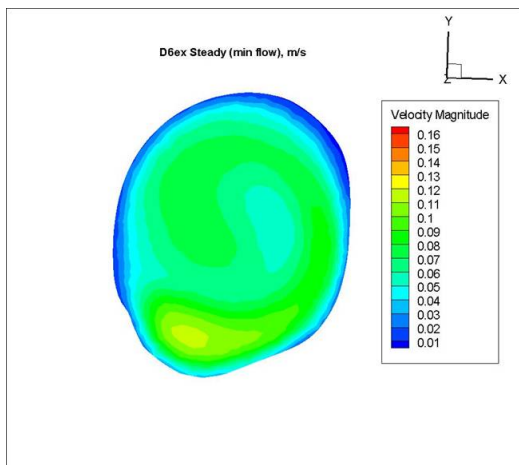
(c) Min Flow

Figure 106: D6 PV Cross-sections displaying Velocity Magnitude (m/s) at same anatomical orientation

117

The flow contribution of blood from the SMV to the right and left portal veins was calculated and results can be found in Table 36. The SMV contributes 7% of the RPV flow and 13% of the LPV. Therefore the outlets are mainly fed by the SV. 59% of the SMV blood goes to the LPV. The streamtraces show the movement of the fluid towards the outlets (Figure 107). A visual representation of the SMV cross-section shows which streamlines went to which corresponding outlet (Figure 108).

Table 36: D6 Flow Contributions

Vessel	Flow Rate (ml/min) (% composed of SMV)
Inlets	
SMV	71
Outlets	
RPV	404
LPV	316
SMV to Outlets	
SMV/RPV	30 (0.07)
SMV/LPV	42 (0.13)
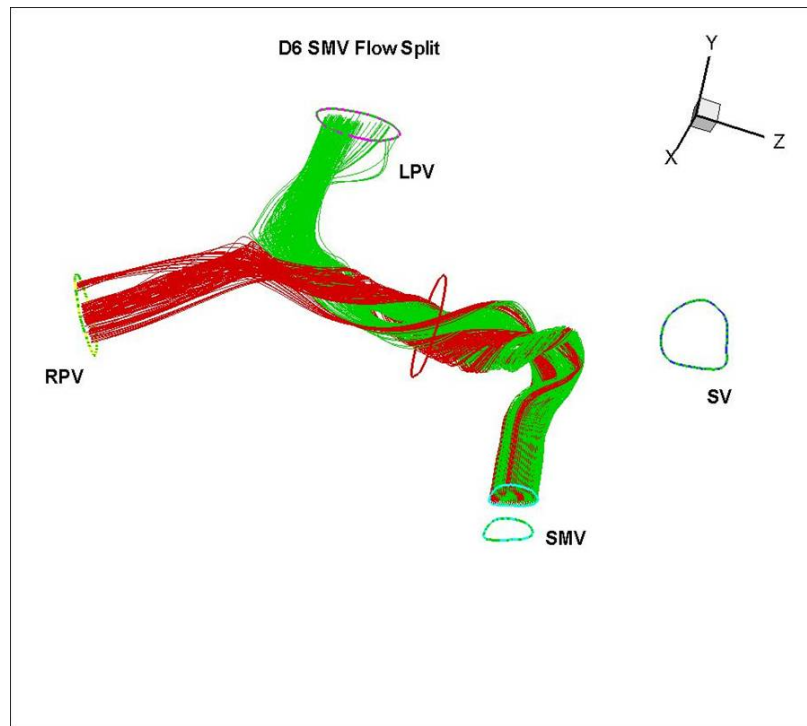
Figure 107: D6 Flow Contribution Streamtraces: RPV (red) and LPV (green).
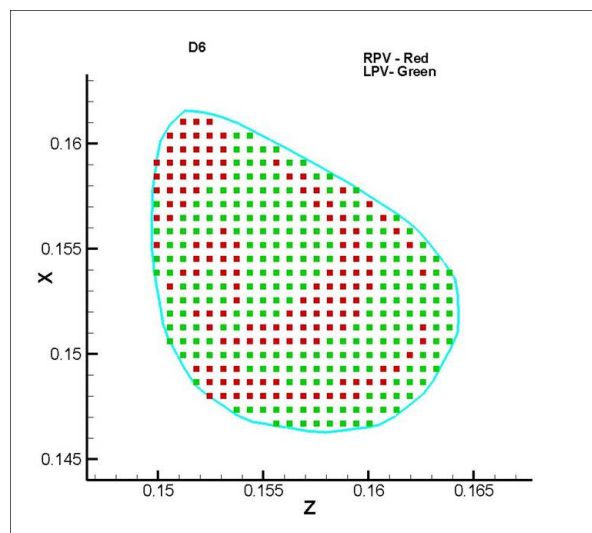
Figure 108: D6 SMV Cross-Section illustrating Flow Contributions

7.2.2.3   Unsteady Flow Calculations

Although there were slight variations in the velocity and flow over the cardiac cycle, unsteady calculations were performed to assess the validity of quasisteady flow. The velocity and flow for D6 from the MR data are presented in Figures 109 and 110.
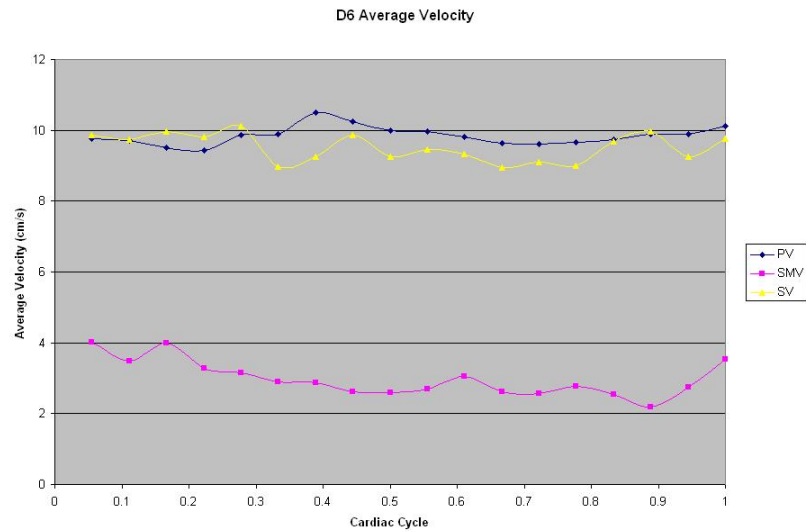
Figure 109: D6 Inlet Velocities (cm/s)
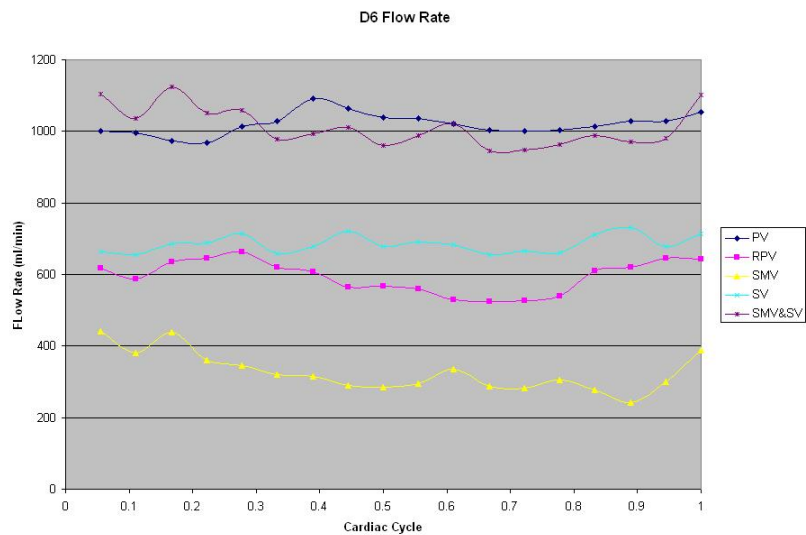
Figure 110: D6 Flow Rate (ml/min)

The inlet velocities for the SMV and SV were used as the boundary conditions for the unsteady calculations. The center PV velocity magnitude cross-sections were similar to the steady flow calculations done at maximum and minimum flow. The cross-sections can be found in Figures 111 & 112. Due to the similar magnitude of velocity and shape of the profile, quasisteady flow is valid in this case.

(a) Unsteady Max Flow   (b) Steady Max Flow
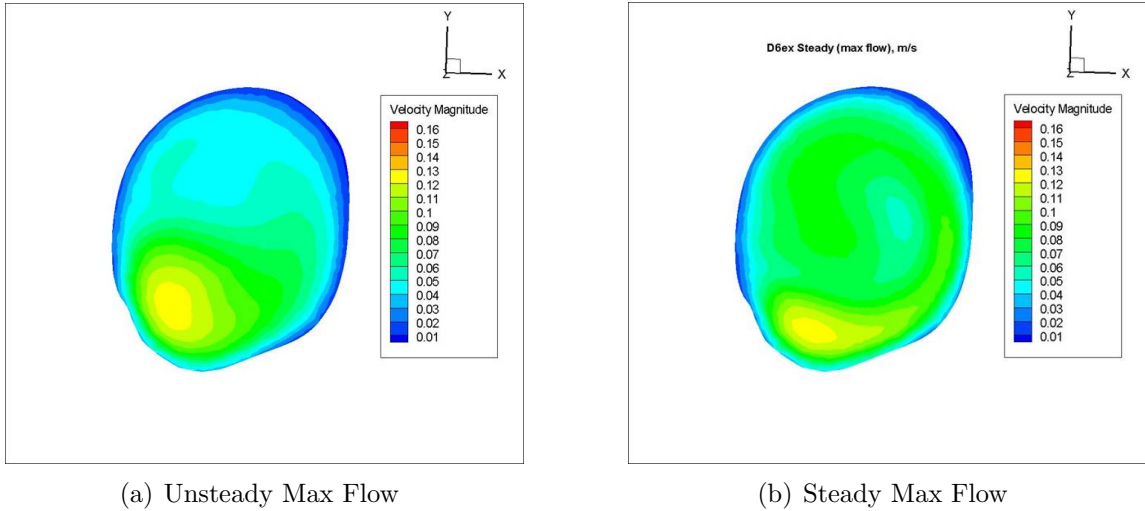
Figure 111: D6 Maximum Unsteady Calculations: PV Cross-sections displaying Velocity Magnitude (m/s)

(a) Unsteady Min Flow   (b) Steady Min Flow
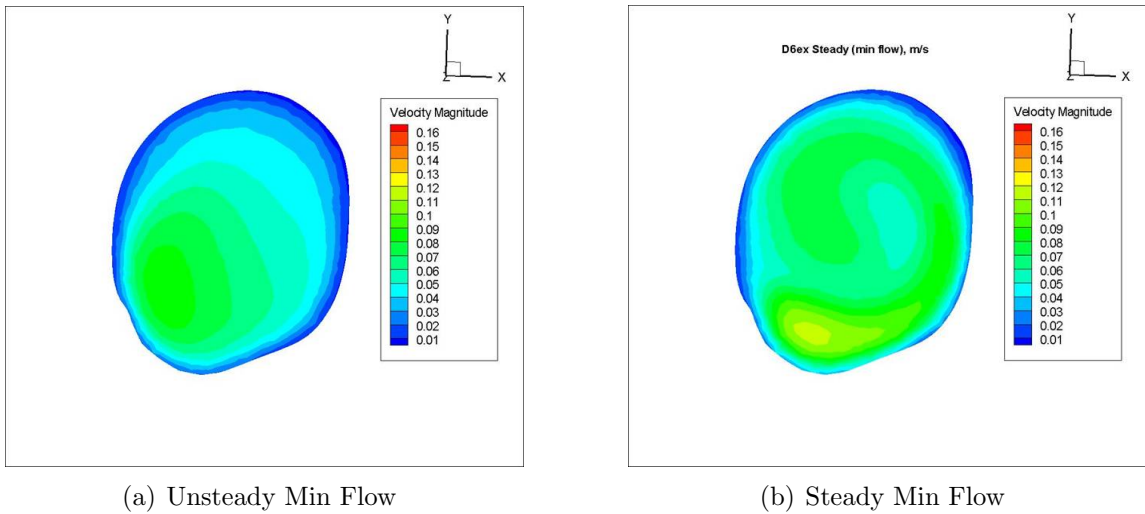
Figure 112: D6 Minimum Unsteady Calculations: PV Cross-sections displaying Velocity Magnitude (m/s)

To validate the model the CFD results were compared to the MR results. The magnitude is lower and the direction of skewing is also not similar. In examining the direction of skewing as you travel along the PV in the steady CFD results, the skewing does change directions going to the posterior inferior side versus the inferior anterior side of the PV. The comparison can be seen in Figure 113.

(a) Average Unsteady Flow   (b) Average MR Time Point 11
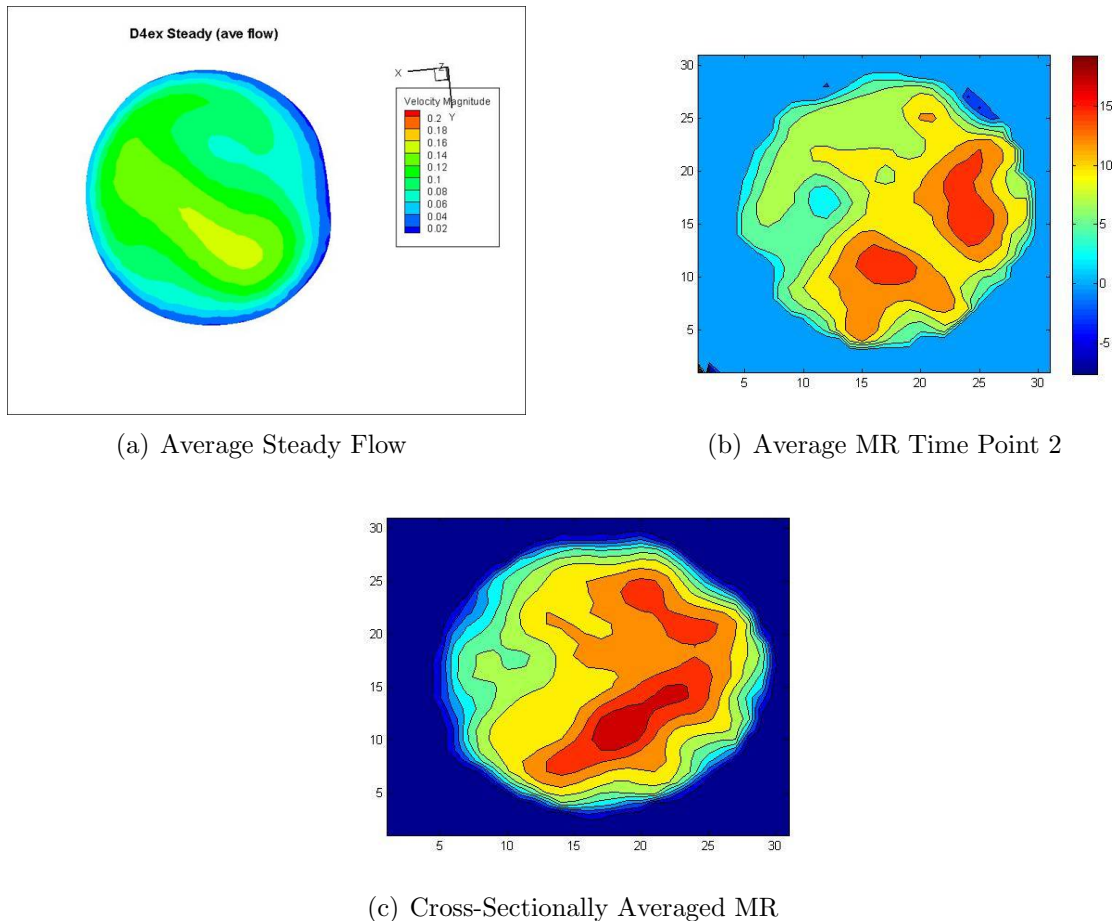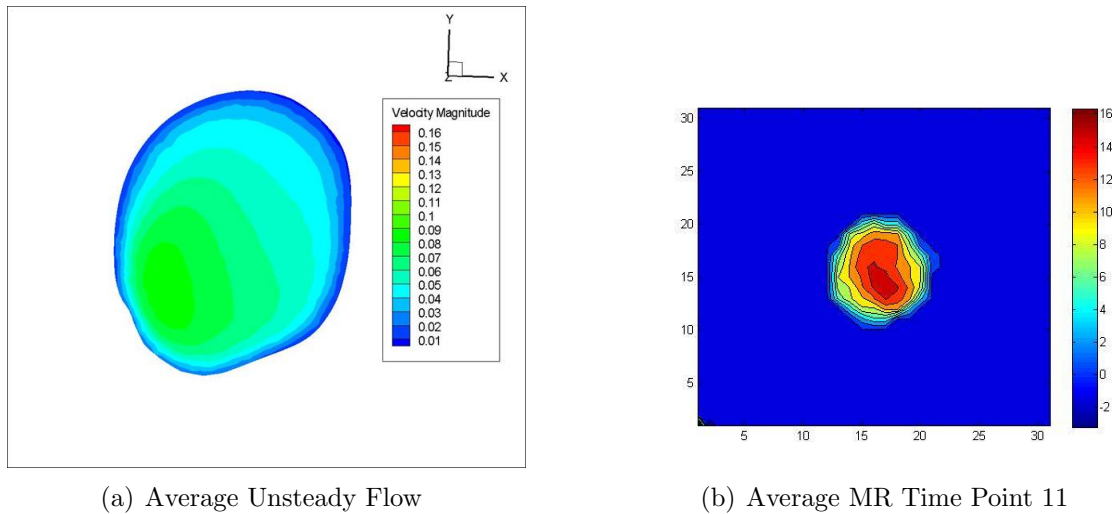
Figure 113: D6 PV Cross-Sections comparing Average CFD Result to MR Data

The results for maximum flow and minimum flow were also compared with their MR counterpart. And again the magnitude is lower in the minimum flow case, but similar in the maximum flow case. In both cases the direction of skewing is not similar. The comparisons can be seen in Figures 114 and 115.
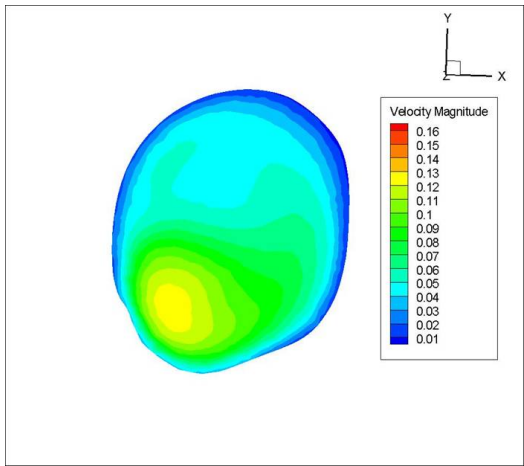
(a) Max Flow
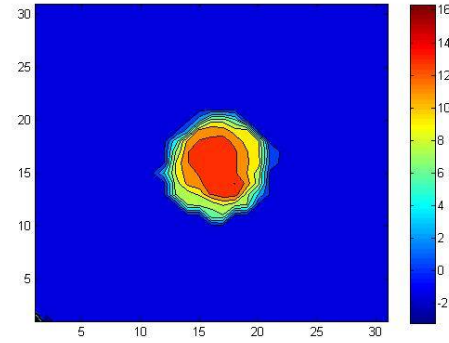
(b) MR Data Time Point 18

Figure 114: D6 PV Cross-Sections comparing Max Flow Unsteady CFD Result to MR Data
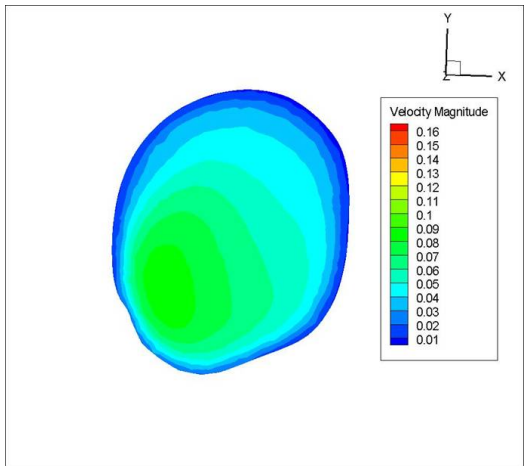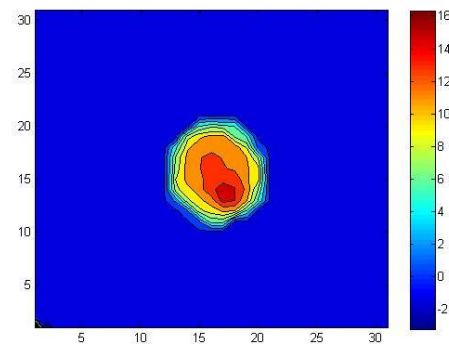
(a) Min Flow

(b) MR Data Time Point 12

Figure 115: D6 PV Cross-Sections comparing Min Flow Unsteady CFD Result to MR Data

CHAPTER VIII

COMPARISON OF PORTAL VENOUS HEMODYNAMICS IN NORMAL SUBJECTS AND PATIENTS

Specific Aim 4: Identify differences in hemodynamic characteristics of the portal venous system between normal.

Due to the limited number of subjects in this study these results are preliminary and are not meant to fully characterize all normal subjects and patients but to lay the foundation for the application of this methodology, initial findings and further research.

8.1 Liver Volume

The patients had a larger average liver volume but the results were insignificant as seen in Table 37. While the liver may enlarge initially in cirrhosis, as the disease develops the right lobes may hypotrophy and the left lobe may hypertrophy, thus calculating the volume per lobe may be an interesting addition.

Table 37: Liver Volumes

	Normal	Patient	p-value
Number of Subjects	6	4	
Average (cm^3)	1350 $\pm$320	1559 $\pm$676	0.595

8.2 Portal Vein

The PV area was significantly different for normals and patients. The PV area increased which is in agreement with the literature findings. The range of values for the area, velocity, and flow rate are within the ranges from literature. The parameters

per liver volume were calculated in an effort to separate changes in velocity and flow due to disease or due to increased liver mass, this has not been done previously to the knowledge of the author. The velocity per liver volume was significantly decreased in the patients. The velocity variance, perhaps an indicator of pulsatility, was significantly decreased in patients and is illustrated in the velocity graphs on pages 66 & 97. The lower velocity variance in patients may imply a steadier flow. In addition to these significantly different parameters, the PV average velocity and the proportion of SV blood in the PV were almost significantly different with the average velocity decreased and SV/PV increased in patients. This is also in agreement with the literature. In comparing the velocity profile cross-sections the patients all had skewing toward the lower posterior side while the normal subject skewing was variable. The comparison results can be seen in Table 38.

Table 38: Portal Vein Comparison

	Normal	Patient	p-value
Number of Subjects	7	4	
Average Area (cm^2)	0.97 ±0.08	1.75 ±3.09	0.048
Average Velocity (cm/s)	12.74 ±3.17	8.74 ±3.09	0.083
Average Flow Rate (ml/min)	783 ±241	1032 ±586	0.47
Number of Subjects	6	4	
Ave Vel/Liver Volume	0.01 ±0.0025	0.0058 ±0.0017	0.002
Ave FR/Liver Volume	0.58 ±0.18	0.64 ±0.187	0.64
Vel Variance	4.4 ±1.7	1.93 ±1	0.02
Flow Variance	285 ±117	228 ±148	0.54
SV/PV	0.36 ±0.069	0.74 ±0.32	0.07

8.3 Superior Mesenteric Vein

The superior mesenteric vein (SMV) has been under-investigated in patients except in the evaluation of changes after a meal. While no results were significant, the general trends were for the patients to have a larger area and a lower average velocity and average velocity per liver volume. The values for area are within the literature range, but the velocities were lower than the limited reportings in literature. This could be due to the timing of exams in relation to meal time, since the SMV flow increases after a meal. There was agreement with one study for the velocity but the study showed a higher area and flow rate [26]. Further investigation is needed for the SMV and perhaps more quantitative pre- and post-prandial studies including comparisons with patients. The comparison results can be seen in Table 39.

Table 39: SMV Comparison

	Normal	Patient	p-value
Number of Subjects	6	3	
Average Area (cm^2)	0.74 ±0.23	1.27 ±0.53	0.22
Average Velocity (cm/s)	9.8 ±7.49	4.97 ±2.49	0.2
Average Flow Rate (ml/min)	386 ±109	394 ±197	0.97
Number of Subjects	5	3	
Ave Vel/Liver Volume	0.007 ±0.005	0.004 ±0.0017	0.23
Ave FR/Liver Volume	0.288 ±0.1	0.209 ±0.18	0.54

8.4 Splenic Vein

Literature provides no consensus on the changes, if any, to the SV velocity. This work illustrates a significant increase in SV area (agreement with literature) with trends of an increase in velocity (not significant) and an increase in flow rate (almost significant). However when the flow rate is taken per liver volume the results do become significant. The magnitude of velocity was lower than literature predicted but the flow rates were within range for both populations. Due to the significant results this vein requires further investigation and attention. The comparison results can be seen in Table 40.

Table 40: SV Comparison

	Normal	Patient	p-value
Number of Subjects	7	4	
Average Area (cm^2)	0.578 ±0.1	1.18 ±0.37	0.043
Average Velocity (cm/s)	7.93 ±1.53	8.88 ±1.65	0.38
Average Flow Rate (ml/min)	300 ±102	666 ±311	0.097
Number of Subjects	6	4	
Ave Vel/Liver Volume	0.0057 ±0.001	0.0068 ±0.003	0.60
Ave FR/Liver Volume	0.202 ±0.033	0.46 ±0.163	0.049

8.5 Right or Left Portal Vein

While no result was significant, perhaps due to the small number of subjects who were successfully imaged, the trend seemed to be for the patients to have a lower RPV flow split. This is consistent with increased resistance on the right side of the liver. The trend was also for a smaller ratio of SMV blood in the RPV which could be related to the overall flow reduction to the RPV as supported by literature. Another important question is why was data acquisition unsuccessful in so many subjects. This was partially due to the variable branching patterns and the need to capture data before any branches. Defining a perpendicular slice through a section of the RPV to acquire data also proved to be difficult. The comparison results can be seen in Table 41.

Table 41: R/LPV Comparison

	Normal	Patient	p-value
Number of Subjects	3	2	
RPV Split	0.73 ±0.21	0.64 ±0.11	0.56
Number of Subjects	2	2	
SMV/RPV	0.6 ±0.24	0.37 ±0.03	0.4

8.6 Individual Patient Comparisons

In addition to the lumped comparisons above, the patients were compared in a few parameters individually with normal subject averages. The first parameter investigated was PV velocity in Figure 116. Each normal subject and patient is plotted separately and horizontal lines show the normal and patient averages and average plus or minus a standard deviation. One patient D5 is far below the normal and patient average. This particular patient had moderate varices, which means blood was shunted from the PV, mild spleen enlargement, which means there was less of an increase in splenic venous return, and no SV, the SV was replaced by a shunt also

indicating low splenic venous return.

The next parameter was PV flow rate. Figure 117 plots the values for all subjects. One patient, D2, had an increased PV flow rate when compared to both averages and D5 had a relatively decreased flow rate in comparison. D2 presented with severe spleen enlargement, thus increased splenic return, and mild varices, indicating that only small amounts of blood were being shunted from the PV. These two classifications together would present as increased PV flow. D5, as mentioned above, had no SV, which is presumably the reason for the reduced PV flow.

Individual comparisons of the PV flow rate per liver volume showed some interesting results (Figure 118). Since D2 has such increased flow, this patient was expected to have increased flow rate per liver volume which indeed was true. However, D6 also showed increased flow rate per liver volume. The complication that both of these patients had was severe spleen enlargement. Patients D4 and D5 who had decreased flow rate per liver volume showed only marked and mild spleen enlargement.

The last parameter is SMV flow rate as seen in Figure 119. While the normal and patient averages were similar, patient D4 showed an increase in SMV flow. D4 had only minimal inflammation which would provide less resistance to flow or the patient had recently eaten temporarily increasing flow. The other two patients D5 and D6 had moderate varices which in addition to shunting blood from the PV can shunt blood from the SMV as well. However the normal subjects also presented in a wide range of values so these data are difficult to interpret.
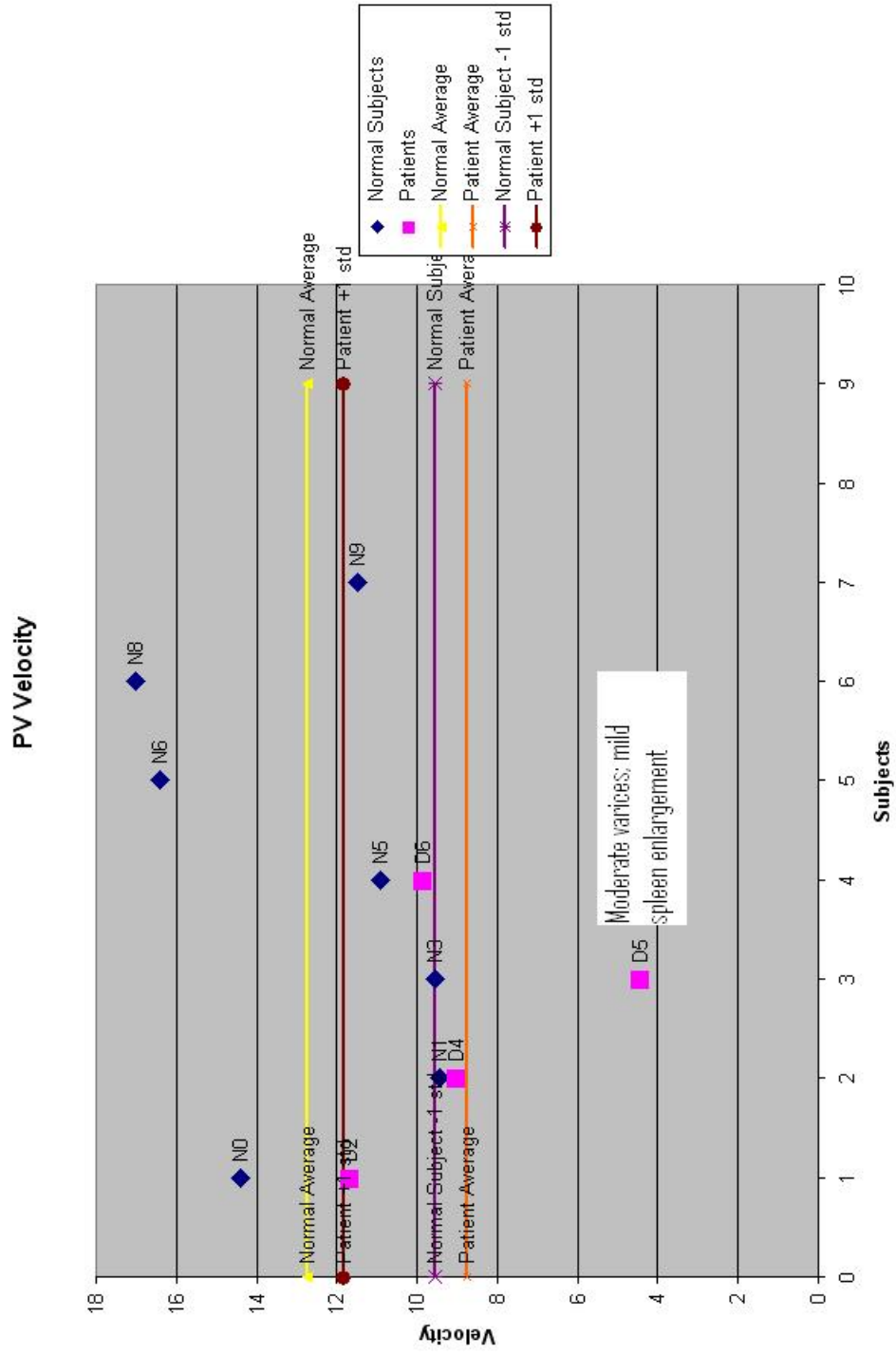
Figure 116: Portal Vein Velocity Individual Comparison
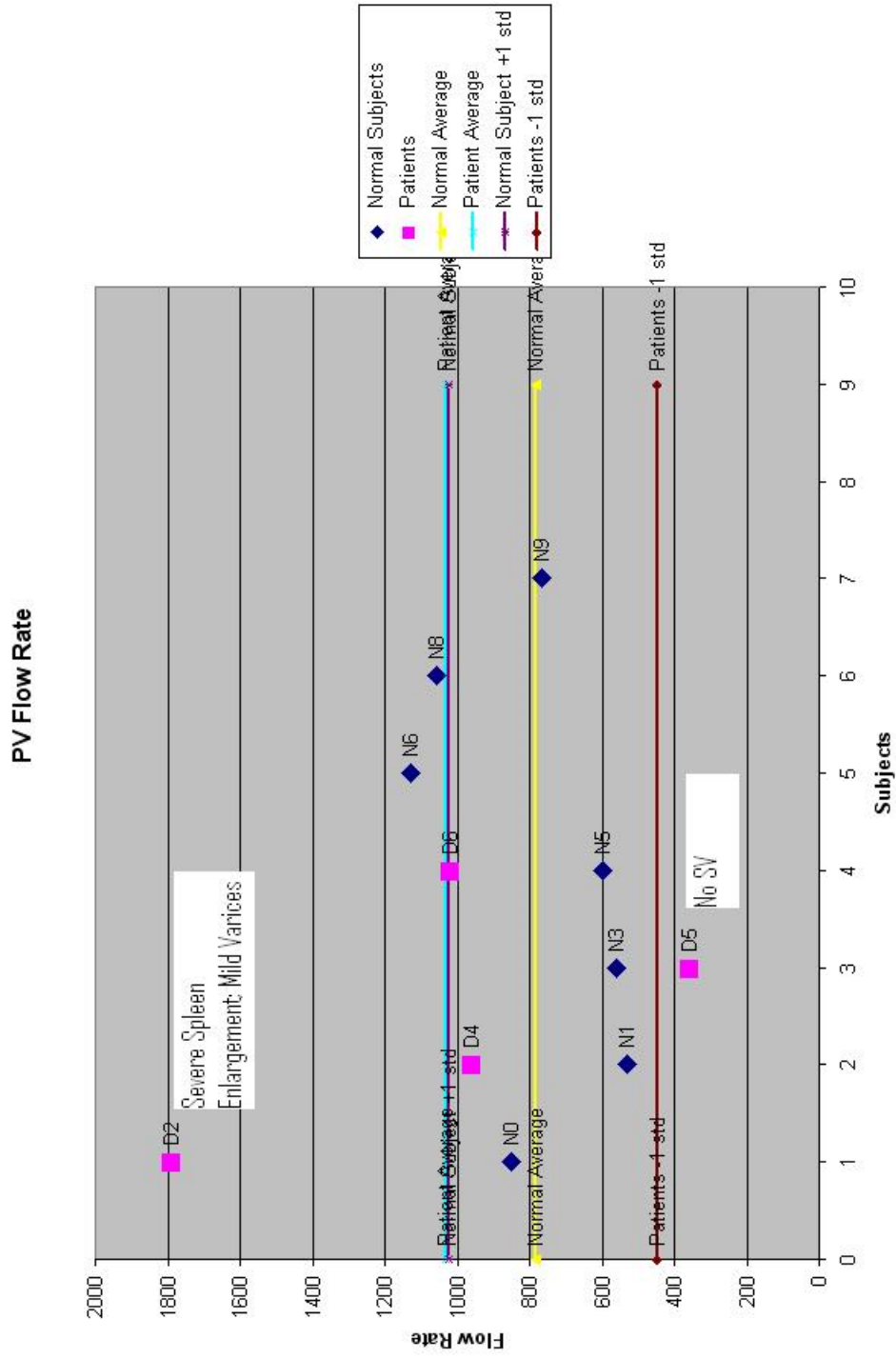
Figure 117: Portal Vein Flow Rate Individual Comparison
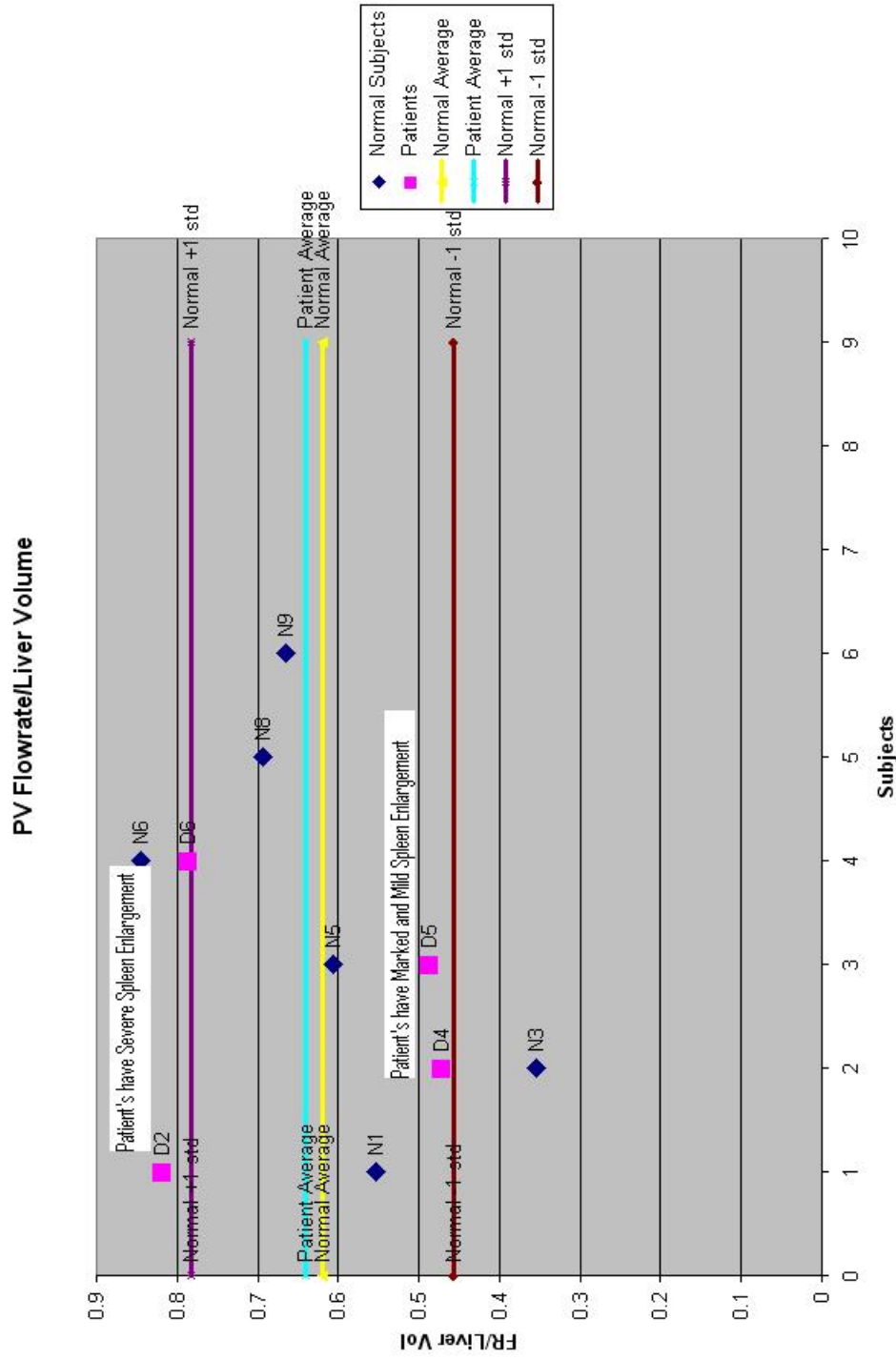
Figure 118: Portal Vein Flow Rate per Liver Volume Individual Comparison
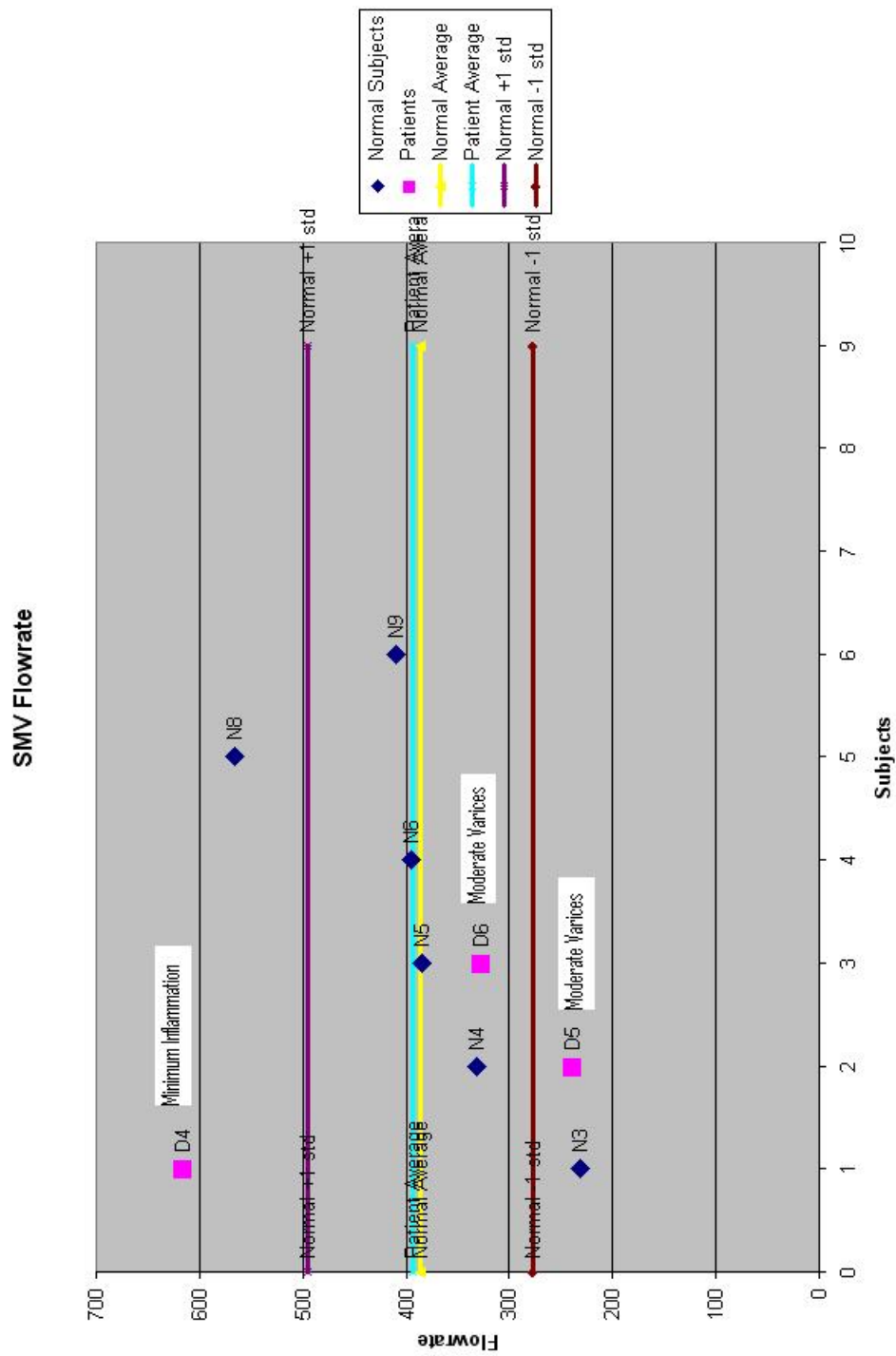
Figure 119: SMV Flow Rate Individual Comparison

8.7 CFD

Although there are only two normal models and two patient models, some preliminary conclusions include increased rotation and secondary flow in the patients as compared with the normal subjects. The streamlining theory held true for the normal subjects but in the patients the streamlines rotated. While MR will be most clinically useful, the CFD models supplement the MR data and provide information on streamlining and blood tracking to the outlets.

8.8 Comparison Summary

Even with the limited number of subjects a few parameters were significant. Patients with cirrhosis had a significantly increased PV area and a significantly decreased average velocity per liver volume and velocity variance. Patients with cirrhosis had a significantly increased SV area and average flow rate per liver volume. While these results are preliminary due to small sample size, they are promising and require further investigation and more subjects including varying stages of disease. In addition most of the parameters had values that were within the ranges reported by literature, suggesting validation of the methodology.

CHAPTER IX

DISCUSSION

The development of an idealized model allowed for an initial adaptation of CFD methodology to the portal venous system. The only geometric change that affected the flow in the PV was the altered 90-degree model which increases the angle between the PV and SMV. The flow within the portal vein was parabolic-like although slightly skewed to the superior side of the PV. However, this pattern shifted to a more centered parabolic-like flow by the bifurcation. There was little mixing of the blood from the SMV and SV as evidenced by the streamtraces and nearly zero cross-sectional velocities. This was as previous research suggested. A program was also developed to calculate the contribution of an inlet flow to the outlets. There is some error in this method as the velocities were multiplied by the grid area. For this aim the blood from the SV was followed and percentages obtained for the two outlets. The results showed that the SMV contributed 75% of the RPV and LPV flow, which supports the hypothesis that the SMV mainly supplies the RPV. Also, unsteady calculations were run in order to evaluate whether the flow was quasisteady. In the idealized model case the quasisteady assumption held, which was promising for subject specific modeling.

The idealized model demonstrated the feasibility of conducting a CFD analysis on the portal venous system. The results were as expected from literature. While human portal vein geometries are more complex than the idealized models, we believe that in moving forward to subject specific models this work allows us to postulate that the velocity profiles within the PV will be parabolic-like with little mixing of the blood and that the quasisteady flow assumptions will be valid.

Normal subject volunteer data were collected after the method of MR data acquisition was optimized allowing viable results to be gathered. Geometric variations were observed as had been expected from the literature. Of note is a general anatomical narrowing of the SMV before the PV confluence. We believe this to be due to the pancreas and the supine position of the patient. For the PV the velocity profile was skewed, although in no preferential direction, with an average velocity of 12.74 cm/s and average flow rate of 783 ml/min. Thus, we believe that there is not a standard skewing direction within the PV and that the direction is largely dependent on the geometry. There was some variation in the velocity and flow rate waveforms. This variation could be a product of the error inherent in the PC-MR acquisition method. The SMV profiles showed a range from parabolic-like to jet-like characteristics, with an average velocity of 9.8 cm/s and average flow rate of 386 ml/min. The SV profiles were parabolic-like but skewed as were the RPV profiles. In all vessels the skewing appears to be the result of the geometry orientation. The PV area was fairly consistent across the normal population. The SMV velocity in subject N8 was over 200% greater than the average velocity. However, when you look at the area of N8's SMV, it was much smaller than the average, thus the flowrate was in line with the other subjects. The RPV/LPV flow split confirmed that the majority of the PV flow feeds the RPV which supplies the right, larger, lobe of the liver. Another consistent result was the composition of the PV blood. The SMV composed the majority of the PV flow.

The MR data provided sufficient boundary conditions to create subject specific converging CFD models. In both cases the PV velocity profile was parabolic-like but the skewing was subject specific. This was the trend for the normal MR data. There was little mixing of blood within the PV although N9 illustrated slightly more mixing than N3 and also some rotation. One explanation is that N9 had a larger angle between the SMV and SV than N3. In both cases the quasi-steady assumption

136

was valid. In both cases the majority (95% for N3 and 63% for N9) of the SMV blood ultimately goes to the RPV. For the N3 case, the SMV composed 84% of the RPV flow and for N9 the SMV composed only 48% of the RPV flow. This difference could be the result of anatomical differences in the veins as the LPV in N3 was very small and most likely branches from the RPV fed portions of the LPV. We believe these calculations to be important as the hypothesis is that liver disease is preferentially located on the right side due to the SMV contribution to the RPV. While these data do not prove the hypothesis, they do support it. Although the validation slices for N3 were not taken exactly perpendicular to the vessel, the velocity profile skewing was similar in both subjects. The velocity magnitude was approximately similar in N3 and slightly lower in N9 when compared to the MR data. Thus, we believe the CFD models to be validated, keeping in mind the accuracy of the MR measurements.

All patients in the study had moderately-advanced to advanced cirrhosis. Again geometry variations were as expected although the narrowing of the SMV from the pancreas appeared to be less pronounced. Perhaps that may reflect a higher pressure in the vessel or stiffening of the vein. For the PV the direction of skewing was always to the posterior side of the PV. There was also little velocity variation in the PV. For the SMV the flow was parabolic-like, and reverse flow was seen in one subject perhaps due to varices. The SV was difficult to image in some subjects and not all data were of high quality. Generally, the flow was skewed and parabolic-like. In one case the SV had disappeared entirely, replaced by a shunt. The RPV or LPV was difficult to capture. For the one RPV case the flow was parabolic-like and for the LPV case the image was not quite perpendicular to the vessel but otherwise the profile was parabolic-like. Due to the range of disease states the results were not as consistent as the normal subjects.

Again the MR data provided sufficient boundary conditions to create two subject

specific converging CFD models. The D4 computational model showed skewing towards the inferior posterior side of the PV that did not change under maximum or minimum flow conditions. D6 model data showed skewing towards the inferior side of the PV. These skewing results differ slightly from the trend seen in the MR data. There was modest mixing of the blood in D4 with more rotation than was seen in the normal subjects. In D6 there was definitely mixing of the blood and rotational flow. The angle between the SMV and SV was large, almost 180 degrees. The quasi-steady assumption is also valid for both cases. The majority of the SMV blood (53% for D4 and 59% for D6) went to the LPV. For D4 the SMV composed 99% of the LPV and only 37% of the RPV. For D6, the SMV composed 13% of the LPV and 7% of the RPV. D6 had a very small SMV contribution in general. When CFD results were compared with the MR images, the areas of high velocity matched although there was noise in the D4 MR images. For D6, in comparing the CFD results to the MR images the magnitudes were similar but the areas of high velocity were not. However in additional slices from the CFD results, the center of high velocity shifted from the anterior side to the posterior side. While the quality of patient MR data was less than for the normal subjects, we believe it was sufficient to allow the CFD models to represent the *in vivo* flow again allowing for errors inherent in the measurement method.

We must preface this section by saying that while we feel that the number of normal subjects is sufficient to provide average normal values, we recognize that our pool of patients is small and limited and the comparisons drawn are meant to be preliminary and represent areas for further research. In looking for anatomical differences between the two groups the architecture of the liver tissue was obviously different and has been documented elsewhere in literature. However, there was no statistical difference in liver volume. This could be due to the fact that with cirrhosis the liver may increase in size but then as the disease progresses the right lobe may

hypotropy and the left lobe may hypertrophy maintaining a relatively normal liver volume. It may be interesting to calculate the volume per liver lobe and map the changes as the disease progresses. Other anatomical differences include a significantly larger PV and SV area in patients as compared to normal subjects. The PV enlarges due to the increase in pressure and the SV enlarges due to the increased blood supply to the spleen and ultimately the SV.

In order to tease out whether differences in velocity were true or due to the volume of the liver, we calculated velocity per liver volume values. While the PV velocity was decreased in patients it was not statistically significant, however, the PV velocity per liver volume was significantly lower in patients than in normals. Also, the velocity variance was significantly lower in patients indicating near steady flow or possibly variations due to measurement error. The SV flow rate per liver volume was significantly greater in patients again indicating increased flow to the spleen. Also of interest, the ratios of SV flow to PV flow were almost significantly higher in patients than in normals.

In addition to the lumped comparisons above, the patients were compared individually with the normal subject averages. For PV velocity D5 had the greatest difference from both the normal and patient averages. D5 had moderate varices which means blood was bypassing the PV and liver as well as only mild spleen enlargement and thus a smaller increase in flow to the SV. While the patients trended to have increased but not statistically different PV flow, one patient, D2, had a flow rate that was 80% greater than even the patient average. D2 also had severe spleen enlargement and only mild varices which means that the flow from the SV was increased and the flow to the PV was not being diverted by varices. Another patient, D5, had a 60% decrease in flow from the patient average and had no SV which limited the SV contribution to the PV flow. For PV flowrate per liver volume D2 and D6 were

over 1 standard deviation away from the normal average and D4 and D5 were almost 1 standard deviation the other way from the normal average. Thus, the patient and normal averages were not that far apart. The parameter that separates these two groups is that D2 and D6 have severe spleen enlargement and D4 and D5 have only marked and mild spleen enlargement. We can then hypothesize that with severe spleen enlargement the flow increase from the spleen is not a result of an increase in liver volume since the PV flowrate per liver volume increases. Otherwise if the liver volume did increase, the flow per liver volume would remain the same. The SMV flowrate averages for normals and patients were within 8 ml/min. However, D4 had increased SMV flow and only minimal inflammation. Perhaps the low amount of inflammation allowed the flow to be higher or the patient had recently eaten which can also increase flow temporarily. D5 and D6 had decreased SMV flowrates and also moderate varices, which could in addition to diverting blood from the PV also divert blood from the SMV.

In comparing the CFD models, the patients had greater mixing of the blood and more rotational flow. The SMV also contributed a majority of its flow to the LPV versus the RPV as the normal subjects showed. This could be due to changes in the flow split and increased resistance in the right portion of the liver due to the disease. However, further work is needed to determine at what stage of disease that change occurs and if it can be used as a marker or predictive parameter.

9.1 Future Directions

This work is meant to draw preliminary conclusions about the portal venous system and apply the MR/CFD methodology. Future work would involve more normal subjects and more patients including a range of disease stages. The parameters mentioned above should be investigated further to see if indeed they are significant or if any other parameters emerge as significant with the addition of more subjects. Once

the number of subjects is sufficient, the diagnostic significance or applicability will be assessed. Further studies may also include before and after meal measurements of the parameters to see if there is an enhanced or diminished response to food in patients.

CHAPTER X

CONCLUSIONS

Cirrhosis is a leading cause of death in the United States and has severe and costly complications. Because of the clinical significance of cirrhosis, it is important that noninvasive methods be developed to detect cirrhosis early and to monitor its progression with advancing liver disease. Previous studies on portal venous hemodynamics have been performed mainly with ultrasound with mixed results. Magnetic Resonance Imaging offers several advantages over ultrasound including acquisition of both high quality anatomical and hemodynamic information.

Phase-Contrast MR was used to gather velocity data for the portal venous system. Methods were developed to perform registration, segmentation and isolation of the portal vein geometries and velocity data. Computational Fluid Dynamics was also employed to further investigate the flow within the portal vein, beginning with idealized models and then subject specific models.

The idealized models provided a simple initial adaptation of the CFD methodology and provided some insights that were carried forward to the normal subjects and patients such as parabolic-like velocity profiles, streamlining in the portal vein and quasisteady flow assumption.

The data set included nine normal subjects and four patients. Velocity data for the portal vein, superior mesenteric vein, splenic vein and the right or left portal vein was acquired in varying numbers for both data sets. Even with the limited number of subjects a few parameters were significant. Patients with cirrhosis had a significantly increased portal vein area and a significantly decreased average velocity per liver volume and velocity variance. Patients with cirrhosis had a significantly increased

splenic vein area and average flow rate per liver volume. Two other parameters that were almost significant were a decreased portal vein velocity and an increase in splenic blood in the portal vein. CFD results showed some interesting differences between normal subjects and patients which include greater mixing of the blood and more rotational flow in the patients. Whether the rotational flow is a result of the subject's geometry or the disease is yet to be determined. The CFD results also supported the hypothesis that the superior mesenteric vein predominately feeds the right portal vein. This was found to be true for the normal subjects but reversed for the patients perhaps due to the diseased state.

While these results are preliminary due to small sample size, they are promising and require further investigation and more subjects including varying stages of disease. The long term clinical significance is to develop non-invasive diagnostic methods to evaluate and monitor the progression of cirrhosis in patients with chronic liver disease.

REFERENCES

[1] "Cirrhosis." http://janis7hepc.com/cirrhosis6.htm, 2008. Janis and Friends Hepatitis C Support Web Site.

[2] "Division of gastroenterology." http://www.uwgi.org/, 2008. University of Washington.

[3] "Liver, biliary and pancreatic disorders." http://www.ohsuhealth.com/, 2008. Oregon Health and Science University.

[4] "Liver cancer network." http://www.livercancer.com/, 2008. Allegheny General Hospital.

[5] "Pathophysiology of the digestive system: Colorado state university." http://arbl.cvmbs.colostate.edu/hbooks/pathphys/digestion/index.html/, 2008.

[6] "Research center for alcoholic liver and pancreatic diseases and cirrhosis." http://www.usc.edu/schools/medicine/research/alcohol$_c$enter/, 2008.

[7] "United network for organ sharing." http://www.unos.org/, 2008.

[8] ARAIS, I., *The Liver Biology and Pathobiology*. New York: Lippincott, Williams, and Wilkins, 2001.

[9] BOLOGNESI, M., SACERDOTI, D., MERKEL, C., GERUNDA, G., MAFFEI-FACCIOLI, A., ANGELI, P., JEMMOLO, R., BOMBONATO, G., and GATTA, A., "Splenic doppler impedance indices: influence of different portal hemodynamic conditions," *Hepatology*, vol. 23, pp. 1035–1040, May 1996.

[10] BORSE, N., SAWANT, P., and GALA, B., "Assessment of renal and hepatic hemodynamics in cirrhosis of liver.," *Indian Journal of Gastroenterology*, vol. 21, no. 6, pp. 213–215, 2002.

[11] BURCHARTH, F. and AAGAARD, J., "Total hepatofugal portal blood flow in cirrhosis demonstrated by transhepatic portography," *Rofo: Fortschritte auf dem Gebiete der Rontgenstrahlen und der Nuklearmedizin*, vol. 148, no. 1, pp. 47–49, 1988.

[12] BURKART, D., JOHNSON, C., MORTON, M., WOLF, R., and EHMAN, R., "Volumetric flow rates in the portal venous system: measurement with cine phase-contrast mr imaging.," *American Journal of Roentgenology*, vol. 160, pp. 1113–8, May 1993.

[13] CHAWLA, Y., SREEDHARAN, A., DHIMAN, R., JAIN, S., and SURI, S., "Portal hemodynamics in fulminant hepatic failure as assessed by duplex doppler ultrasonography.," *Digestive Diseases Sciences*, vol. 46, no. 3, pp. 504–508, 2001.

[14] GALLIX, B., TAOUREL, P., DAUZAT, M., BRUEL, J., and LAFORTUNE, M., "Flow pulsatility in teh portal venous system: a study of doppler sonography in healthy adults.," *American Journal of Roentgenology*, vol. 169, no. 1, pp. 141–144, 1997.

[15] HAAG, K., ROSSLE, M., OCHS, A., HUBER, M., SIEGERSTETTER, V., OLSCHEWSKI, M., BERGER, E., LU, S., and BLUM, H., "Correlation of duplex sonography findings and portal pressure in 375 patients with portal hypertension," *American Journal of Roentgenology*, vol. 172, pp. 631–5, Mar 1999.

[16] HAKER, S., SAPIRO, G., and TANNENBAUM, A., "Knowledge-based segmentation of sar data with learned priors," *IEEE Tran. on Image Processing*, vol. 9, pp. 298–302, 2000.

[17] HEFFRON, T., PILLEN, T., WELCH, D., SMALLWOOD, G., REDD, D., and ROMERO, R., "Hepatic artery thrombosis in pediatric liver transplantation," *Transplantation Proceedings*, vol. 35, no. 4, pp. 1447–1448, 2003.

[18] HINO, S., KAKUTANI, H., IKEDA, K., UCHIYAMA, Y., SUMIYAMA, K., KURAMOCHI, A., KITAMURA, Y., MATSUDA, K., ARAKAWA, H., KAWAMURA, M., MASUDA, K., and SUZUKI, H., "Hemodynamic assessment of the left gastric vein in patients with esophageal varices with color doppler eus: factors affecting development of esophageal varices.," *Gastrointestinal Endoscopy*, vol. 55, no. 4, pp. 512–517, 2002.

[19] HOLDEN, M. and HILL, D., "Voxel similarity measures for 3-d serial mr brain image registration," *IEEE Tran. Medical Imaging*, vol. 19, no. 2, pp. 94–102, 2000.

[20] KAYACETIN, E., EFE, D., and DOGAN, C., "Portal and splenic hemodynamics in cirrhotic patients: relationship between esophageal variceal bleeding and the severity of hepatic failure.," *Journal of Gastroenterology*, vol. 39, no. 7, pp. 661–667, 2004.

[21] KOK, T., VAN DER JAGT, E. J., HAAGSMA, E. B., BIJLEVELD, C. M. A., JANSEN, P. L. M., and BOEVE, W. J., "The value of doppler ultrasound in cirrhosis and portal hypertension," *Scandinavian Journal of Gastroenterology,*, vol. 34, pp. 82–88, Jul 1999.

[22] KUTLU, R., KARAMAN, I., AKBULUT, A., BAYSAL, T., SIGIRCI, A., ALKAN, A., ALADAG, M., SECKIN, Y., and SARAC, K., "Quantitative doppler evaluation of the splenoportal venous system in various stages of cirrhosis: differences between right and left portal veins.," *Journal of Clinical Ultrasound*, vol. 30, no. 9, pp. 537–543, 2002.

[23] LIN, L.-W., DUAN, X.-J., WANG, X.-Y., XUE, E.-S., HE, Y.-M., SHANG-DA-GAO, and YU, L.-Y., "Color doppler velocity profile and contrast-enhanced ultrasonography in assessment of liver cirrhosis," *Hepatobiliary Pancreat Dis Int*, vol. 7, pp. 34–9, Feb 2008.

[24] LJUBICIC, N., DUVNJAK, M., ROTKVIC, I., and KOPJAR, B., "Influence of the degree of liver failure on portal blood flow in patients with liver cirrhosis.," *Scandinavian Journal of Gastroenterology*, vol. 25, no. 4, pp. 395–400, 1990.

[25] LU, L., ZENG, M., WAN, M., LI, C., MAO, Y., LI, J., QIU, D., CAO, A., YE, J., CAI, X., CHEN, C., WANG, J., WU, S., ZHU, J., and ZHOU, X., "Grading and staging of hepatic fibrosis, and its relationship with noninvasive diagnostic parameters," *World Journal of Gastroenterology*, vol. 9, pp. 2574–8, Nov 2003.

[26] LYCKLAMA, A., NIJEHOLT, G., BURGGRAAF, K., MN, M. W., KOOL, L. S., SCHOEMAKER, R., COHEN, A., and DE ROOS, A., "Mr velocity mapping under fasting and post-prandial conditions–comparison with echo-doppler," *Journal of Hepatology*, vol. 26, pp. 298–304, Feb 1997.

[27] MARTIN, D. R., MOREIRA, R., TUDORESCU, D., SALMAN, K., SPIVEY, J. R., MARTINEZ, E., and LAUENSTEIN, T. C., "Non-invasive evaluation of liver inflammation and fibrosis using multi-phase gadolinium-enhanced gradient echo magnetic resonance imaging. submitted for publication," 2008.

[28] MARTINI, *Fundamentals of Anatomy and Physiology*. New Jersey: Prentice Hall, 1998.

[29] MAS, V., FISHER, R., MALUF, D., WILKINSON, D., GARRETT, C., and FERREIRA-GONZALEZ, A., "Hepatic artery thrombosis after liver transplantation and genetic factors: prothrombin g20210a polymorphism," *Transplantation*, vol. 76, no. 1, pp. 247–249, 2003.

[30] MOLMENTI and KLINTMALM, *Atlas of liver Transplantation*. 2002. Reprinted as Vol. A of *Computers & Typesetting*, 1986.

[31] MORIYASU, F., NISHIDA, O., BAN, N., NAKAMURA, T., SAKAI, M., MIYAKE, T., and UCHINO, H., ""congestion index" of the portal vein.," *American Journal of Roentgenology*, vol. 146, pp. 735–9, Apr 1986.

[32] NANASHIMA, A., SHIBASAKI, S., SAKAMOTO, I., SUEYOSHI, E., SUMIDA, Y., ABO, T., NAGASAKI, T., SAWAI, T., YASUTAKE, T., and NAGAYASU, T., "Clinical evaluation of magnetic resonance imaging flowmetry of portal and hepatic veins in patients following hepatectomy.," *Liver International*, vol. 26, pp. 587–94, Jun 2006.

[33] O'DONOHUE, J., NG, C., CATNACH, S., FARRANT, P., and WILLIAMS, R., "Diagnostic value of doppler assessment of the hepatic and portal vessels and ultrasound of the spleen in liver disease," *European Journal of Gastroenterology Hepatology*, vol. 16, pp. 147–155, Feb. 2004.

[34] OLVER, P., SAPIRO, G., and TANNENBAUM, A., "Invariant geometric evolutions of surfaces and volumetric smoothing," *SIAM J. Applied Math*, vol. 57, pp. 176–194, 1997.

[35] SHAH, S., HAYES, P., ALLAN, P., NICOLL, J., and FINLAYSON, N., "Measurment of spleen size and its relation to hypersplenism and portal hemodynamics in portal hypertension due to hepatic cirrhosis.," *American Journal of Gastroenterology*, vol. 91, no. 12, pp. 2580–2583, 1996.

[36] SHERLOCK and DOOLEY, *Disease of the Liver and Biliary System*. Blackwell Science, 2002.

[37] STANGE, B., GLANEMANN, M., NUESSLER, N., SETTMACHER, U., STEINMULLER, T., and NEUHAUS, P., "Hepatic artery thrombosis after adult liver transplantation," *Liver Transplantation*, vol. 9, no. 1, pp. 612–620, 2003.

[38] TAOUREL, P., BLANC, P., DAUZAT, M., CHABRE, M., PRADEL, J., GALLIX, B., LARREY, D., and BRUEL, J., "Doppler study of mesenteric, hepatic, and portal circulation in alcoholic cirrhosis: relationship between quantitative doppler measurements and the severity of portal hypertension and hepatic failure.," *Hepatology*, vol. 28, no. 4, pp. 932–936, 1998.

[39] TSUKUDA, T., ITO, K., KOIKE, S., SASAKI, K., SHIMIZU, A., FUJITA, T., MIYAZAKI, M., KANAZAWA, H., JO, C., and MATSUNAGA, N., "Pre- and postprandial alterations of portal venous flow: evaluation with single breath-hold three-dimensional half-fourier fast spin-echo mr imaging and a selective inversion recovery tagging pulse.," *Journal of Magnetic Resonance Imaging*, vol. 22, pp. 527–33, Oct 2005.

[40] VYAS, K., GALA, B., SAWANT, P., DAS, H., KULHALLI, P., and MAHAJAN, S., "Assessment of portal hemodynamics by ultrasound color doppler velocimetry in liver cirrhosis.," *Indian Journal of Gastroenterology*, vol. 21, no. 5, pp. 176–178, 2002.

[41] WHITE, F. M., *Fluid Mechanics*. New York: McGraw-Hill Inc., 1994. Third Edition.

[42] YANG, Y., TANNENBAUM, A., and GIDDENS, D., "Knowledge-based 3d segmentation and reconstruction of coronary arteries using ct images," *In Proceedings of the 26th Annual International Conference of the IEEE EMBS*, pp. 1664–1666, 2004.

[43] YIN, X., LU, M., HUANG, J., XIE, X., and LIANG, L., "Color doplar velocity profile assessment of portal hemodynamics in cirrhotic patients with portal hypertension: correlation with esophageal variceal bleeding.," *Journal of Clinical Ultrasound*, vol. 29, no. 1, pp. 7–13, 2001.

[44] Zhang, X., Zhong, T., Zhai, Z., and Zeng, N., "Mr venography of the inferior mesentery vein.," *European Journal of Radiology*, vol. 64, pp. 147–51, Oct 2007.

[45] Zoli, M., Iervese, T., Merkel, C., Bianchi, G., Magalotti, D., Marchesini, G., Gatta, A., and Pisi, E., "Prognostic significance of portal hemodynamics in patients with compesated cirrhosis.," *Journal of Hepatology*, vol. 17, no. 1, pp. 56–61, 1993.

VITA

Stephanie M. George was born in Fort Wayne, Indiana. She moved to Newport News, Virginia and is a product of Newport News Public Schools. She attended Virginia Tech and earned a Bachelor's Degree in Engineering Science and Mechanics in 2002. Her doctorate research has focused on studying portal venous hemodynamics using MRI and CFD. She has been actively involved in graduate women's issues as well as student parent issues. Stephanie also enjoys teaching and was awarded the Gandy/Diaz Fellowship and the PBL Across the Curriculum Fellowship.